Master Thesis

MSc in Energy Engineering

Hydro/Battery Hybrid Systems for Frequency Regulation

Author: Danilo Laban

Supervisor: Oriol Gomis Bellmunt

July 2019

Escola Tècnica Superior

d'Enginyria Industrial de Barcelona

1 Summary

An innovative Hydro/Battery Hybrid System (HBHS), composed of a hydropower plant (HPP) and a Battery Energy Storage System (BESS) is proposed to provide frequency regulation services in the Nordic Power System (NPS). The HBHS is envisioned to have a faster and more efficient response compared to HPPs currently providing these services, whilst retaining their high energy capacity and endurance, thus alleviating stand-alone BESS operation constraints. This Thesis aims to explore the operation and optimization of such a hybrid system in order to make it efficient and economically viable. A power plant perspective is employed, evaluating the impact different control algorithms and parameters have on the HBHS performance.

Providing Frequency Containment Reserves for Normal Operation (FCR-N), to the national TSO in Sweden, is defined from technology and market analyses as the use case for the HBHS. The characteristics of HPPs suitable for HBHS implementation are found theoretically, by evaluating HPP operational constraints and regulation mechanisms. With the aim of evaluating the dynamic performance of the proposed HBHS, a frequency regulation model of the NPS is built in MATLAB and Simulink. Two different HBHS architectures are introduced, the Hydro Recharge, in which the BESS is regulating the frequency and the HPP is controlling its state of charge (SoC), and the Frequency Split, in which both elements are regulating the frequency with the HPP additionally compensating for the SoC. The dynamic performance of the units is qualitatively evaluated through existing and proposed FCR-N prequalification tests, prescribed by the TSO and ENTSO-E. Quantitative performance comparison to a benchmark HPP is performed with regards to the estimated HPP regulation wear and tear and BESS degradation during 30-day operation with historical frequency data.

The two proposed HBHS architectures demonstrate significant reductions of estimated HPP wear and tear compared to the benchmark unit. Simulations consistently report a 90 % reduction in the number of movements HPP regulation mechanism performs and a more than 50 % decrease in the distance it travels. The BESS lifetime is evaluated at acceptable levels and compared for different architectures. Two different applications are identified, the first being installing the HBHS to enable the HPP to pass FCR-N prequalification tests. The second application is increasing the FCR-N capacity of the HPP by installing the HBHS. The Frequency Split HBHS shows more efficient performance when installed in the first application, as opposed to the Hydro Recharge HBHS, which shows better performance in the second application. Finally, it is concluded that a large-scale implementation of HBHSs would improve the frequency quality in the NPS, linearly decreasing the amount of time outside the normal frequency band with increasing the total installed HBHS power capacity.

2 Table of Contents

3 Introduction

The search for environmentally sustainable solutions and the advancement of technology have been transforming many industry sectors, including the electrical energy sector. The most evident trend is the transition from traditional to renewable energy production, which entails the introduction of more and more Renewable Energy Sources (RES) into the electrical power system as sustainable alternatives to fossil fuel power plants. However, the introduction of RES into the power system is bringing new challenges for the system's reliable and stable operation.

One of the more prominent challenges is the regulation of grid frequency. As the power system cannot store electrical energy on a large scale, any discrepancies between power produced and consumed are continuously accumulated as kinetic energy in the system's spinning elements, increasing or decreasing their speed i.e. the system frequency. The amount of these spinning elements defines the inertia of the system, which can be regarded as the sensitivity of the system frequency to power imbalances. This mismatch between production and consumption traditionally originates from inaccurate load forecasts or reliability issues with different grid elements. With the introduction of intermittent RES such as wind and solar power, new mismatches occur originating from inaccurate RES production forecasts and their inherent unpredictability. The resulting imbalances in the electrical grid are becoming larger and more frequent. In addition, the inertia of the system is decreasing, as less rotating electrical machines are being connected directly to the system, and more through Power Electronic converters. These converters control the power flow to and from the system and thus do not inherently participate in the kinetic energy exchange when the frequency deviates. As a result, the system's sensitivity to the more frequent and larger power imbalances is also growing.

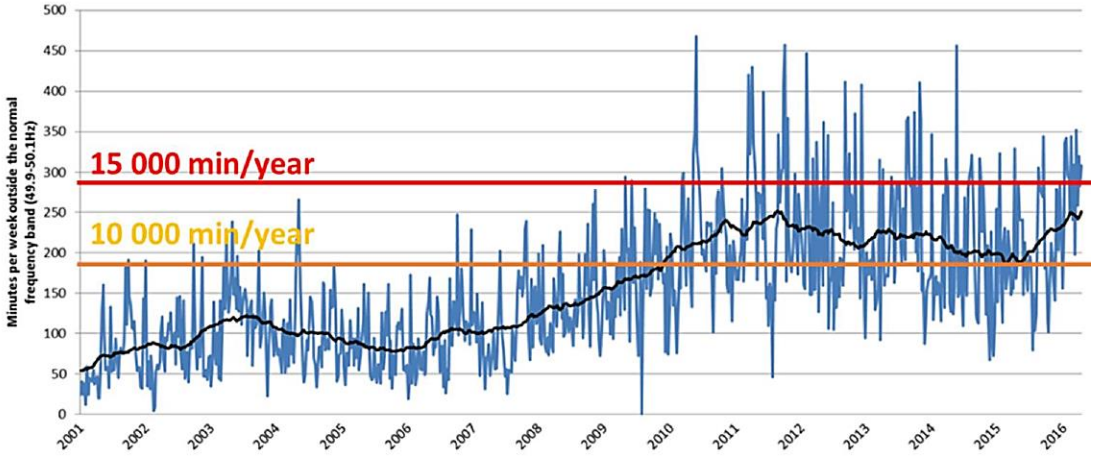

Figure 3.1. Evolution of frequency quality in the NPS 2001-2016 [1]

In the NPS, these negative effects on the functioning of the electrical grid are compounded in the quality of the frequency in the system. The amount of time the AC

system is operating outside the normal frequency band from 49,9 Hz to 50,1 Hz is displayed in Figure 3.1, with weekly values in blue and a floating average in black. This time is increasing and is over the goal of 10 000 minutes per year, set by Nordic Transmission System Operators (TSO) [1]. The most recent reports indicate a total of over 14 000 minutes outside the normal frequency band for 2016, and just under 12 000 minutes for 2017 [2], [3]. This declining power quality trend underlines the need to improve the way the frequency is regulated in the Nordic system. Furthermore, concerning behaviour of the system within the normal frequency band has been identified. Slow oscillations in the grid frequency with a period of 60 to 90 seconds, also called floating, are often present in the system with an amplitude which has been increasing in recent years [3].

The Nordic TSOs are the responsible parties for maintaining the real-time power balance and thus for keeping the system in the normal frequency band. These indicators of quality deterioration are what is motivating the TSOs to rethink and redesign the way frequency is regulated in the NPS. So far, this has resulted in the re-evaluation of frequency regulation products and requirements for their provision. The European Network of Transmission System Operators for Electricity (ENTSO-E) has went on to propose new technical requirements for delivering frequency regulation services in the Nordic countries [4]. Although not yet implemented, these requirements aim to stimulate the implementation of faster and more efficient regulations units, which are able to preserve the frequency quality in today's volatile electrical system.

3.1 Project Objective

Almost all frequency regulation capacity in the Nordic system is provided by hydropower plants (HPP). However, the majority of HPP units were designed and constructed before the 1990s, when the Nordic countries deregulated their electricity markets [5]. These units are therefore intended to operate in a system with slower and more predictable dynamics and their regulation systems are not envisioned to cope with such frequent and large frequency deviations. The control systems are calibrated only to meet current TSO provision requirements. With this, the speed and stability of HPP-provided frequency regulation is becoming an issue in today's power system [6].

Due to their high controllability and the required energy storage timespan, Battery Energy Storage Systems (BESS) are considered to be the best candidates to provide almost instantaneous frequency regulation power to the grid and help mitigate frequency deviations [7]. However, their limited energy capacity and power output pose important issues as they are closely linked to the BESS price. Additionally, due to the inflexible nature of frequency regulation, which does not guarantee a zero-mean reference signal, and its conversion efficiency, the unit needs to periodically purchase energy from the grid during operation in order to restore its state of charge (SoC) [8].

This Thesis project aims to explore the implementation of an innovative Hydro/Battery Hybrid System (HBHS) to participate in frequency regulation in the NPS. The idea is that a hybrid unit, composed of an HPP and a BESS, could adopt the strengths of both components when operating in frequency regulation mode whilst mitigating their individual weaknesses. In other words, the hybrid unit is expected to provide a faster and more efficient response to frequency deviations, due to the superior BESS dynamics, while retaining the high energy capacity and endurance of the HPP. Due to the lack of experience in the industry and no commercial availability of such hybrid systems, there is a need to investigate the design of the BESS aimed at this application and the influence of the HBHS specifications on system performance. The performance of the hybrid system toward the grid is defined by future provision requirements for frequency regulation, however, its internal operation, cost-effectiveness and the impact of a large-scale implementation of such systems on the NPS are not defined. Therefore, the objective of this Thesis is to explore the optimization of such a hybrid system in order to make it economically efficient and viable. The underlying research questions stemming from the project objective are:

1. What type of HPP can benefit the most from the installation of this hybrid system?
2. How should the HBHS operate internally when regulating the frequency?
3. What is the required power and energy capacity of the installed BESS?

3.2 Project Methodology and Scope

This Thesis is carried out in collaboration with Fortum, an energy company which owns and operates over a hundred HPPs in the Nordic countries. The work begins by introducing the current state-of-the-art frequency regulation services and their provision in the NPS. Following this, the theoretical concepts of power generation and varying the power output in hydropower plants and in BESS are introduced as background. Considerations regarding the first research question are given. As a result of a literature review and the introduction of theoretical concepts, the work in the project is limited to one frequency regulation product and one corresponding market i.e. Frequency Containment Reserves for Normal Operation (FCR-N) in Sweden.

A model of the HBHS is then created in MATLAB and Simulink, designed to deliver FCR-N, considering the relevant dynamic processes according to their timescale. The model is limited to frequency regulation, disregarding static HPP production and water levels, in order to simplify it and allow for easier understanding. The frequency dynamics of the NPS and all other units participating in frequency regulation are modelled as the environment in which the HBHS is to operate. Model parameters are taken from previous

research and empirical data, in order to represent the real unit response as accurately as possible. The resulting model is tested against full-scale measurements from Fortum HPPs.

With all the components modelled, two different architectures for the proposed HBHS are introduced and modelled accordingly. The HBHS units are tested for performance dynamics using established FCR-N provision tests for Sweden and operation in the NPS with historical frequency data. The resulting conclusions are aimed at answering the second research question. Next, the parameters of the proposed HBHS units are varied, in an attempt to maximise the cost-effectiveness of the unit. Conclusions are drawn for the performance improvements compared to the benchmark unit and between the two architectures themselves. In the end, a discussion about the sensitivity of the performed parameters optimization is given. The third research question is thus answered.

Finally, a different perspective of evaluating the performance of the HBHS units is taken. An analysis of the impact of a large-scale implementation on the frequency quality, of proposed hybrid units in the NPS, is done. The work is concluded with proposals for further development.

3.3 Previous Research

Intensified research around the performance of HPPs providing frequency regulation is present in the last ten years. The faster dynamics in today's power system raised the question of the increased interaction between the electrical, mechanical and hydraulic systems in a hydropower plant during transients. To this extent, modelling HPP dynamics is classified in three categories [9]: models focusing on the electrical perspective (usually done within small-signal stability studies), models reducing the electrical system to a swing equation (usually done when analysing mechanical transients and frequency responses), and new models coupling all three systems. The authors of [9] continue to give common ranges of different time constants which demonstrate this coupling. The influence of different parameters on the response performance of HPPs is addressed as well. The authors of [10] give an extensive study on the effects of the regulation control and water way modelling on the response time of the hydro unit. The development and classification of various HPP models for frequency regulation is given in [11], with the author continuing to give a list of recommendations for modelling FCR behaviour.

In addition to developing more accurate and detailed models, research has been done into improving and optimizing the performance of HPPs. The need for this performance improvement and its quantification for frequency control is described in [12]. Multiple approaches to this issue can be found in existing literature. A market approach is seen in [13], where three different performance-based remuneration schemes are proposed and modelled against governor control settings to identify the most stimulating solution. A

power system approach is presented in [14], where the authors propose a system of dispatch instructions and optimization constraints, which should ensure the quality and speed of the frequency response. In other works, a more unit-based approach is taken. In [11] the author discusses governor tuning and the introduction of filters among other possibilities. In [15] the governor is optimized to tackle a more specific issue – the occurrence of the 60-second frequency floating. The possibility of improving the HPP performance by adding another product, named fast FCR-N, is introduced in [16]. The fast FCR-N product can be seen as a general concept in which the HBHS can be classified.

The research around the dynamic behaviour of grid-connected BESS has been developing with regards to the application and the timescale of interest. For applications with a longer timeframe, such as providing frequency regulation, the state of the battery system becomes a priority over the stability and control considerations. Changes in the state of the BESS are simulated in order to evaluate the performance of the system from a functional and lifetime point-of-view. Much of the work is then aimed towards the design of the higher-level controller. Many studies are tackling the issue of necessary battery recharge when performing frequency control. In [8], the authors propose different SoC control strategies which should slow down battery degradation while remaining economically efficient. In [17] a historical frequency signal is used to obtain the minimum BESS size which complies with TSO requirements. A comprehensive study on the effects of different SoC controls on the lifetime of the battery system is presented in [18]. In general, the research trend gravitates towards employing different higher-level control algorithms and analysing their impact of the BESS state, through various ageing and degradation indicators for batteries, such as depth of discharge, cycling and charge or discharge current.

It can be concluded that most of the research in hydropower is addressing the HPP as a stand-alone unit acting towards the grid. A study of a combined, hybrid system is done in [16], but does not detail the type or characteristics of the storage unit. The research around battery systems performing frequency regulation again addresses stand-alone battery systems, employing one or more storage technologies, and envisions purchasing energy from the grid. A combination of battery and pumped hydro storage performing frequency regulation is tested in [19], built with similar intentions as combining two different BESS technologies. One study on a hybrid combination of a generation-based and storage-based unit is presented in [20], where a hydropower plant and a flywheel operation is coordinated to provide frequency regulation to the grid. Therefore, very little research is present on the topic of combining a generation-based and an energy-storage-based unit into one hybrid unit. Furthermore, the internal interaction between these two units during frequency regulation and their coordination has not been researched in detail. To the best of the author's knowledge, there is no study addressing the optimization of the storage unit size or control algorithm for the Hydro/Battery Hybrid System concept.

4 Background

4.1 The Nordic Power System

The NPS incorporates the national electrical grids of Finland, Norway, Sweden and Zealand (East Denmark) into one synchronous area. These national electrical transmission grids are connected via direct AC interconnections, resulting in the uniform spinning of all synchronous power generation in the area and thus in one AC grid frequency, with a nominal value of 50 Hz. The power system has been deregulated during the 1990s, allowing free trade of electricity between different actors and establishing a joint market shared by the Nordic and Baltic countries, except for Iceland. Today, electricity trading is done on multiple markets and in different timeframes, with most of the electricity traded on the Nord Pool day-ahead Spot Market. Bids for both electricity production and consumption are submitted by different market participants to the Spot Market for every hour of the following day, containing the offered energy production and consumption and a desired price. When the hourly Spot Market closes, a balance of total generation and consumption capacity is reached by a price cross, and the bids captured within this cross are accepted. To support the participants in maintaining this balance until activation, trading is also done at the Nord Pool intra-day market, where bids are submitted up to the delivery hour. This is an opportunity for the participants to anticipate and compensate for events such as incorrect weather forecasts or outages, or to make additional profits by restoring the power balance [21]. When the traded hour begins, the TSOs are tasked with maintaining the balance in their national control area in real-time. To this end, the TSOs have established a portfolio of frequency products in the Nordics to balance the active power in the grid.

4.1.1 Frequency Regulation Products

Traditionally, frequency regulation is divided into primary and secondary control. Primary control is the capability of the units to react to the sudden changes of frequency in the grid by changing their output power, in order to reduce the frequency deviation. The change in the output power of these units is directly proportional to that deviation and these units constitute what is regarded as the spinning reserve in the system. When an imbalance occurs, primary control is automatically activated and is active as long as the grid frequency is deviating from the nominal value. In order to make the used spinning reserves available for future grid events, the production from primary control is substituted by increasing production from secondary control. The task of secondary control units is to restore the frequency to its nominal value whilst unloading all the primary control units in the system. Secondary control can be activated automatically or manually from the dispatch centre [22]. More recent classifications refer to manually-activated secondary control as tertiary control, with the output power change occurring slowly and lasting for longer, again

acting in order to substitute the production from secondary control and thus make it available for future grid events. In the NPS, these frequency control processes are called Frequency Containment Reserves (FCR) and Frequency Restoration Reserves (FRR). The names of the different products rather accurately depict their role. Their specifications are given in Figure 4.1, as published by the Swedish TSO, Svenska kraftnät (SvK) [23].

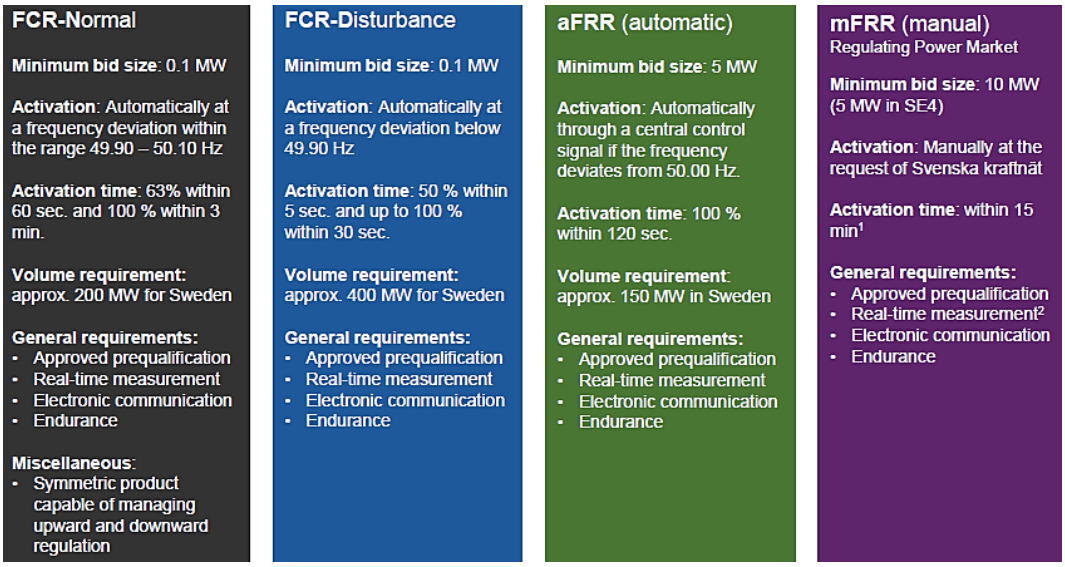

Figure 4.1. Frequency product specifications in Sweden [23]

Primary control is divided into FCR-N and FCR-D, with the former being active inside the normal frequency band of ±0,1 Hz. The volume of FCR-N procured every hour in the Nordic synchronous area is at least 600 MW. There is usually a larger amount since some TSOs procure more than is required [13]. FCR-D is sized according to the largest generation unit outage or major transmission line disconnection in the system, as it pertains to larger disturbances and is activated when the frequency falls below 49,9 Hz. Both products are triggered automatically by local frequency measurements in the units but have different activation times. Since FCR-D corresponds to more severe grid conditions, the activation time is 5 seconds for 50 % of regulation power, as opposed to 60 seconds for FCR-N. The secondary control automatic FRR (aFRR) product is required to respond to an automated central control signal with 100 % regulation power within 120 seconds. The manual FRR (mFRR) product responds to a manual signal (traditionally a telephone call) within 15 minutes. One should point out the relatively small volume of aFRR provision, which is due to the novelty of this product, first introduced in 2013. It is currently active only during periods with the largest power variations, i.e. morning and evening hours. However, its application throughout the whole day is planned due to the positive impact on the frequency quality it has displayed [11].

To date, there is no unified approach to the requirements for or provision of these frequency services in the Nordics, although initiatives for a Nordic-wide frequency

regulation system are present [24]. These differences impose the need to limit the work in this project to Sweden, as being the country of choice.

The Reserve Markets, where FCR-N and FCR-D capacity is purchased, are also organized differently in the Nordic countries. In Sweden, both FCR-N and FCR-D are traded twice for each delivery hour – two days ahead and one day ahead. By introducing these two different timeframes, Swedish Reserve Market participants are allowed to carry out more efficient hydropower production scheduling and to harmonize their trading activities between the Reserve Market and Spot Market [25]. In both timeframes, the participants submit one-hour bids detailing the available regulation power capacity and desired price. The only purchaser of regulation power in Sweden is SvK, which pays the bid price to selected regulation resources. In addition to the capacity, the providers are also compensated for the energy produced or consumed according to the hourly price of upward or downward regulation [26]. It should be pointed out that the regulation capacity is paid according to the bid specification and not according to production power measurements, which can present a discrepancy between actual unit performance and remuneration [6].

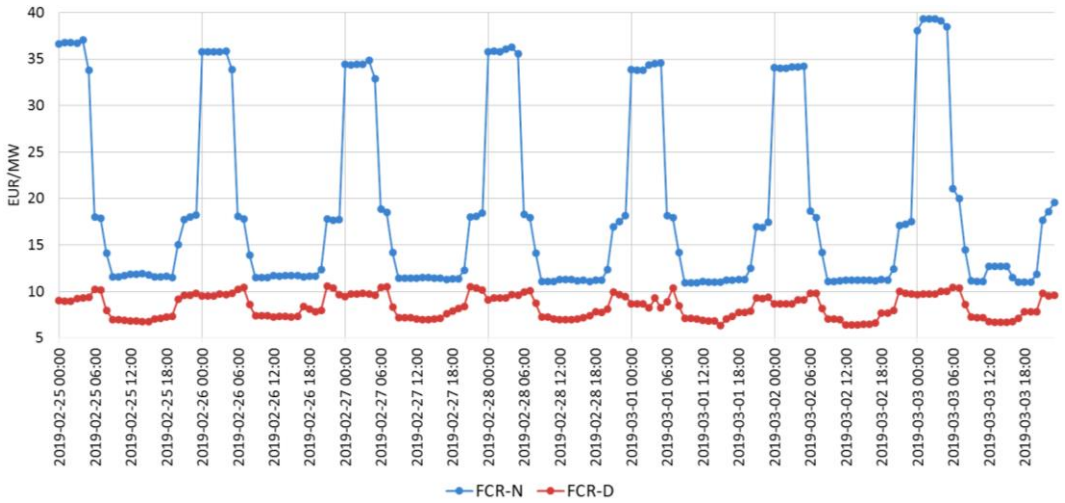

Figure 4.2. Hourly prices of FCR products in Sweden for a period of one week [27]

The hourly prices of these FCR products, as published by SvK, are displayed in Figure 4.2. As this is a pay-as-bid market, the values displayed represent the weighted averages for the hour while individual bids are confidential. Two important characteristics of the Reserve Market in Sweden can be identified from the price behaviour. Firstly, the price of FCR-D is considerably lower than the price of FCR-N. This is due to the less frequent use of the FCR-D product, which occurs only during larger outages, and the fact that capacity that is offered for FCR-D is usually available capacity in power plants already in operation [21]. Secondly, the day and night price oscillations are significant and uniform, especially for FCR-N, with the price increasing around three times during the night. This behaviour is very much linked to Spot Market trading activities and water value optimization.

During the day, the load in the grid is high and a large portion of HPPs are active, operating at maximum efficiency with the existing water constraints. A major portion of the FCR-N price comes from opportunity costs, i.e. water value and loss of efficiency of the units running frequency control [28]. Since the unit is already running and doing so at high efficiency during the day, these costs are minimal. During the night the load is lower and less HPPs are active. This in turn means that some regulation units have to be activated solely to perform frequency control, causing high opportunity costs, as this water could have been sold during daytime when the spot prices are higher, and high loss of efficiency since the unit will probably run at lower discharge, i.e. lower efficiency.

From this market analysis, it can be concluded that the FCR-N product has better market conditions for provision from the proposed HBHS. Furthermore, it is directly responsible for maintaining the system within the normal frequency band i.e. directly influences the frequency quality indicator chosen in this project. Due to its higher price and effect on frequency quality, FCR-N is taken as the frequency regulation product of choice for the HBHS. With the HBHS product and market identified, the influence of market dynamics is disregarded in further work, in order to limit its complexity.

4.1.2 FCR-N Prequalification Tests

In order to be able to participate in the Reserve Market, every generation unit must pass certain prequalification tests which are designed to verify its performance during a frequency deviation event. The results of these tests, together with other unit information, constitute an application for FCR-N or FCR-D provision which is submitted to SvK [29]. The technical information required in the application differs for generation-based and energy-storage-based units.

The testing procedure is prescribed in detail by SvK and includes instructions on how the tests should be conducted and what signals are to be recorded. The units are set up for testing by replacing the grid frequency measurement with an artificial frequency signal whose shape is outlined in Figure 4.3. The unit output remains connected to the grid and the following values are logged:

- Instantaneous active power [MW] and calculated available capacity [MW] of the unit, with a minimum sampling rate of 1 Hz,
- Measured grid frequency [Hz] and applied frequency signal [Hz], with a minimum sampling rate of 5 Hz,

for hydropower units:

- Turbine governor output signal,

- Guide vane opening and, for Kaplan units also the runner blade angle,
- Upstream and downstream water levels above sea level [m],

and for batteries:

- State of charge (SoC).

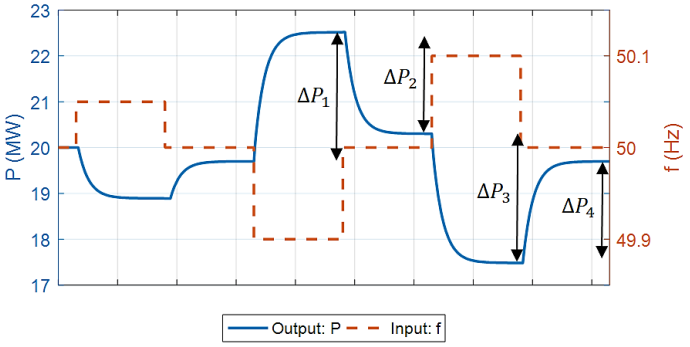

Figure 4.3. Example step response to a frequency signal of an FCR-N prequalification test [30]

Example results of a properly conducted prequalification test are also given in Figure 4.3. This test represents a step response test as the input frequency is changed instantly and kept at the new value until a steady state is reached. The periods when 49,9 Hz and 50,1 Hz are applied are required to last at least one hour, so that the endurance of the unit is tested. This represents a quantification of the energy storage limits which are problematic for stand-alone BESS used for frequency regulation. Namely, the unit must have at the very minimum the same amount of MWh as the MW they intend to sell to the market. This limit is practically higher because of the symmetrical requirements for FCR-N delivery. Another interesting point is the recognition of the HPP backlash effect in the testing procedure. The amount of power output attributed to backlash $2D$ is directly subtracted from the reported regulation capacity of the unit C_{FCR-N} i.e.

$$2D = \frac{(||\Delta P_1| - |\Delta P_2|| + ||\Delta P_3| - |\Delta P_4||)}{2} \tag{4.1}$$

$$C_{FCR-N} = \frac{(|\Delta P_1| + |\Delta P_3| - 2D)}{2} \tag{4.2}$$

using the measured HPP power output changes $\Delta P_1, \Delta P_2, \Delta P_3$ and ΔP_4 as displayed in Figure 4.3.

In recent years, the Nordic system TSOs have started the process of requirement and procurement harmonization for FCR products, with the aim of jointly mitigating frequency quality issues. The initial stage consisted of reaching common definitions of quality standards and frequency products, outlined in [1] in 2016. This work

continued to produce a draft of improved technical requirements for providing frequency regulation products in 2017, as reported in [24]. This draft introduces new dynamic and stability requirements for both FCR-N and FCR-D. Units providing FCR-N are to be subjected to a new dynamic response test outlined in Figure 4.4.

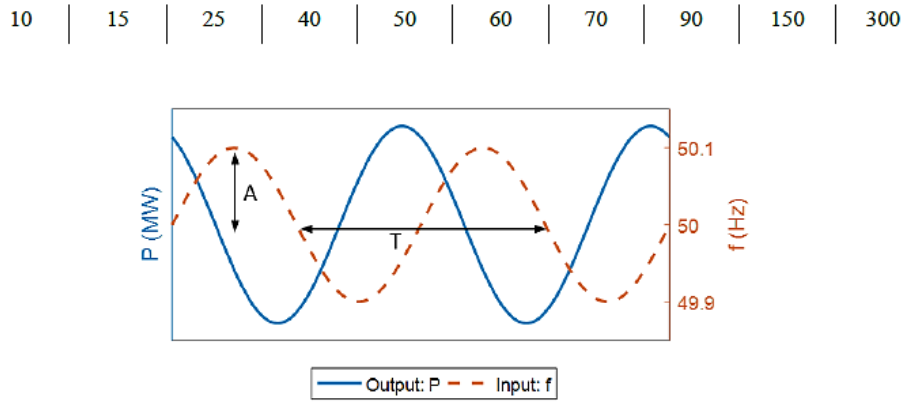

Figure 4.4. Example dynamic response to a frequency signal of proposed FCR-N dynamic test [24]

The aim of this dynamic response test would be to assess the stability and performance of the units with current grid conditions of fast and frequent frequency deviations. The new prequalification test for FCR-N would involve a setup identical to the step response test, but with the artificial frequency signal now sinusoidal with 10 different time periods varying from 10 to 300 seconds, as displayed in Figure 4.4. The output of the test are so-called FCR-N vectors which consist of the power output gain and phase at all listed sinusoidal frequencies. These vectors are then to be used in a stability assessment based on the Nyquist stability criterion, which is still being developed.

Although the new dynamic response test would theoretically aid the TSO in improving the frequency quality, since it is a more accurate study of the regulation unit behaviour compared to step response tests, an important issue is raised about the capability of the current units and their control systems to pass this FCR-N prequalification test [6]. Failure of current units to comply would have a strong negative impact on the price of FCR-N products, which the TSOs would have to compensate for. The proposed requirements are still in draft form to date.

4.2 Hydropower Plants

Hydropower today is the largest source of renewable electricity in the world, producing around 16 % of global electricity needs from over 1 200 GW of installed capacity, including pumped storage plants [31]. Perhaps more importantly, it is a source of renewable electricity that is providing substantial amounts of flexibility and inertia to the power systems. The large synchronous generators which are usually found in HPPs are directly connected to the grid and thus capable of exchanging kinetic energy with the system. During a

frequency deviation, the generators provide or absorb kinetic energy to the grid thus reducing the speed of frequency change, allowing the system to compensate for the power imbalance. Without this inertia, the larger and more frequent power imbalances in the NPS would lead to larger frequency oscillations, resulting in disconnection of generation units and load shedding. This will be demonstrated later. Also, the amount of power production in a hydropower plant can be regulated faster than in other traditional power plants, using the turbine governor. Because of this, hydropower is the dominant provider of production flexibility in power systems. Naturally, the flexibility is conditioned by the amount of water available to the turbine, however, the dynamics of natural water inflow are considerably slower and more predictable than other weather elements, and some types of HPPs have water reservoirs, in Sweden amounting to a storage capacity of around 33 TWh. These characteristics, together with the hydropower production optimization that is regularly used, reduce this water conditioning.

As hydropower technology is very mature and every unit is considered unique because of its placement and construction, a multitude of different hydropower plants can be identified. Two classifications are important for previous flexibility considerations and future work. The first is according to the type of the HPP, with three major types being:

- Run-of-river power plants,
- Reservoir power plants and
- Pumped storage power plants.

As the name suggests, the run-of-river (RoR) HPPs are built to run primarily of the natural river flow and are either constructed crossing the whole riverbed or partly with a diversion canal. These RoR plants do not have a water reservoir but can have a limited accumulation of water upstream built up by the dam or weir, in order to raise the water level or regulate the flow. Reservoir HPPs are built with a water reservoir upstream which can store water during a longer time period. Although from a flexibility point-of-view water reservoirs are beneficial, reservoir HPPs require a large amount of land and impact the local ecosystems, leading to social opposition, long permission processes and limited sites for their construction [32]. Pumped storage plants currently present 99 % of on-grid electricity storage worldwide, i.e. readily available generation, pumping water from a lower to an upper reservoir to store electric energy as gravitational potential energy. The water flows back down through turbines to release the electric energy on command [31].

The second classification is based on the type of turbine which is installed in the HPP. The four most dominant designs of turbines are:

- Pelton turbine,
- Francis turbine,
- Kaplan turbine and
- Bulb turbine.

The Pelton turbine is a representative of the impulse turbine type, which means that it uses the impulse i.e. kinetic energy of the water stream to spin the turbine runner and generator shaft. A powerful jet of water is directed into so-called buckets mounted around the wheel of the Pelton turbine runner, which is suspended in air and transfers the water energy into rotational force acting on the generator shaft. The flow of water can be regulated by adjusting the nozzle, indicated in green in Figure 4.5, to open or close the opening through which the water jet flows. This energy conversion process requires a relatively small but fast stream of water, which limits the application of the Pelton turbine to high heads (over 200 m) and lower flow rates (up to 10 000 litres per second) [32].

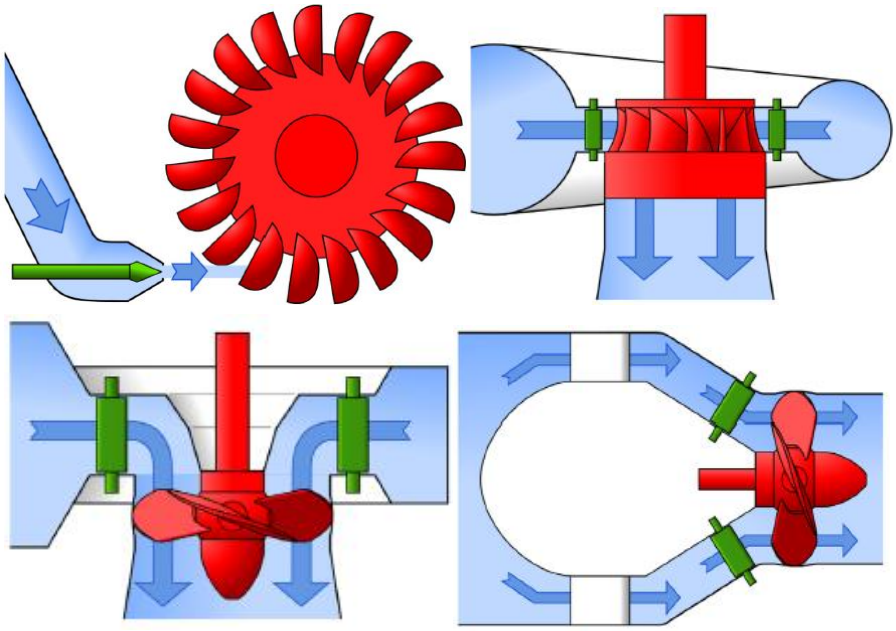

Figure 4.5. Side views of the Pelton (upper left), Francis (upper right), Kaplan (lower left) and bulb (lower right) turbines with indicated water flow [32]

The other turbine designs are representative of reaction turbines, which rely on a combination of impulse and pressure to extract energy from the water. Reaction turbines are placed in a casing and the entire water flow is directed through the casing, entering radially or axially to the shaft, flowing over the turbine runner blades and exiting along the axis. The use of water pressure allows reaction turbines to utilize lower heads,

down to a few meters and much higher flow rates, but also limits their use for very high heads.

The Francis turbine is the most common reaction turbine, suited for a wide range of heads (20 m – 400 m) and a wide range of flows, but delivering the best performance for heads between 100 m and 300 m. The flow of water is controlled at the entry into the casing by turning the guide vanes, indicated in green in Figure 4.5, while the turbine runner blades are fixed. The Francis turbine is also the turbine of choice for pumped hydro storage units, mostly due to the higher head (over 100 m) required for the unit's profitability. When moving to lower heads, the use of a Kaplan turbine is preferred. This is mostly thanks to its main difference to the Francis turbine – adjustable runner blades, indicated in red in Figure 4.5 which, through a combined operation with the guide vanes, allow the Kaplan turbine to utilize different flows to a higher efficiency. For very low heads of down to a few meters, Bulb turbines are preferred. They are essentially horizontally placed Kaplan turbines with the water flowing axially around the shaft before entering the runner [32].

Sweden is relatively flat, meaning that high heads which would suit Pelton turbines are very scarce, available only in the western mountain ridge. Therefore, basically all Swedish hydropower plants are equipped with reaction turbines, mostly Francis and Kaplan units. Considering the high utilization of hydropower resources in Sweden, most rivers have a cascade of HPPs operating on them. The upstream sections, closer to the mountains are dominated by Francis turbines and also the area where most storage power plants can be found. As the water moves downstream, lower heads are encountered and thus most of the HPP are of the RoR type with Kaplan turbines and in some cases Bulb turbines.

These trends have an important impact on the frequency regulation and the quality of the service. This impact stems from several factors. Firstly, thinking in terms of water value optimization, the more downstream the water flows, the less value it has, since it can pass through less hydropower plants, i.e. produce less. Secondly, RoR power plants have limited accumulation capacity, if any, and are sometimes required by law to maintain a certain minimum discharge because of environmental reasons, resulting in more running hours throughout the year. This combines to give a lower price for the regulation capacity of downstream Kaplan units than upstream Francis units. Since the Reserve Market is a financial market, this means that RoR plants with Kaplan units are providing most of the regulation power to the system and are the ones active during day and night [28]. This becomes relevant when it is noted that Kaplan units traditionally have slower and less stable responses to frequency deviations due to their cascaded regulation system of moving both guide vanes and runner blades. This becomes especially troubling when the new dynamic

prequalification test is considered, which is expected to be more challenging for most of the low-head Kaplan units to pass with current settings [6].

4.3 Battery Energy Storage Systems

The main difference between different large-scale energy storage technologies is the timescale in which they can efficiently store energy. Inductors and capacitors store energy on the seconds timescale, flywheels for several minutes up to hours, batteries for hours up to days while other technologies such as pumped storage hydro and compressed air can store energy on a seasonal timescale [33]. According to these and other characteristics, such as response speed and round-trip efficiency, different technologies have found different applications in the energy sector. The resent use of BESSs in the electricity grid is motivated by their mid-term storage timescale and very fast response time, enabling them to provide continuous support to the grid in terms of fulfilling load demands, frequency regulation and alleviating transmission congestion issues [34]. With regards to this, the provision of primary frequency control has been identified as the highest value application for the BESS in the grid [7].

A BESS converts electrical energy into potential chemical energy while charging and vice versa while discharging. The battery cell is the device that provides the conditions for this conversion to happen through reduction and oxidation (redox) chemical reactions. The external contact points, i.e. electrical connections of a battery cell, are its electrodes which have a certain DC voltage between them when energy is stored in the battery cell. The cell possesses an internal resistance which generates a voltage drop during power exchange and thus defines the battery efficiency. The ratio between the electrical energy inserted into the cell and the electrical energy that can then be extracted is called the round-trip efficiency and constitutes an important battery parameter. The energy capacity of a battery is defined as the usable energy at a certain discharge rate. For grid applications, the commonly used unit for energy is Wh, which is equal to 3 600 J and is usually complemented with the battery C rate, which denotes the ratio between the battery output power and energy capacity. The state of charge (SoC) is defined as the ratio between the remaining and the rated energy storage capacity.

The desire to maximize the specific energy capacity, i.e. energy to weight ratio of the battery, led to the development of several battery technologies, differing in electrochemical design. These differences are translated to different operational temperatures, response times and cyclability, which are all very important parameters for battery operation. The different battery technologies which are considered good candidates for grid applications, and thus for the HBHS, are described and compared qualitatively in [33] and [34].

The oldest, lead-acid battery technology is still widely used because of its low cost compared to other technologies. It also has a relatively high efficiency if a low depth of discharge is employed and the SoC is controlled properly. However, it possesses the poorest cycle life and operating temperature as well as low energy and power densities. sodium-sulphur (NaS) technology is regarded as one of the most promising technologies for high-power applications, due to the cell's high specific power and high efficiency. NaS also exhibits low costs, comparable to lead-acid batteries, and low maintenance requirements. This is still a very young technology which implies the need for further research to overcome existing problems with implementation. A more relevant concern for the HBHS is the fact that sodium reacts violently with water, which might result in reliability issues. Lithium-ion (Li-ion) batteries are probably the most popular technology today and are viewed as promising for a wide range of applications. They have a high energy density thanks to the high cell voltage and low weight of lithium and are relatively robust. In addition, they are capable of fast charging and discharging with a high round-trip efficiency. The drawbacks of the lithium-ion technology are narrow voltage and temperature operation ranges, which highlight a need for protection circuits, and the higher capital cost than lead-acid and NaS technologies, caused by the limited supply of the metal lithium. In addition to the previously described conventional battery technologies, there is a family of so-called flow batteries which are characterized by the electrolyte flowing from storage tanks to the cells and back during operation cycles. The energy capacity of flow batteries is proportional to the volume of electrolyte in the system, making them easily scalable. Additionally, they can be fully discharged without any damage, giving better cyclability than conventional batteries. Although their cost is comparable to NaS, the specific energy of flow batteries is low, and the technology is still very young.

Due to its high efficiency and cyclability, the Li-ion battery technology is chosen for the HBHS. This choice is affirmed by current conditions in the market, where Li-ion batteries dominate such high-power, high-energy grid applications. The maturity of the technology and their high energy density are also expected to incur less construction work and lower maintenance costs.

A standard battery cell voltage is in the range of several volts, which means that for high power grid applications the cells need to be stacked. These stacked battery modules can contain cells connected in series in order to increase the output voltage and connected in parallel in order to increase the output current. The operation of individual cells or stacks of cells inside the battery module is governed by a Battery Management System (BMS) which regulates their voltage and temperature by controlling the power electronic devices during charge and discharge cycles.

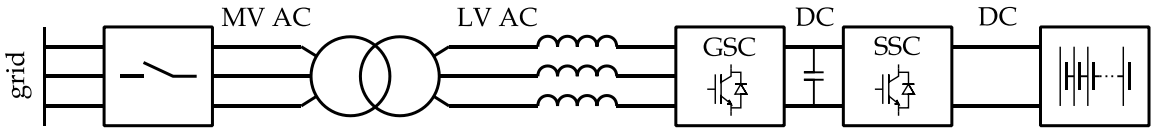

Figure 4.6. An example of a BESS with its connection to the grid

When the battery module is stacked up to the desired power output, which for grid applications can reach the MW range, its external connections are connected to an inverter tasked with transforming the DC battery output to a grid-synchronized AC output. This output is then usually connected to the grid via a transformer to step-up the voltage level and additional filters, if needed. An example of such a topology can be seen in Figure 4.6. The inverter is composed of two power electronic converters which perform different functions. The battery unit is directly connected to a DC-DC converter called the storage-side converter (SSC) which is managing the state and charge of the battery unit based on an active power or SoC regulation command coming from a higher-level controller. The other side of the SSC is connected to a DC-AC converter called the grid-side converter (GSC) through a DC link. The GSC is synchronized to the grid voltage in order to be able to exchange active and reactive power. The standard command for the reactive power import and export to the GSC comes from a higher-level controller while the command for the active power comes from the DC link voltage regulation [33].

The previous description shows the elements and processes of a grid-connected BESS. It can be summarized that, after a higher-level command signal is received, the output is changed by manipulating the power electronic devices and that all parameters influencing the response of the BESS are of an electrical or chemical nature, making the response very fast and efficient. Exactly this characteristic is motivating the combination of a BESS and an HPP in a hybrid system.

5 Modelling

A model of the proposed hybrid system is built in MATLAB and Simulink, as a platform for testing and evaluating the dynamic behaviour of different HBHS specifications and control algorithms. The model is designed to simulate the power output response of such a system to a frequency deviation event i.e. capture the dynamics of the HBHS performing primary frequency regulation. Based on this, it can be said that the model input is the grid frequency change while the model output is the HBHS power output change. This further means that the hourly scheduled production, as a result of the Spot Market trading, is excluded from the model. Frequency regulation dynamics can be modelled using two approaches:

- Assuming the unit does not influence the system frequency, which implies an open-loop regulation system where the frequency is a predefined signal and
- Assuming that the unit regulates the frequency, which implies a closed-loop system in which all regulation units are represented, and their output is fed into a power system model which outputs the grid frequency.

The former approach is taken when observing the open-loop response of the system and is used during the testing procedure for FCR-N provision. The latter is superior in terms of evaluating and optimizing system performance, since it reproduces real operating conditions, and will thus be used for this purpose.

5.1 Nordic Power System Model

First, the environment in which the HBHS is to operate – the NPS – is modelled. For a change in frequency to occur, an imbalance between the power produced and consumed must exist. The reaction of the power system to this imbalance i.e. the frequency change, is described by two phenomena: system inertia and damping. System inertia refers to the stored kinetic energy in the system's rotating elements and can be introduced using a swing equation of a single machine indexed with i as

$$J_i \omega_i \frac{d\omega_i}{dt} = P_{mech_i} - P_{el_i} = \Delta P_i \tag{5.1}$$

From the expression, the moment of inertia of the machine J_i defines the rate of speed change when there is an imbalance between the mechanical power fed into the machine and the electrical power extracted from it. The moment of inertia also defines the machine's stored kinetic energy while rotating at the speed ω_s to be

$$E_{kin_i} = \frac{1}{2} J_i \omega_s^2 \tag{5.2}$$

Substituting the kinetic energy into the swing equation and acknowledging that all rotating elements in a synchronous AC grid are rotating at the same speed ω_g, which is the grid frequency, these expressions can be generalized to the all rotating elements in the grid as

$$2 \frac{E_{kin}}{\omega_s} \frac{\omega_g}{\omega_s} \frac{d\omega_g}{dt} = P_{prod} - P_{cons} \tag{5.3}$$

where

$$E_{kin} = \sum_i E_{kin_i}, \qquad P_{prod} = \sum_i P_{mech_i}, \qquad P_{cons} = \sum_i P_{el_i} \tag{5.4}$$

Adopting ω_s to be the synchronous speed corresponding to the nominal frequency of 50 Hz, the ratio between the grid frequency ω_g and the synchronous speed can be disregarded as these two speed are always of similar value, giving the final expression to be

$$M \frac{d\omega_g}{dt} = P_{prod} - P_{cons}, \qquad M = 2 \frac{E_{kin}}{\omega_s} \tag{5.5}$$

where M is used to denote the total system inertia.

The damping D of the system depicts the presence of loads in the grid whose power is proportional to the grid frequency, so-called frequency-dependent loads. These loads help stabilize the system by reducing their consumption when the frequency decreases and vice versa. The system damping is a measure of this reduction defined as the change in power consumption for a change in frequency f i.e.

$$D = \frac{\Delta P_{cons}}{\Delta f} \tag{5.6}$$

There are multiple hydropower units which provide FCR-N, all contributing to the total system regulation gain R_{FCR-N} defined as the amount of power production change in the system for a change in frequency i.e.

$$R_{FCR-N} = \frac{\Delta P_{prod}}{\Delta f} \tag{5.7}$$

The fact that multiple units are providing FCR-N in unison, requires the total gain to be scaled down to a power plant level. This is accomplished by the so-called HPP droop

constant which acts as the static gain for a single unit. This droop constant in the Nordics is traditionally called the Ep setting and is inversely proportional to the gain, i.e.

$$E_{p_i} = \frac{\Delta f}{\Delta P_{mech_i}} \tag{5.8}$$

The introduced parameters of the NPS were measured during full-scale experiments in 2016 [35]. These experiments were performed by creating an artificial power disturbance through a large fleet of HPPs in the north of Sweden and measuring the grid frequency and power flow along major connections between Sweden, Finland and Norway, giving separate parameters for the three grid sections. The experiment was performed on two occasions: during the day and during the night to capture the variability of the parameters. The amounts of kinetic energy and frequency-dependent loads in the system are around 20 % lower during the night. This decrease is explained by lower power production and consumption during the night, which translates into fewer units being active. The amount of FCR-N capacity purchased remains the same however, supporting the explanation behind higher prices of FCR-N during the night, seen in Figure 4.2.

Table 5.1. Nordic Power System experimental measurements from 2016 [35]

Parameter	Symbol	Time	Sweden	Norway	Finland	Total
Kinetic energy of rotating elements [MWs]	E_{kin}	day night	112 605 92 152	81 177 60 152	48 187 42 520	241 969 194 824
Frequency dependent load [MW/Hz]	D	day night	246 204	184 136	87 76	517 416
Activated FCR-N gain [MW/Hz]	R_{FCR-N}	day night	2 500 2 500	4 230 4 230	800 800	7 530 7 530

Enough information is obtained to represent the Nordic system with a three-area model i.e. with three separate inertia and damping constants. However, since there is no automatic control of inter-area oscillations, which also occur at a higher frequency than frequency regulation, a one-area dynamic model is used [35]. Therefore, the power system is represented by its total inertia and damping, as denoted in Table 5.1. As it is assumed there are no interactions between different HPPs performing FCR-N, the entire regulation capacity can be accumulated into one lumped HPP, having the total gain R_{FCR-N} i.e. the total droop E_p.

At this point, it is prudent to introduce a per-unit system which will be used throughout the Thesis. A per-unit system consists of unique definitions of base values for system variables. Several per-unit systems, commonly used for frequency regulation, are defined in [4], differing in the base power value. As the model will contain the total Nordic system gain, the base power is scaled according to it. Considering that the droop constant used by most HPPs in the Nordics is the so-called Ep0 setting, the defined base power

should preserve this value when delivering total system gain. The nominal frequency is taken as the base and so is the full opening of the turbine guide vanes, with position denoted by Y.

$$Y_{base} = 1\,pu, \qquad f_{base} = 50\,Hz, \qquad P_{base} = R_{FCR-N} E_{p0} f_{base} = 37650\,MW \tag{5.9}$$

Now, the final model parameters in per-unit can be calculated. For a one-area model, the total inertia of the system is obtained by summing up the kinetic energy in all three areas and taking the average of the day and night values. The same is done for the damping constant.

$$M = 2 \sum_{j=1,2,3} \frac{E_{kin_{j,day}} + E_{kin_{j,night}}}{2P_{base}}, \qquad D = \sum_{j=1,2,3} \frac{D_{j,day} + D_{j,night}}{2} \frac{f_{base}}{P_{base}} \tag{5.10}$$

The final power system model in the Laplace domain is finally obtained from the expression in (5.5) by acknowledging the frequency-dependent loads.

$$\Delta f(s) = \frac{1}{Ms + D} \Delta P(s) \tag{5.11}$$

5.2 Lumped HPP Model

All hydropower units providing FCR-N react to a frequency deviation by changing their active power output according to (5.8). If the frequency decreases, the power output increases and vice versa. As was introduced, the entire FCR-N capacity in the Nordics will be modelled with one lumped HPP. The dynamic process of increasing the power output involves the electrical, mechanical and hydraulic subsystems of the unit. From the time constants of these subsystems estimated in [9], it is assumed that the electrical subsystem, containing the generator, is an order of magnitude faster. Therefore, it is reduced to the swing equation already included in the power system model in (5.11). The HPP model is thus composed of the governor control system and mechanical and hydraulic subsystems.

The standard governor control system employed in Sweden is a PI controller with droop. The droop constant defines the control loop static gain while the PI controller ensures there is no steady-state control error. The closed-loop controller can have two feedback variables: guide vane position or HPP power output. The position feedback is common practice in Swedish HPPs, as it is regarded to have better stability margins and is therefore used in the model [6]. In the chosen per-unit system, the droop constant has the same value for both feedbacks i.e.

$$E_p = \frac{\Delta f}{\Delta P_{prod}} = \frac{\Delta f}{\Delta Y} \tag{5.12}$$

To generate the control error signal e_f, the grid frequency is measured locally, subtracted from the reference and then compared to the measured and drooped position feedback i.e.

$$e_f(s) = f_{ref} - f_{meas}(s) - E_p \Delta Y_{meas}(s) = \Delta f(s) - E_p \Delta Y_{meas}(s) \tag{5.13}$$

From the error calculation, it can be concluded that the control mechanism is in steady state if the measured frequency is equal to the reference or if the position change is proportional to the frequency deviation. This error signal is first filtered by a low-pass filter with the time constant T_{meas} to suppress measurement noise. Then, it is forwarded to the PI control law which calculates the guide vane position reference in the Laplace domain as

$$\Delta Y_{ref}(s) = \left(K_p + \frac{K_i}{s}\right)\frac{1}{T_{measf}s + 1} e_f(s) \tag{5.14}$$

As the FCR-N service is delivered only inside the normal frequency band while the frequency can also assume values outside, the controller output needs to be limited to the FCR-N dedicated volume and capacity. This is also necessary for safe HPP operation and water value optimization as the limits for FCR-N capacity are set by several different factors and used in HPP operation planning. The limit is defined using the normal frequency band in (5.12) as

$$\Delta Y_{max} = \frac{\Delta f_{max}}{E_p}, \qquad \Delta f_{max} = \frac{0{,}1\ Hz}{f_{base}} \tag{5.15}$$

This gives the final controller output expression below.

$$\Delta Y_{ref}(s) = \begin{cases} \left(K_p + \frac{K_i}{s}\right)\frac{1}{T_{meas}s + 1} e_f(s)\,, & |\Delta f| \le \Delta f_{max} \\ \pm \Delta Y_{max}\,, & |\Delta f| > \Delta f_{max} \end{cases} \tag{5.16}$$

The guide vane servo mechanism acts based on the controller reference and mechanically moves the guide vanes into the position ΔY_{ref}. The dynamic behaviour of this servo system is modelled based on full-scale test results, from three HPPs in Sweden [36]. The tests identified the dynamic behaviour of the servo as a first-order lag with the time constant T_y and with a time delay of T_{del_y} i.e.

$$\Delta Y_{meas}(s) = \frac{1}{T_y s + 1} e^{-sTdel_y} \Delta Y_{ref}(s) \tag{5.17}$$

A ramp rate limitation is also put on the guide vanes movement to limit their maximum speed, replicating actual system limitations [37].

While the governor system of a Francis turbine regulates only the guide vane position, the system of a Kaplan turbine regulates the runner blade angle as well. This added mechanism needs to be included in a Kaplan governor servo model. A secondary servo, which adapts the runner blade angle according to the measured guide vane position, is added. This is the most common control loop cascade, however, some Kaplan units have guide vane servos which adapt their position according to the runner blade angle. The runner blade servo model is built from the same elements as the guide vane servo: a first-order lag with the time constant T_a, a time delay of T_{del_a} and a ramp rate limitation with the full-opening time limit being T_{lim_a}.

$$\Delta A_{meas}(s) = \frac{1}{T_a s + 1} e^{-sTdel_a} \Delta Y_{meas}(s) \tag{5.18}$$

The governor control and mechanical subsystem models for both turbines are complete now, giving the measured guide vane and runner blade position as an output.

As was mentioned, the vast majority of HPPs in Sweden use the so-called Ep settings for the tuning of their governor systems. These settings were created and adopted by the largest HPP owners and are designed to satisfy the dynamic requirements put forth by the TSO for frequency provision. Four sets of standard settings exist, defining the PI controller gains and droop constant as listed in Table 5.2. The most common HPP governor setting is Ep0, followed by Ep1 [35]. The other two settings are not common, although a general trend is to move towards higher Ep settings to decrease the influence of the backlash effect, which will be discussed later.

Table 5.2. Standard governor Ep settings [36]

Parameter	Symbol	Ep0	Ep1	Ep2	Ep3
Controller proportional gain [pu]	K_p	1	1	1	2
Controller integral gain [pu/s]	K_i	1/6	5/12	5/6	5/6
Droop constant [pu/pu]	E_p	0.1	0.04	0.02	0.01
Controller limit [pu]	$\Delta Y_{max} = \frac{\Delta f_{max}}{E_p}$	0.02	0.05	0.10	0.20
Controller time constant [s]	$T_{gov} = \frac{1}{K_i E_p}$	60	60	60	120

As can be seen from the controller limit and time constant, different settings give a different static gain to the HPP while satisfying TSO speed requirements. In other words, a higher Ep setting gives a higher ratio of regulation to static power, with the maximum guide vane

movement for FCR-N ranging from 2 % to 20 %. Therefore, increasing the settings would reduce the number of HPPs needed to reach R_{FCR-N} but might also bring about other issues such as water level management and turbine mechanics. To replicate the majority of HPPs in Sweden, the Ep0 setting is chosen for the model. Other model parameters are taken from standard value ranges in literature and are listed in Table 5.3.

Table 5.3. Governor and servo model parameters

Parameter	Symbol	Value
Controller proportional gain [pu]	K_p	1
Controller integral gain [pu/s]	K_i	1/6
Droop constant [pu/pu]	E_p	0.1
Frequency measurement filter time constant [s]	T_{measf}	2
Guide vane servo lag time constant [s]	T_y	0,2
Guide vane servo time delay [s]	T_{del_y}	0,3
Guide vane time limit for full opening [s]	T_{lim_y}	10
Runner servo lag time constant [s]	T_a	1
Runner servo time delay [s]	T_{del_a}	0,5
Runner time limit for full opening [s]	T_{lim_a}	30

With the servo model completed, it is time to address the backlash effect that occurs in hydropower turbines. Namely, it was concluded from practical tests that there is empty movement of the regulation mechanism resulting in an offset between the mechanism's physical position and the one given and measured by governor control. This effect pertains to guide vanes and extends to Kaplan runner blades with an even higher amplitude. The empty movement can be described as a hysteresis floating around the current guide vane position and is called backlash. This means that the physical movement is always offset by the width of the hysteresis compared to its desired position. The effect is demonstrated in Figure 5.1 with a backlash hysteresis width of 1 pu applied to a 5 pu amplitude sinusoidal signal. The backlash effect is applied to both the measured guide vane position ΔY_{meas} and measured runner blade angle ΔA_{meas}. With backlash included, the physical positions of these two regulation elements ΔY_{pos} and ΔA_{pos} are obtained and only the hydraulic subsystem remains.

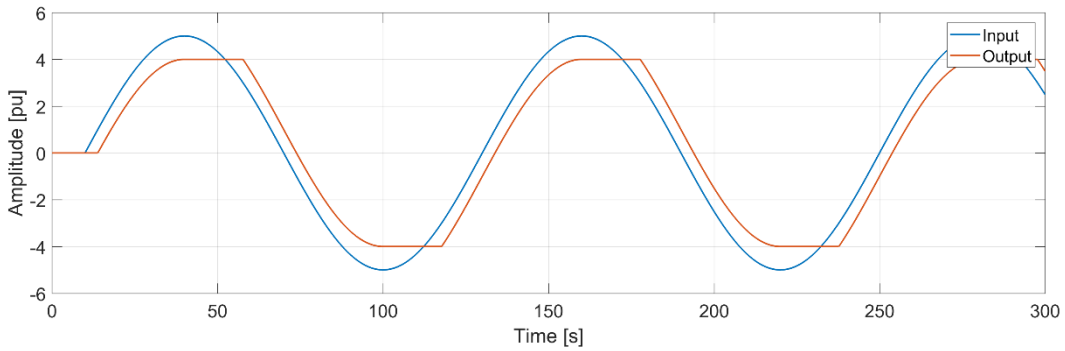

Figure 5.1. Demonstration of the backlash effect

Now, the water dynamics of the HPP can be introduced, as the water flow through the turbine is proportional to its mechanical power output. This proportionality is known as the HPP efficiency curve and displays an increase in efficiency with the increase of water flow up to around 70-80 % guide vane opening for Francis turbines. After this maximum, the efficiency decreases steadily. Since the hourly HPP production is not modelled, this efficiency curve is disregarded, and a single scaling factor is used.

$$K_{pow} = \frac{\Delta P_{mech}(s)}{\Delta Y_{pos}(s)} \tag{5.19}$$

This single scaling factor is used for Francis turbines since the guide vane position is the only regulated variable. For a Kaplan turbine, the power output depends on the runner blade position as well, which is regulated according to the guide vane position as in (5.18). In practice, this is done using look-up tables which contain the vane-to-runner combinations with the highest efficiency. In order to model the fact that this combination produces the desired power output, the scaling factor from guide vane opening to mechanical power is split into two contribution factors K_y and K_a, for guide vanes and runner blades respectively. The sum of these factors must be equal to the total Francis turbine scaling factor K_{pow} to ensure coherency of the two turbine models.

Finally, the water dynamics are introduced in order to obtain the output mechanical power. The model is built with the base assumption for reactive turbines that the power is exerted on the turbine through water pressure and velocity and is derived using fluid dynamics [38]. The result is a non-minimum phase first-order model with a water time constant T_w. This behaviour stems from the fact that, upon opening the guide vanes for example, the water pressure on the turbine drops until the higher volume of water accelerates back to its steady-state velocity. The non-minimum phase represents the power drop caused by the lower pressure while T_w denotes the time needed for the water to reach steady-state velocity. The hydraulic models for a Francis and a Kaplan turbine are given in (5.20) and (5.21) respectively.

$$\Delta P_{prod}(s) = K_{pow}\frac{-T_w s + 1}{0.5T_w s + 1}\Delta Y_{pos}(s) \tag{5.20}$$

$$\Delta P_{prod}(s) = \frac{-T_w s + 1}{0.5T_w s + 1}\left[K_y \Delta Y_{pos}(s) + K_a \Delta A_{pos}(s)\right] \tag{5.21}$$

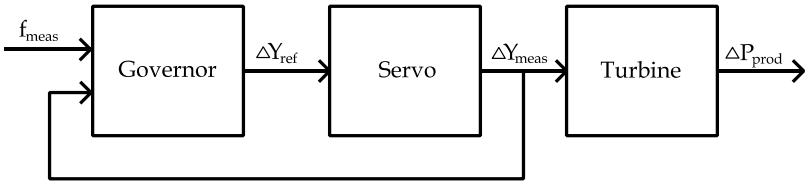

Figure 5.2 Lumped HPP complete model

The introduction of turbine hydraulics completes the lumped HPP model, with its final structure displayed in Figure 5.2. The introduced model parameters are taken from standard value ranges and listed in Table 5.4, thus completing the lumped HPP model.

Table 5.4. Turbine model parameters

Parameter	Symbol	Value
Guide vane backlash [%]	Bl_y	0,1
Runner blade backlash [%]	Bl_a	0,2
Francis power scaling factor [pu/pu]	K_{pow}	1
Kaplan guide vane contribution factor [pu/pu]	K_y	0,3
Runner blade angle contribution factor [pu/pu]	K_a	0,7
Water time constant [s]	T_w	1,5

5.3 Nordic Power System Test

With the NPS and all the HPP units participating in FCR-N included in the model, the system dynamics can be tested with a simple consumption power step acting as a disturbance. The disturbance step is sized according to the FCR-N gain of the system in order to produce a frequency deviation of 0,1 Hz i.e.

$$\Delta P_{cons} = R_{FCR-N}\Delta f = 753\ MW \tag{5.22}$$

It should be noted that, since there is no FCR-D in the system, the total regulation power is limited to the 753 MW of FCR-N. Therefore, the regulation limit ΔY_{max} is removed for this test in order to observe the linear dynamics of the system, which are easier to interpret and a more realistic response.

In Figure 5.3, the consumption power increase can be seen, followed by the FCR-N units' reaction. When the disturbance occurs, the frequency drops to almost 49,5 Hz, which is the instantaneous frequency deviation. The regulation power sharply increases

during this drop and stops it when the produced power is equal to the disturbance. Following this the frequency increases while the produced power is higher, finally returning the frequency inside the normal band, settling at just over 49,9 Hz. The direct connection between the power imbalance and frequency behaviour is easily observed during this test.

Two important observations can be made about the steady state after the disturbance. Firstly, it is reached around 200 s of simulation time, corresponding to the FCR-N requirement of 180 s for full deployment. Secondly, the steady-state value is close to the expected 49,9 Hz. The reason for it not being exactly 49,9 Hz as calculated, can be extracted from regulation power ΔP_{prod} in steady state. Namely, the system damping reduced the power disturbance i.e. the frequency-dependent loads reduced their consumption since the frequency decreased, resulting in less than 753 MW of FCR-N activated and thus a higher frequency.

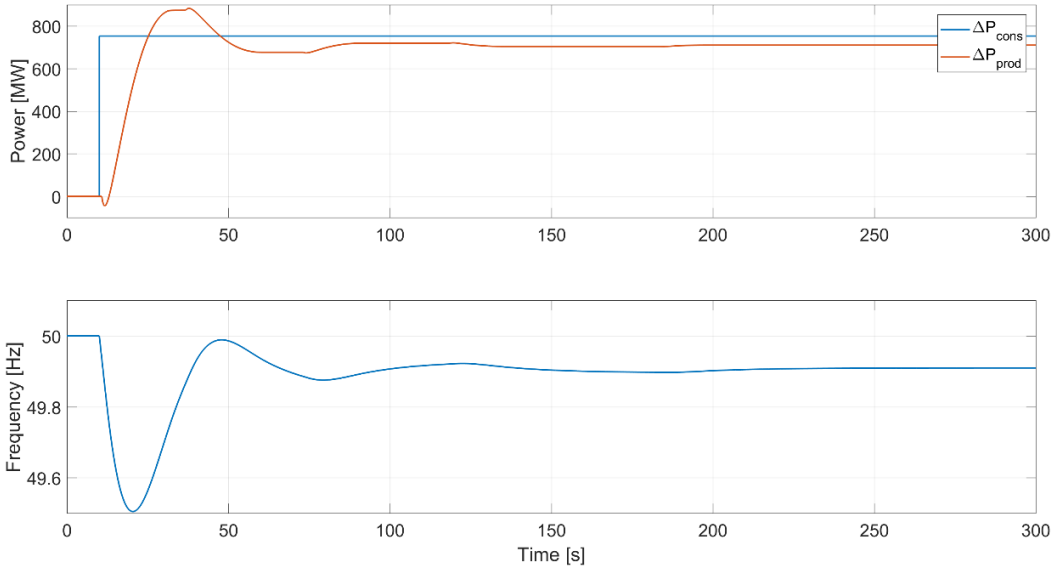

Figure 5.3. Nordic Power System dynamics test

Based on these results, the test is deemed successful and the power system and lumped hydropower models are validated.

5.4 Historical Power Disturbance Model

The previous test revealed an issue when the system is operating under the assumption that the FCR-N units are regulating the grid frequency. Namely, in order to provoke a reaction of the regulation mechanism, a consumption and production imbalance needs to be introduced to the model in the form of a power disturbance. This power imbalance is never measured during grid operation since the frequency signal is more accessible and uniform for the entire system. This means that the information about the operating conditions of the NPS exists in the form of a historical frequency measurement

signal, which needs to be translated into a power disturbance signal to replicate these realistic operating conditions in the modelled environment.

Detailed historical grid frequency data from the power system is made available by the Finnish TSO Fingrid [39]. The frequency measurements are performed at several 400 kV substations with a 10 Hz sampling rate. For the purposes of replicating realistic operating conditions for the HBHS, measurements from May 2018 to April 2019 are used. The quality of the frequency during each of these 12 months is displayed in Figure 5.4, listing the number of minutes spent outside the normal frequency band. The average for this one-year time period is 1 097 minutes per month, corresponding to 13 161 during the whole year. Since months differ in the number of days, these values can also be normalized to a period of 30 days, as displayed in Figure 5.4.

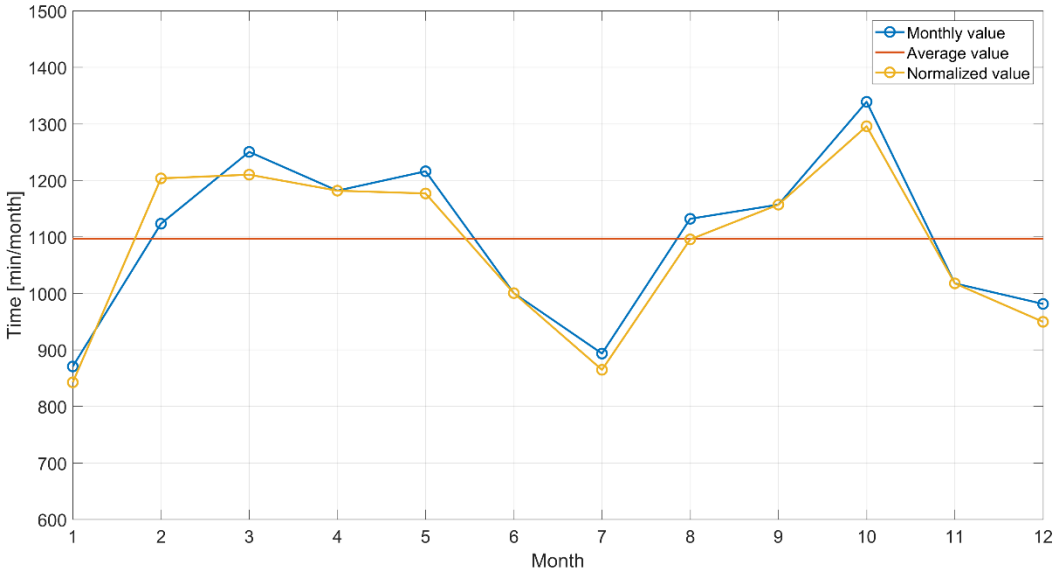

Figure 5.4. Frequency quality in the NPS for the previous 12 months

It can be concluded that the frequency quality is better during summer and winter. During the spring and autumn, the quality deteriorates significantly. Furthermore, the frequency conditions during 30 days of August 2018 and 28 days of February 2019 are the closest to the yearly average. Based on this, the month of August 2018 is regarded as a representative frequency data sample. However, it should be noted that this is not the only parameter for evaluating grid frequency quality, meaning that there might not be a direct dependency between the time spent outside the normal band and the amount of action which is provided by FCR-N units.

To generate the power disturbance signal from the frequency, the reactions of the NPS and FCR-N units to a frequency deviation need to be inverted. As was shown in the Figure 5.3, the frequency deviation that results from a disturbance is defined by the system inertia and damping and the action of the units providing FCR-N. Therefore, by reversing the effects of these elements, the power disturbance that leads to the

corresponding frequency deviation can be reconstructed. The effect of the lumped HPP is simply inversed by introducing the historical frequency signal to the HPP model, which outputs the corresponding FCR-N power. The effect of the power system is inversed by obtaining the inverse transfer function of the power system model from (5.11). This gives

$$\Delta P_{hist}(s) = \frac{Ms + D}{T_{ff}s + 1}\Delta f_{hist}(s) + \Delta P_{prod}(s) \tag{5.23}$$

where ΔP_{hist} denotes the obtained historical power disturbance, Δf_{hist} the historical frequency data and ΔP_{prod} the output of the lumped HPP when Δf_{hist} is fed to its regulation mechanism. A low-pass filter with the time constant T_{ff} is added in order to limit the pure derivative action of the inverse grid model.

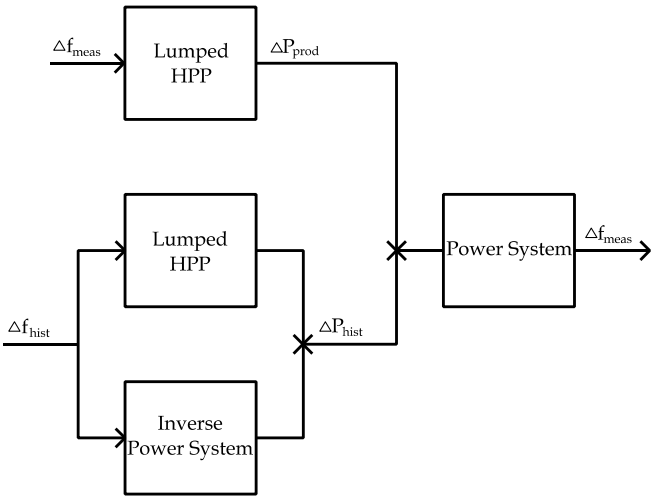

Figure 5.5. Historical power disturbance test model

With all other parameters set, the power disturbance generation is tested against the filter time constant. The historical measured frequency data is compared to the simulated frequency i.e. the output of the power system model with the lumped HPP when ΔP_{hist} is introduced as the power disturbance. The aim is to obtain the historical values of grid frequency from the model simulation, displayed in Figure 5.5. The lumped HPP model contains all the elements in Figure 5.2. The comparison is made based on the absolute difference between the two frequency values and the difference in time spent outside the normal frequency band. The best match is obtained for the filter time constant of 0,2 s with both frequency parameters increasing with higher time constants, giving a poorer match to the historical data. A sample of the measured and simulated frequencies with $T_{ff} = 0{,}2\ s$ is displayed in Figure 5.6.

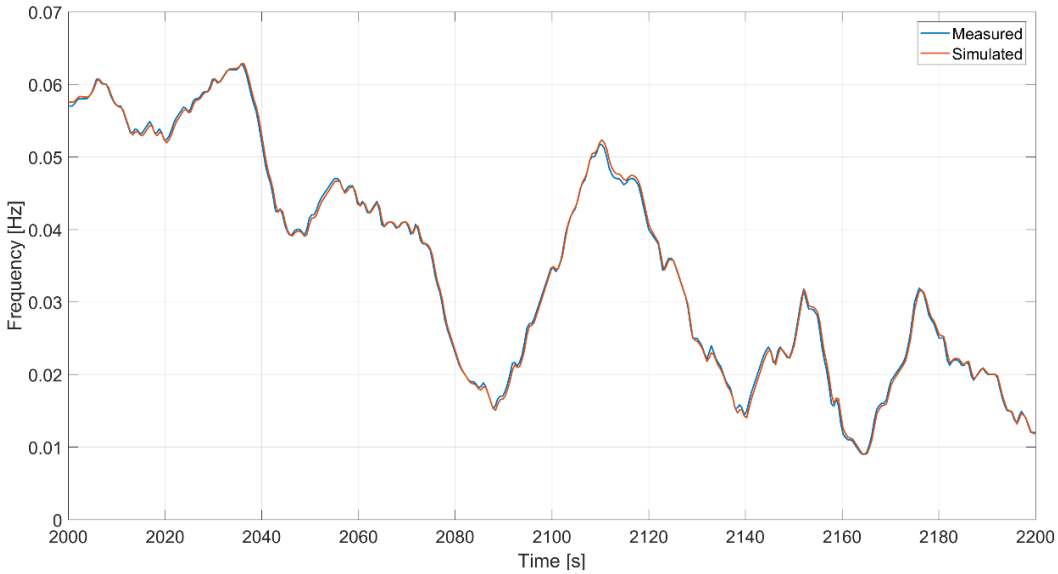

Figure 5.6. Frequency samples during the power disturbance generation test

This very good match of the two frequencies means that introducing ΔP_{hist} as a disturbance to the model will result in the same operating conditions for the FCR-N units as introducing historical grid frequency data. Therefore, the operating conditions present in the NPS during the selected time period are accurately recreated.

5.5 Single HPP Model

As the main goal of this project is to investigate the operation of the HBHS as a single unit inside the NPS, a model of this single unit needs to be connected to the power system model. The lumped HPP represents all n hydropower units providing FCR-N in the system. Therefore, for the system dynamics to be preserved, the lumped HPP needs to be altered to represent $(n-1)$ hydropower units while this one HPP, where the HBHS is to be implemented, is modelled separately.

As was mentioned before, the dynamics of all FCR-N providing HPPs are assumed to be the same when lumped into one model. This means that the dynamics of the model do not need to be altered, only the amount of regulation power delivered needs to correspond to $(n-1)$ units. This is done by modifying the droop constant, as it is designed to do just that – split up FCR-N gain between different power plants. The total gain in the system still needs to remain equal to R_{FCR-N} i.e. the total droop needs to be equal to E_p from Table 5.3. Assuming the single HPP has a gain of R_h the expressions become

$$R_h + R_{sys} = R_{FCR-N} \tag{5.24}$$

$$\frac{1}{E_{p_h}} + \frac{1}{E_{p_{sys}}} = \frac{1}{E_p} \tag{5.25}$$

where R_{sys} and $E_{p_{sys}}$ refer to the $(n-1)$ lumped HPP unit, named to indicate that it models the response of the rest of the system. In order to simplify the calculations, a scaling ratio of the single HPP gain compared to the total system gain is defined as

$$K_h = \frac{R_h}{R_{FCR-N}} \tag{5.26}$$

and used to adapt the parameters of both the system and single HPP models.

Firstly, the controller parameters are adapted to both HPP models. The governor mechanism will continue to operate with the same frequency change input while the output is now scaled down to the single unit and system size respectively. This further means that, in order to retain the same governor dynamics such as the response time constant and proportional action, all the controller parameters from Table 5.3 need to be scaled accordingly i.e.

$$E_{p_h} = \frac{E_p}{K_h}, \qquad E_{p_{sys}} = \frac{E_p}{1-K_h} \tag{5.27}$$

$$K_{p_h} = K_h K_p, \qquad K_{p_{sys}} = (1-K_h)K_p \tag{5.28}$$

$$K_{i_h} = K_h K_i, \qquad K_{i_{sys}} = (1-K_h)K_i \tag{5.29}$$

Secondly, other model parameters which are dependent on the HPP static gain are scaled as well. All time constants in the model remain the same since they are independent. The controller limitation ΔY_{max} is scaled automatically since it is defined over the droop constant in (5.15) i.e.

$$\Delta Y_{max_h} = \frac{\Delta f_{max}}{E_{p_h}}, \qquad \Delta Y_{max_{sys}} = \frac{\Delta f_{max}}{E_{p_{sys}}} \tag{5.30}$$

The other model parameter that is dependent on the static gain i.e. guide vane movement is the backlash, as it is defined in percentages of the distance. Therefore, it is scaled accordingly as well.

$$Bl_{y_h} = K_h Bl_y, \qquad Bl_{y_{sys}} = (1-K_h)Bl_y \tag{5.31}$$

$$Bl_{a_h} = K_h Bl_a, \qquad Bl_{a_{sys}} = (1-K_h)Bl_a \tag{5.32}$$

With this, the guide vanes movements of both models ΔY_{pos_h} and $\Delta Y_{pos_{sys}}$ and thus their powers ΔP_{prod_h} and $\Delta P_{prod_{sys}}$ represent the action of a single and $(n-1)$ HPPs

respectively. Therefore, the power system model now contains a separate single HPP which is used to implement the HBHS.

5.6 BESS Model

The hybrid system consists of an HPP and a grid-connected BESS which act together as one unit delivering FCR-N to the system. Therefore, as the next step towards modelling the HBHS and its behaviour, a model of the BESS is built and introduced to the system.

The dynamics of a BESS are governed by its chemical and electrical subsystems. The chemical subsystem encompasses the processes inside the battery cells whilst all elements between the battery electrodes and the grid connection are part of the electrical subsystem. Considering the timescale of frequency regulation, the chemical processes are assumed to be at least an order of magnitude faster, delivering instantaneous power to the converter. The BESS model is thus composed of the power control mechanism and the electrical subsystem.

Like the turbine governor, the BESS power control measures the grid frequency and subtracts it from the reference value to obtain the frequency deviation i.e.

$$e_f(s) = f_{ref} - f_{meas}(s) = \Delta f(s) \tag{5.33}$$

This error signal is first filtered for measurement noise and then used to calculate the power reference which is forwarded to the converter. The controller output is again limited to the power capacity dedicated to FCR-N, usually also the BESS power rating, giving the expression

$$\Delta P_{ref_b}(s) = \begin{cases} K_{p_b} \dfrac{1}{T_{meas}s + 1} e_f(s), & |\Delta f| \leq \Delta f_{max} \\ \pm \Delta P_{max}, & |\Delta f| > \Delta f_{max} \end{cases} \tag{5.34}$$

As can be seen, the control law consists only of a proportional gain which is equal to the FCR-N gain of the unit i.e.

$$K_{p_b} = R_b = \frac{\Delta P_{ref_b}(s)}{\Delta f} \tag{5.35}$$

which gives adequate performance assuming this is a higher-level controller, for example a Power Plant Controller (PPC), which is the case for the HBHS. This means that the calculated power reference will be reached by the internal converter controllers without any steady-state error.

For the electrical subsystem model, a power plant perspective is employed. Most grid-connected converters contain the abovementioned internal controllers for output current and power [33]. In a BESS converter, the power controller computes the current reference based on a reference received from the higher-level controls. The GSC power output then tracks this reference with a dynamic response that is defined by the internal power controller itself. Based on these considerations and the frequency regulation timescale, the dynamics of the BESS can be defined through the dynamics of this power controller. Therefore, the standard response of a power converter to a reference is set to be a time delay T_{del_c} accounting for the action of the measurement and control circuits, and a first-order lag behaviour with the time constant T_c when reaching the reference value i.e.

$$\Delta P_{prod_b} = \frac{1}{T_c s + 1} e^{-sTdel_c} \Delta P_{ref_b}(s) \tag{5.36}$$

With the power output obtained, the BESS model is complete and is added to the power system model. It should be stressed that, considering that the regulation power controller is a simple proportional law, the speed of the BESS power response is defined by (5.36) and is therefore almost instantaneous in a frequency regulation timescale. The parameters of the model are given in Table 5.5. The proportional controller gain and power limit directly depend on the BESS power rating and are thus subject to optimization. Therefore they are defined through the FCR-N gain of the BESS, which will be used in the optimization together with the undefined FCR-N gain of the single HPP.

Table 5.5. BESS model parameters

Parameter	Symbol	Value
Proportional controller gain [pu]	K_{p_b}	R_b
Frequency measurement filter time constant [s]	T_{measf}	2
BESS power limit [pu]	ΔP_{max}	$R_b \Delta f_{max}$
Converter lag time constant [s]	T_c	0,3
Converter time delay [s]	T_{del_c}	0,1

5.7 HPP Wear and Tear Estimation

The fatigue experienced by the governor of an HPP and its mechanisms, while it is performing frequency regulation, is usually called the regulation wear and tear. The constant changes in the grid frequency lead to frequent movements of the guide vanes and runner blades. Since these components are mechanical and experience large forces during HPP operation, their systems wear down with every movement, eventually requiring maintenance and replacement. The runner blade bearings have been identified as the element with the shortest maintenance interval, followed by guide vane bearings [40]. Performing repairs on any of these elements requires the HPP to completely shut down its

production, resulting in great production losses due to unavailability and thus high expenses for such works. This is why reducing the wear and tear on the HPP is a crucial factor for its operation and why it is an important parameter to be estimated for the HBHS.

From previous research and industry experience, two parameters have been found indicative of the amount of wear and tear: the distance travelled by the guide vanes and the number of movements the regulation mechanism makes [41], [42]. One movement is defined as the guide vanes first starting to move and then stopping, because the reference is reached or in order to change the moving direction. If both of these parameters, as a result of regulation actions, can be evaluated, the amount of wear and tear the HPP experiences from these regulation actions can be quantified.

The distance L_{wt} the guide vanes travel can be easily calculated from their position ΔY_{meas}. This variable represents the signal measured by the control system and therefore is a good indicator of the control actions performed by the governor. The physical position ΔY_{pos} is not chosen since it does not account for the movements performed by the servos which are absorbed by the backlash and since it is not easily measurable in real cases. The distance travelled is a sum of the position change during the simulation time T_{sim} i.e.

$$L_{wt} = \int_0^{T_{sim}} \frac{d|\Delta Y_{meas}|}{dt} dt = \int_0^{T_{sim}} d|\Delta Y_{meas}| \tag{5.37}$$

As the signal ΔY_{meas} is the absolute value of the position, with regards to the hourly static production reference, a derivative is taken to avoid integrating the position itself but rather the position change.

The number of movements N_{wt} the regulation mechanism makes is evaluated from the same guide vanes position signal. A straight-forward approach can be taken to evaluate this parameter, which would mean counting the number of times $d\Delta Y_{meas}$ is equal to zero i.e. the number of times guide vanes come to a complete stop. However, in the simulation environment, ΔY_{meas} almost never comes to a complete stop because of the asymptotic nature of the model. Different HPP elements are modelled using first-order lags which theoretically never reach their exact asymptotic value, meaning that $d\Delta Y_{meas}$ is never exactly zero. Furthermore, an exact zero is a value MATLAB, as a numerical environment, can have trouble evaluating. Practically, this issue is solved by introducing a tolerance ε_{wt} to the zero value, which would mean that the guide vanes are considered to have stopped if they have moved less than the tolerance value during a certain sampling time T_{wt}. The evaluation is implemented using a counter which reacts on the rising edge of the inequality

in (5.38), resulting in a count increase whenever the mechanism is considered to have stopped and started moving again.

$$\Delta N_{wt} = \begin{cases} 1, & |\Delta Y_{meas}(t) - \Delta Y_{meas}(t - T_{wt})| > \varepsilon_{wt} \\ 0, & |\Delta Y_{meas}(t) - \Delta Y_{meas}(t - T_{wt})| < \varepsilon_{wt} \end{cases} \quad (5.38)$$

When the output of this counter ΔN_{wt} is accumulated during the simulation time, the total number of movements performed N_{wt} is obtained.

Whereas the introduction of the tolerance is easily motivated, another modification of the counter can be considered. Considering the random nature of the frequency, it is possible to assume that the final count is highly dependent on the chosen tolerance ε_{wt}. One way of decreasing this dependency can be through the introduction of a floating hysteresis, much like the one used to model the turbine backlash effect. In this way, the obtained signal would resemble ΔY_{pos} and is denoted with ΔY_{wt}, giving the final counter definition below.

$$\Delta N_{wt} = \begin{cases} 1, & |\Delta Y_{wt}(t) - \Delta Y_{wt}(t - T_{wt})| > \varepsilon_{wt} \\ 0, & |\Delta Y_{wt}(t) - \Delta Y_{wt}(t - T_{wt})| < \varepsilon_{wt} \end{cases} \quad (5.39)$$

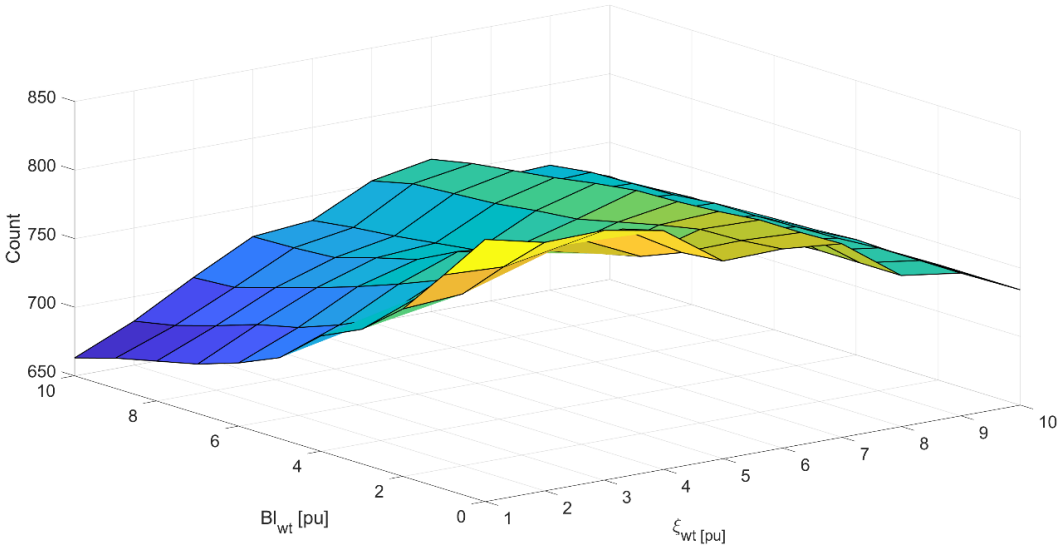

Figure 5.7. HPP wear and tear counter test

The effect of this added backlash on the sensitivity of the counter and its final value is examined by including the wear and tear model from (5.39) to the single HPP in the power system model. A five-hour operation is simulated using the historical load disturbance from (5.23), replicating real grid conditions. The tolerance of the counter ε_{wt} and the backlash width Bl_{wt} are varied and the change of the counter is observed in Figure 5.7. Both varied parameters are given in per-unit of turbine backlash Bl_y to preserve a sense of scale. It can be observed that the introduction of a small backlash decreases the dependency of the counter value on the tolerance significantly. Therefore, the modification of the wear and tear

evaluation is accepted. With the aim of obtaining the lowest sensitivity and an average count from the test, the following values are used for the wear and tear parameters.

$$Bl_{wt} = 2Bl_y, \qquad \varepsilon_{wt} = 5Bl_y, \qquad T_{sim} = 2\ s \tag{5.40}$$

Validating these counter values would require comparing the modelled counter result with measurements from a real HPP while using the same historical frequency data. Since this is out of the scope of the Thesis, these counter values are assumed valid based on industry experience and similar model results from literature. For example, the settings from (5.40) result is a count of 24 624 movements during a one-week period, whereas the counter from [42] records 25 345 movements for the same time length. Nevertheless, if these settings are kept constant during the optimization of the HBHS functioning, a quantitative comparison of the wear and tear values for different settings can be made.

5.8 BESS Degradation Estimation

Much like the wear and tear of the HPP turbine, the degradation of the BESS is a crucial parameter for evaluating the operating conditions and performance of the HBHS. During energy conversion, the battery cells lose a certain amount of energy capacity due to the mechanical stress on its chemical elements [18]. This results in a storage capacity degradation that is closely linked to the way in which the BESS is operated. The considerable cost of BESS units makes the operational lifetime of a BESS a deciding factor for the profitability of its implementation [43].

From these considerations and the nature of energy storage, it is obvious that the SoC signal will have to be created in the model in order to evaluate the degradation of the BESS. In practice, the SoC is usually estimated by the BMS from the cell voltage level which varies with the SoC. There is no need to measure cell voltage levels in the simulation environment, since the SoC can easily be tracked by establishing an initial state and accumulating the power the BESS is exchanging through the converter. Considering that the BESS energy conversion has a round-trip efficiency of η_{rt}, the expression for the SoC change becomes

$$SoC(s) = \begin{cases} \sqrt{\eta_{rt}}\,\dfrac{1}{s}\Delta P_{prod_b}(s), & \Delta P_{prod_b} < 0 \\ \dfrac{1}{\sqrt{\eta_{rt}}}\,\dfrac{1}{s}\Delta P_{prod_b}(s), & \Delta P_{prod_b} > 0 \end{cases} \tag{5.41}$$

In other words, when the BESS is absorbing power from the grid, the energy stored is $\sqrt{\eta_{rt}}$ less than what the grid is providing and vice versa. The initial SoC for BESS providing FCR-

N in Sweden can be extracted from the requirements for a symmetrical product [30]. They dictate that regulation power should be provided in the same manner during over- and under-frequency events, setting the desired and initial SoC at half i.e.

$$SoC_{ref} = SoC_0 = 50\ \% \tag{5.42}$$

Finally, the SoC signal is limited to the actual battery energy capacity by putting a minimum charge of 0 % and a maximum charge of 100 %. This is done to imitate realistic BESS behaviour and thus allow for a better degradation estimate. This also introduces the possibility of accurately tracking the time period in which the BESS is not able to supply regulation power, due to a lack or excess of energy.

The SoC values require the definition of the battery storage capacity which is used as the base value. Following industry standards introduced in Section 4.3, the battery C rate is used for this purpose. With the FCR-N gain of the BESS directly defining its power rating, and the C rate defining the ratio between battery power and energy, the battery capacity in Wh is obtained as

$$SoC_{base} = \frac{R_b \Delta f_{max}}{C_{rate}} \tag{5.43}$$

The BESS experiences capacity loss as a result of cycling and of ageing, therefore this degradation is evaluated differently over time spent charging and discharging and over time spent idling [43]. The modelled operation of the HBHS is presumed to be continuous, therefore the entire simulation time is assumed as cycling time and the idling capacity loss is disregarded. The cycling capacity fade is calculated from an empirically formulated expression for Li-ion batteries at an operating temperature of 25 ˚C [44]. The energy capacity fade depends on the average SoC during operation SoC_{av}, depth of the cycles the BESS performed cd and the number of these cycles nc i.e.

$$C_{fade} = 0{,}021 e^{-0{,}01943 SoC_{av}} cd^{0{,}7162} nc^{0{,}5} \tag{5.44}$$

all given in percentages of full charge.

The calculation in (5.44) is valid for uniform cycling, meaning that only a single cycle depth can be applied to it. As the SoC is expected to exhibit stochastic behaviour, all cycles of varying depth need to be accounted for. This calls for an introduction of a counting algorithm which can identify all the cycles the SoC goes through. To this end, the SoC signal is put through the so-called Rainflow counting algorithm, which gives multiple results as an output, all applicable to the expression in (5.44) [45]. As preparation for the counting, the local extremes of the SoC signal are found, as marked in an example in Figure 5.8.

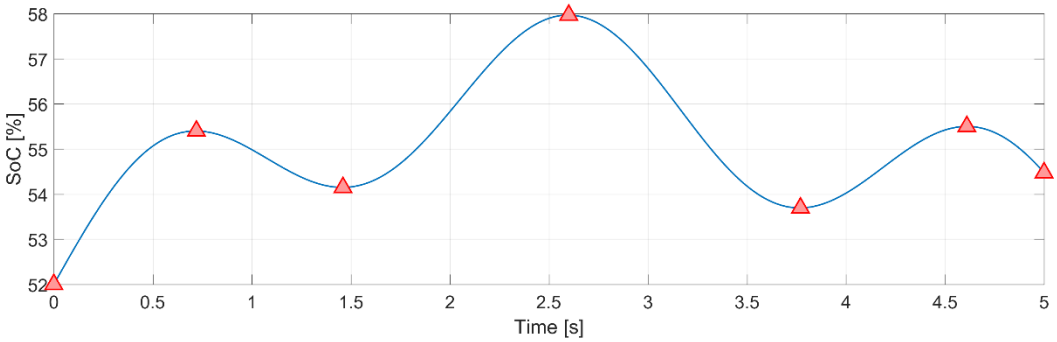

Figure 5.8. Example of SoC signal processed by the Rainflow counting algorithm

These extremes are then processed by the algorithm which identifies the different cycles and their depths, not limited to two adjacent local extremes but rather taking into account the whole array. The name comes from the philosophy behind the counting, which can be described as rotating the graph in Figure 5.8 clockwise for 90 degrees, letting rain drops flow downwards over the signal and observing the flow behaviour. From this, cycle amplitude, mean value and cycle number are obtained in a histogram format with defined data bins. The fatigue from each of these data bins can then be individually estimated. To obtain the overall BESS degradation, Miner's rule of mechanical fatigue accumulation is applied, stating that the life consumption LC from varying loads i.e. cycle depths can be summed as

$$LC = \sum_j \frac{nc_j}{nf_j} \tag{5.45}$$

where j denotes the data bin i.e. cycle depth, nc_j is the number of cycles that occurred with that depth and nf_j the number of cycles of that depth which would lead to the end of life for the BESS. The end of life for a BESS is commonly defined in the industry as the point when a 20 % capacity fade is reached [18]. Therefore, the Rainflow algorithm cycle counts are used as nc_j and (5.44) is altered to obtain the end of life criterion for each bin nf_j as

$$nf_j = \left[\frac{20\ \%}{0{,}021e^{-0{,}01943SoC_{av_j}} cd_j^{0{,}7162}}\right]^2 \tag{5.46}$$

The obtained result is the per-unit life consumption LC, which the BESS experiences during the simulated time. In order to obtain more understandable results, this can be scaled to the predicted BESS life consumption for one year or the lifetime in years can be estimated.

6 HBHS Architectures

The NPS and all its components necessary for the implementation of the HBHS, have been introduced and modelled in the simulation environment, as well as the HPP wear and tear and BESS degradation estimators. This gives all the tools and definitions needed to introduce the HBHS architectures and exemplify the behaviour of the hybrid system. At this point it is decided that the HBHS is to be developed without altering the HPP governor and systems. The only thing that can be altered is the frequency deviation signal used by the governor. This is done for two reasons, to model the implementation and performance of such a hybrid system at an existing HPP and to decrease the number of optimization variables, as will be seen later.

Several parameters were left undefined previously, because of their impact on HBHS operation. These include the FCR-N gains for the HPP and the BESS i.e. regulation power ratings R_h and R_b respectively, and the BESS capacity SoC_{base}, defined over the battery C_{rate}. It is now set that an HBHS providing 5 MW of FCR-N to the NPS will be used as a study case, with a preliminary $C_{rate} = 1$, which amounts to 5 MWh of BESS storage capacity. For easier understanding, a new gain value is introduced as the HBHS unit's FCR-N gain. This gain is the result of the combined action of the HPP and BESS comprising the HBHS and is what the unit is delivering to the grid, therefore

$$R_{unit} = \max\{R_h, R_b\} \tag{6.1}$$

First, the operation of a single HPP providing these 5 MW of FCR-N will be evaluated and set as a benchmark for the HBHS operation. The hybrid system performance during FCR-N prequalification tests, introduced in Section 4.1.2, will be examined, as well as its operation in the NPS with a historic load disturbance signal defined in (5.23). After this, two different HBHS architectures will be described: Hydro Recharge and Frequency Split. The same prequalification tests are run, allowing for a qualitative comparison between the systems.

6.1 Benchmark Operation

A single HPP operating in the NPS is taken as a benchmark, with the goal of evaluating the performance and regulation wear and tear of standard HPP units that are currently delivering FCR-N to the grid. Thus, no BESS is present in the model at this point.

All the values for the power system, lumped HPP and single HPP models were defined before, giving the single HPP the said study case gain i.e.

$$R_{unit} = R_h = 50\frac{MW}{Hz}, \qquad R_b = 0, \qquad R_{sys} = R_{FCR-N} - R_h = 7480\frac{MW}{Hz} \tag{6.2}$$

with both HPP models using the Ep0 settings, allocating 2 % of the guide vane opening for FCR-N regulation. What is left is to choose if the unit has a Francis or a Kaplan turbine. For the benchmark model, both turbine types are implemented in order to demonstrate their behaviour and identify performance differences. The described model can be seen in Figure 6.1, where the single HPP model is now displayed with same three components as the lumped HPP in Figure 5.2.

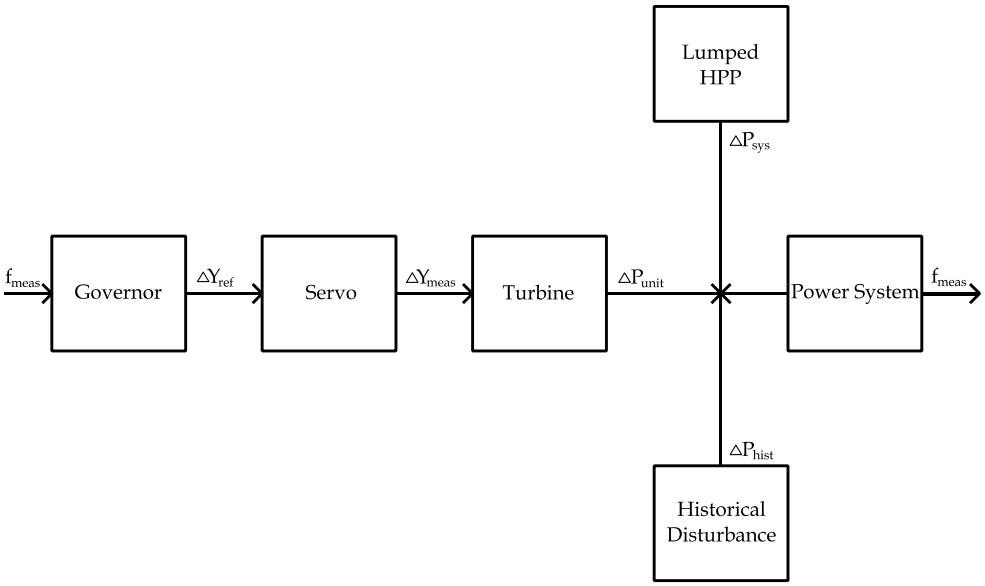

Figure 6.1. Benchmark system model

First, a single step with a deviation of Δf_{max} is introduced to the model. This represents the most simple and understandable dynamic test for the model and is therefore used to observe its behaviour.

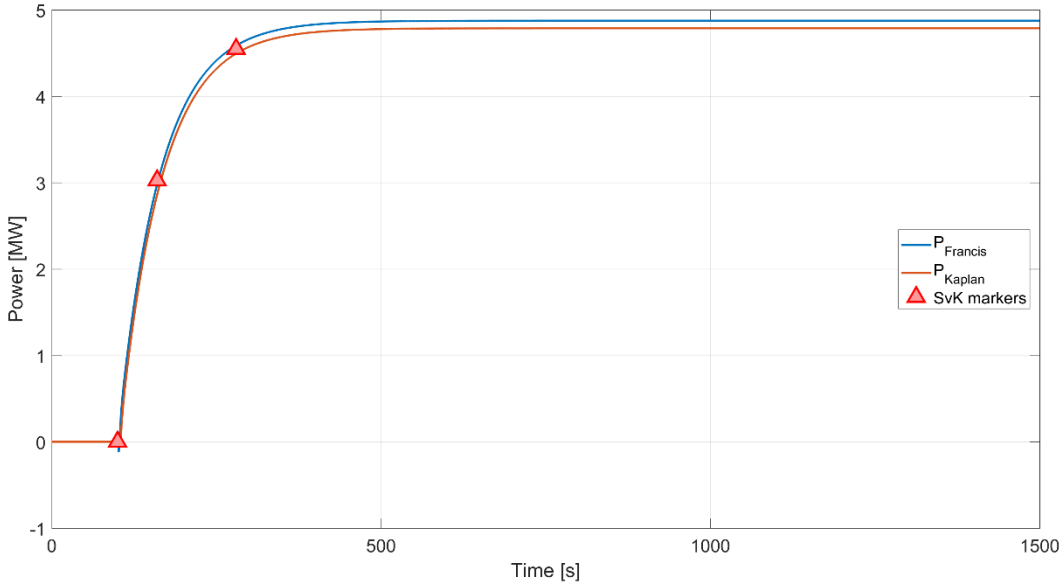

Figure 6.2. Benchmark unit step response test with both turbine types

Apart from the unit power response, the markers from the SvK FCR-N provision test are displayed to evaluate the unit response speed. SvK requires the unit to reach 63,3 % of regulation power within 1 minute, and steady state i.e. 95 % of regulation power within 3 minutes. Figure 6.2 shows the step response both a Francis turbine and a Kaplan turbine unit. The power response of both turbines is of a first-order lag nature, without any overshoot but with a small negative reaction immediately after the frequency step. This is a result of the non-minimum phase turbine models from (5.20) and (5.21). Furthermore, the response follows the SvK markers, which have the same time constant as the governor. This confirms that the speed of the HPP regulation is defined primarily by the governor settings. A slight delay of the Kaplan unit is visible compared to its Francis counterpart, caused by its two-tier governor system. The most notable difference is in the steady-state value of the regulation power. Both benchmark models fail to deliver exactly the reference value of 5 MW due to the backlash effect, while the steady-state value is lower for the Kaplan turbine. To conclude, the step response test confirms that the benchmark model is behaving as expected, both regarding its dynamic and steady-state responses.

This confirmation of model behaviour allows for the continuation of testing with the FCR-N prequalification tests as defined by SvK. Next, the static prequalification test comprising of several frequency steps is performed. The frequency sequence, displayed in Figure 4.3, is introduced to the model with the steps of ±0,1 Hz lasting for one hour, in order to test the unit endurance, and other steps lasting until a steady state is reached. The results from a Francis and a Kaplan turbine are displayed in Figure 6.3. The power reference is obtained by multiplying the frequency deviation signal by the gain R_{unit}.

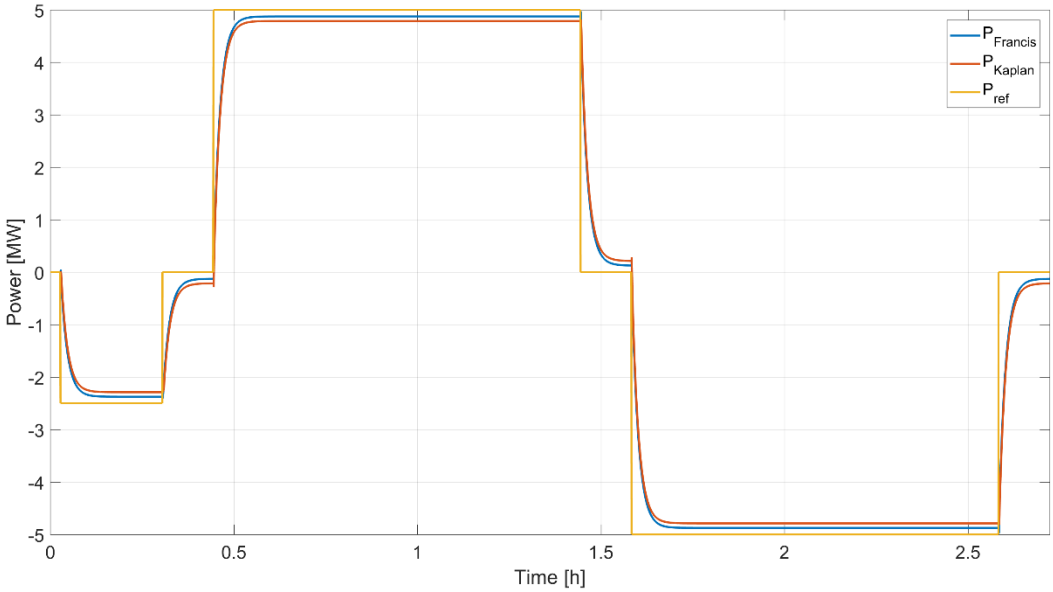

Figure 6.3. Benchmark unit static prequalification test with both turbine types

The same behaviour as during step response tests can be seen, which is expected since the nature of the frequency disturbance is the same. Again, the backlash

effect is visible in the steady-state values and the unit endurance poses no problem, since it is only an HPP. The formulas in (4.1) and (4.2), given by SvK, can now be used to calculate the amount of backlash in the system and the available FCR-N capacity. The SvK calculations give

$$2D = 0{,}10\ \%, \qquad C_{FCR-N} = 4{,}87\ MW \tag{6.3}$$

and

$$2D = 0{,}17\ \%, \qquad C_{FCR-N} = 4{,}78\ MW \tag{6.4}$$

for the Francis and Kaplan units respectively. Comparing these values with the parameters Bl_y and Bl_a, a match is identified when the scaling for the guide vane opening to power for the Kaplan turbine is taken into account. Therefore, another confirmation of a sound model functioning is obtained, as well as the real FCR-N capacity which is available from the unit.

After subjecting the unit to static prequalification tests, the scarcity of the information they provide is visible. Although much can be said about the dynamic characteristics of the unit based on a step response, these tests do not describe the behaviour of the unit when exposed to oscillations in the frequency. As such oscillations are present in the actual grid frequency, the proposed sinusoidal dynamic FCR-N provision tests are envisioned to give more detailed information about the unit's performance in today's system. As depicted in Figure 4.4, frequency oscillations with 10 different time periods and an amplitude of Δf_{max} are fed to the regulation mechanism and the gain and phase delays of the unit regulation power are observed. What is obtained is effectively a Bode diagram defined by the 10 measurement points, as can be seen in Figure 6.4.

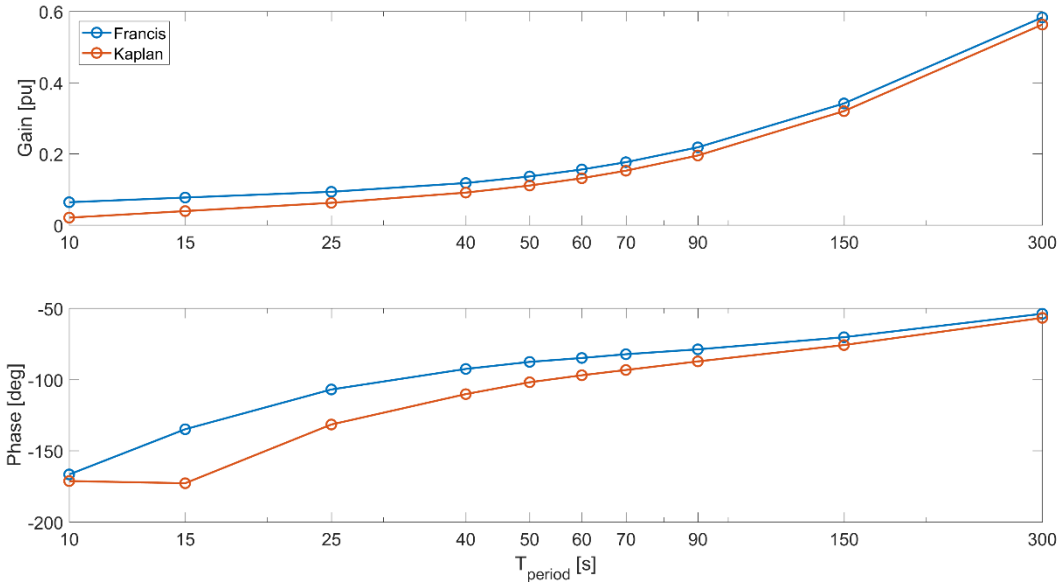

Figure 6.4. Benchmark unit dynamic prequalification test with both turbine types

The performance degradation of HPP units providing FCR-N when exposed to fast frequency oscillations, which was introduced as the motivation behind this project, can be clearly seen from the sinusoidal tests. Namely, when the oscillation time period decreases below 90 seconds, the regulation power provided by the unit is less than 20 % of the capacity from (6.3) and (6.4) and the phase delay goes over 90 degrees. This means that the little power that is provided does not positively affect the system balance as the unit outputs maximum power while the frequency in the system is over the nominal value and vice versa. To demonstrate this undesired behaviour, the result of the dynamic prequalification test with a 60-second and a 15-second time period is displayed in Figure 6.5. It can be concluded that, for the 60-second period, the delay results in no regulation power delivered at the moments the frequency assumes its extreme values. This translates into very little or no damping for oscillations at this frequency and can be the phenomenon causing the mentioned grid frequency floating. For the 15-second time period, the frequency maximum and power output maximum occur at the same time, effectively destabilizing the system. However, these frequency oscillations are not observed in the grid frequency.

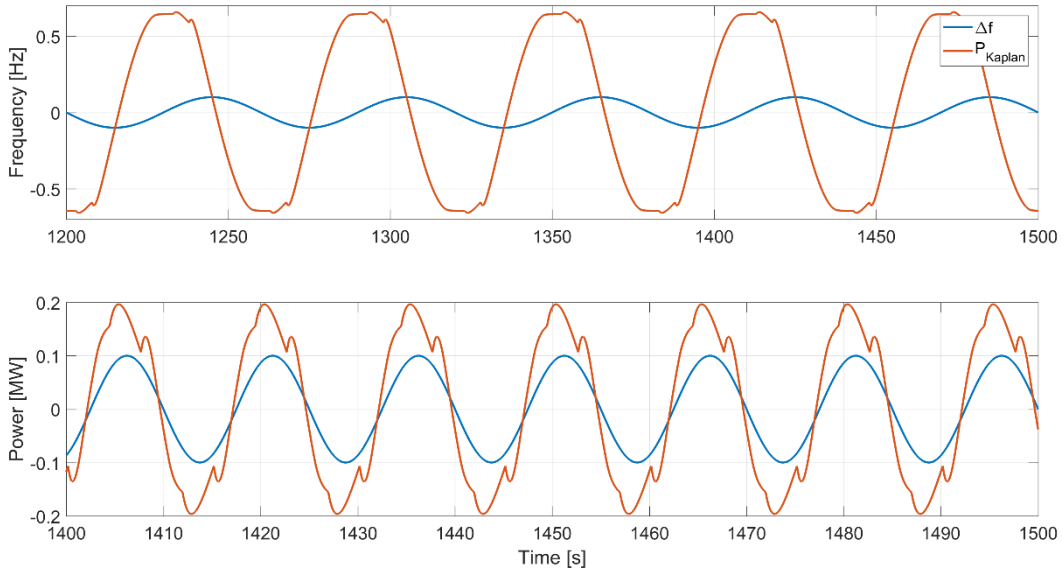

Figure 6.5 Benchmark unit sinusoidal tests with 60-second (upper) and 15-second (lower) period

Overall, the performance degradation is more prominent for Kaplan turbines, with the gain difference a result of more prominent backlash and the two-tier regulation mechanism causing the phase difference to increase together with the oscillation speed.

With the model performance during dynamic prequalification tests evaluated, it is useful to compare the results to full-scale tests performed on existing HPPs. Several sinusoidal tests were performed by Fortum on existing Kaplan units in Sweden. Three different frequency deviation signals, with a period of 90, 60 and 30 seconds, were fed to the HPP governors of four different units and their power responses were recorded in the same manner as in Figure 6.5. The resulting Bode plot points can be seen in Figure 6.6, compared to the modelled Kaplan unit response. The full-scale results display more

variability when the oscillation speed increases, with only one unit having a measurable output during the 30-second oscillation. The modelled phase delay matches the results adequately while possibly underestimating the delay for faster frequency oscillations. The modelled gain is underestimated for slower oscillations while possibly providing a good match for faster sinusoidal signals. Observing the scarcity of full-scale results, it can only be concluded that the model is exhibiting valid behaviour trends and responses which are in the same value range as existing HPPs.

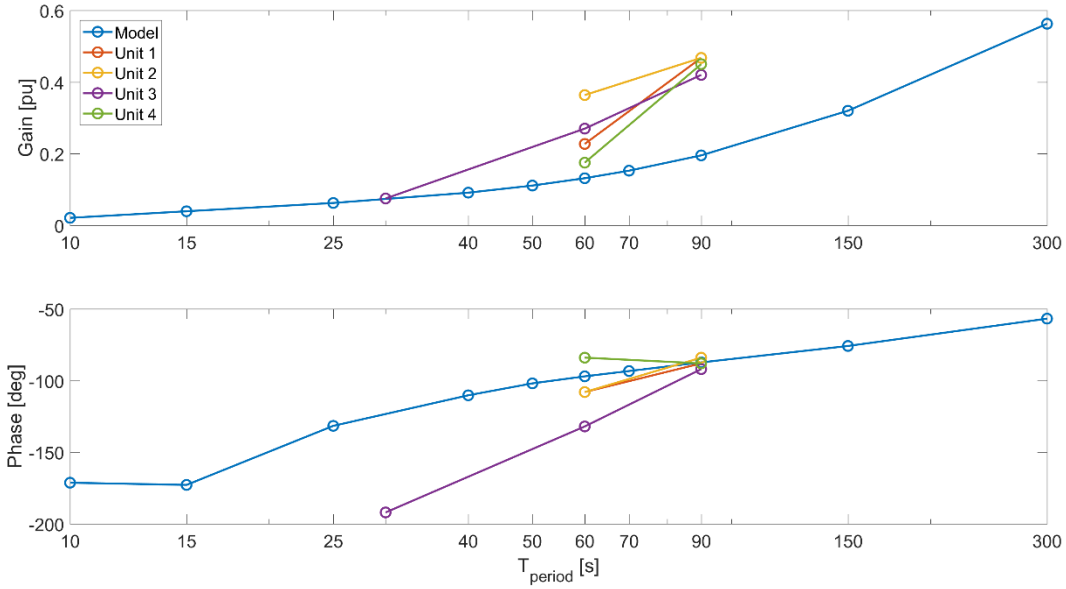

Figure 6.6 Benchmark model performance comparison to full-scale tests

This completes the qualitative performance testing of the benchmark unit. It is concluded that the unit would pass the static prequalification test with the capacity calculated in (6.3) or (6.4), depending on the turbine type. It is also concluded that the requirements of the envisioned dynamic prequalification test would pose an issue for certain HPPs, especially those with Kaplan turbines. This result, together with different considerations from Section 4, suggests an answer to the first research question which HPPs are good candidates for the installation of the proposed hybrid system. If a certain unit is not able to pass the FCR-N provision tests, it is a prime candidate for the HBHS, as this upgrade would enable the entire regulation capacity of the HPP to be sold. This would significantly increase the profits of installing such a system. On the other hand, if the unit is able to pass the test, the possible profits of installing an HBHS decrease. Nevertheless, the many running hours, that downstream Kaplan units have, could translate into low-cost and frequently available charging power for the HBHS, still favouring them for the HBHS installation over Francis units. Based on these conclusions, further optimization work and comparisons are done using a Kaplan turbine model.

After the qualitative, the quantitative performance benchmark is set. As was already mentioned, the unit performance will be analysed based on its operation in the NPS

with historical frequency data. The evaluation parameters are obtained by the HPP wear and tear estimator, which measures the amount of stress the regulation mechanism of the HPP endures during a certain time period. The time period for unit testing is taken to be 30 days of August 2018. As a result, the benchmark unit performs as exemplified in Figure 6.7. The frequency governed reference and the power output of the benchmark unit are displayed for a five-hour sample. It is apparent that the reference is heavily filtered by the governor mechanism but followed as required. The FCR-N limitation of 5 MW can also be seen around one hour of simulation time when the frequency exits the normal frequency band.

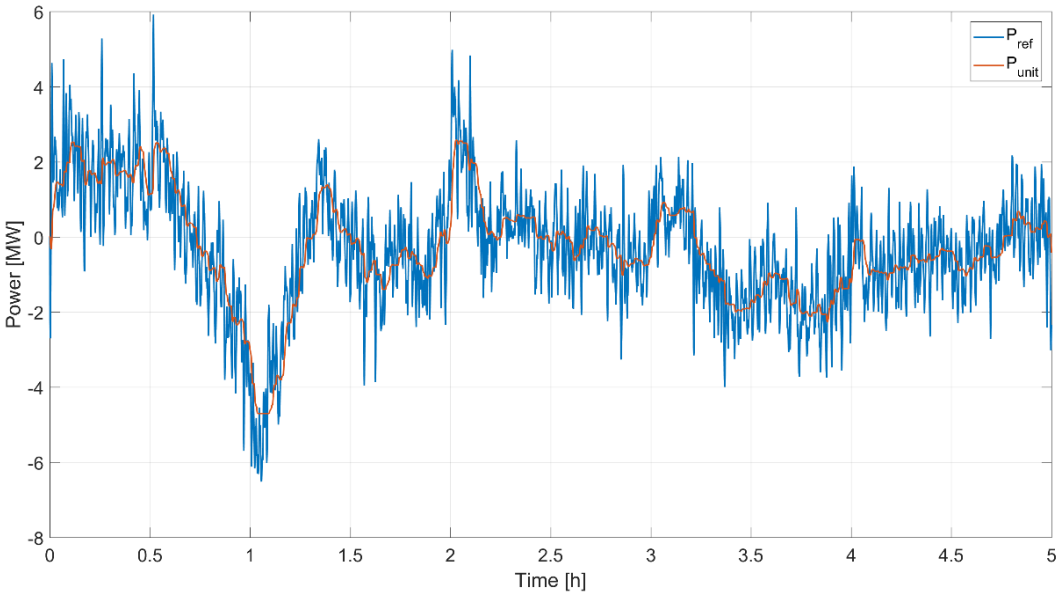

Figure 6.7. Benchmark unit operation in the NPS

The regulation wear and tear on the HPP during these 30 days of operation, expressed through the distance and number of movements, is evaluated to be

$$L_{wt} = 16\,670{,}2\ \%, \qquad N_{wt} = 122\,011 \tag{6.5}$$

which gives an average movement distance of 0,14 %, coherent with existing wear and tear estimations in literature [42]. Therefore, this is accepted as a valid measure of the stress a single HPP would experience during 30 days of continuous frequency regulation. Another parameter that is evaluated is the frequency quality in the system i.e. the minutes spent outside the normal frequency band during operation. The month of August 2018 returned 1 171 minutes outside the band, which is slightly over the 1 132 minutes measured by Fingrid. This difference is attributed to the fact that the simulation calculates the time with a smaller time step than the one-second measurements in Figure 5.4. This comparison confirms that the power system is accurately modelled in the simulation environment. With this, the benchmark is defined for both qualitative and quantitative analysis, thus the hybrid

system architectures can be developed, and their performance compared to the benchmark HPP unit.

6.2 Hydro Recharge HBHS

The first hybrid architecture is designed using an opposite approach to the benchmark HPP unit performing frequency regulation. This means that the HPP is not delivering any regulation power at all i.e. the BESS is providing all of the unit's regulation power. In the Hydro Recharge HBHS, the HPP is controlling the state of charge of the BESS during operation, giving the architecture its name. The HBHS model is thus composed of a single HPP and a BESS model, with the already defined parameters.

The presence of both an HPP and a BESS, operating together towards the grid, invites the introduction of another component into the system, the Power Plant Controller (PPC) of the HBHS. In order to coordinate the actions of both elements, the PPC takes over the function of measuring the grid frequency f_{meas} and is tasked with creating the error signals e_{f_h} and e_{f_b} for both the HPP governor and the BESS power controller. If this is accomplished, the control circuit is closed again with the PPC being cascaded over the existing control elements, giving the model structure as displayed in Figure 6.8.

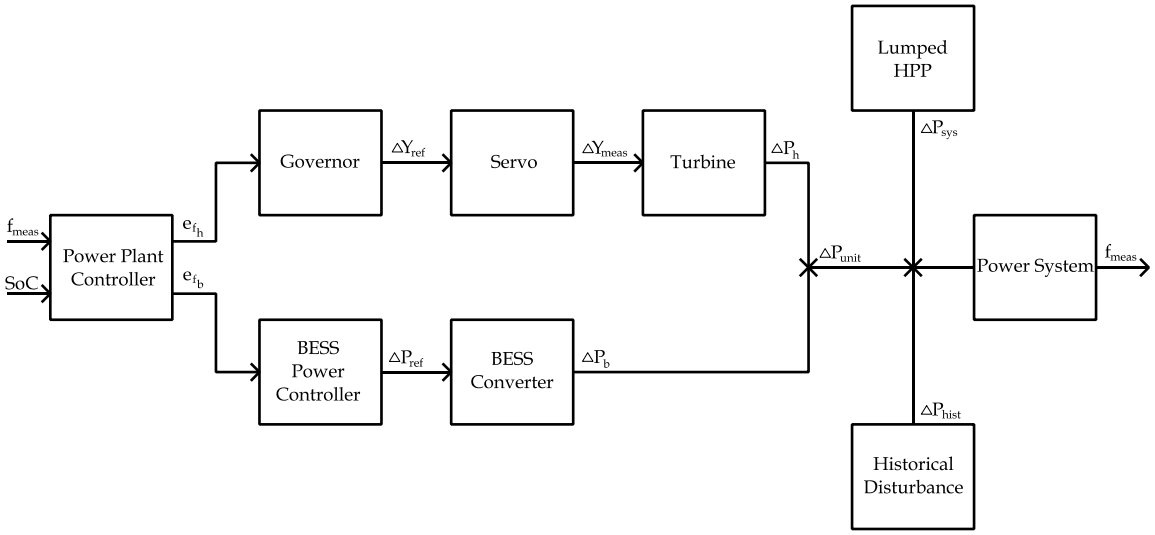

Figure 6.8. Hydro Recharge HBHS model

Following the introduced architecture, the frequency error which is forwarded to the HPP is created from the SoC signal. If the BESS charge falls below a permissible SoC band, the HPP output power will increase with the aim of recharging the BESS and if it goes over the permissible SoC band, the HPP output power will decrease with the aim of discharging the BESS. The HPP regulation power output will return to zero when the reference SoC defined in (5.42) is reached. Using the same signal structure as for frequency regulation, the HPP error signal is formed as

$$e_{f_h}(s) = \begin{cases} \Delta f_{max}, & SoC < SoC_{lo} \\ 0, & SoC_{hi} \geq SoC \geq SoC_{lo} \\ -\Delta f_{max}, & SoC > SoC_{hi} \end{cases} \quad (6.6)$$

where SoC_{lo} and SoC_{hi} are the lower and upper limits of the permissible SoC band. The error value returns to zero when $SoC = SoC_{ref}$. The maximum frequency deviation Δf_{max} is used in order to provoke the maximum power reaction from the HPP. This way, all of the power dedicated to FCR-N is used during Hydro Recharge operation, maximizing the capability of the unit to maintain the SoC. In addition, this complies with the current model settings in which R_h is the sizing parameter.

For the HBHS to operate as a single unit towards the grid, the PPC needs to compensate for the HPP power output change caused by the SoC level by adapting the BESS power output. This is done during the formation of the frequency error signal for the BESS. As was already mentioned, the BESS is delivering FCR-N on behalf of the HBHS, and adjusts for the SoC controlled HPP power output i.e.

$$e_{f_b}(s) = f_{ref} - f_{meas}(s) - \frac{\Delta P_h(s)}{R_b} = \Delta f(s) - \Delta f_h(s) \quad (6.7)$$

Dividing the HPP power output by the BESS regulation gain gives the frequency deviation value proportional to the HPP power output. This produces a BESS frequency error signal which will produce the required FCR-N capacity while compensating for the HPP output.

With the compensation in place, it is time to shape the FCR-N power output of the HBHS unit. If the expression from (6.7) is directly implemented in the PPC, the HBHS would have an FCR-N capacity of 5 MW, compared to the benchmark 4,78 MW from (6.4), and a response speed defined by the BESS converter i.e. under one second. While it is debatable whether an increase in capacity is desirable or not, it is clear that such a fast FCR-N response is not desirable. Although it would inevitably have a positive effect on the frequency quality in the grid, this fast response is not remunerated in any way by SvK and causes significantly more BESS degradation, making it undesirable for the HBHS owner. One simple way of slowing down the HBHS regulation response is filtering the measured frequency deviation with a desired time constant. Since the BESS reacts almost instantaneously in the FCR-N delivery timescale, this would result in an HBHS power reaction with a time constant inherited from the filter. Following SvK requirements, this translates into

$$e_{f_b}(s) = \frac{1}{T_{unit}s + 1}\Delta f(s) - \Delta f_h(s), \qquad T_{unit} = 60\ s \quad (6.8)$$

If it is desired to retain the same FRC-N capacity as the single HPP, the frequency signal can be put through a backlash model with Bl_f. One reason for doing so would be to allow the BESS to establish a zero power output during steady state if $R_h = R_b$. This scaling modification is also implemented in the Hydro Recharge HBHS.

$$Bl_f = \frac{K_y Bl_y + K_a Bl_a}{R_b} \tag{6.9}$$

The HPP power compensation from (6.7) also introduces an issue with the SoC control algorithm in (6.6). Namely, adding a charging power reference on top of the regulation power reference, implies that the BESS has to have the power rating that accommodates both. As this is not the case and the BESS is rated to ΔP_{max} dedicated to regulation, adjustments must be made to (6.6). The primary function of the HBHS is to deliver FCR-N to the grid, therefore the regulation power reference has priority. In order to guarantee that the HBHS unit delivers exactly C_{FCR-N}, the HPP error signal is modified to account for the power limits of the BESS. In other words, if the HPP charging power summed with the BESS regulation power is higher than the BESS power capacity, the HPP charging signal is set to zero. The nature of the SoC control process moving between charging, discharging and idling states, based on the SoC value and grid frequency is now obvious. Therefore, this modified control algorithm is implemented in a Stateflow chart in the simulation environment, displayed in Figure 6.9.

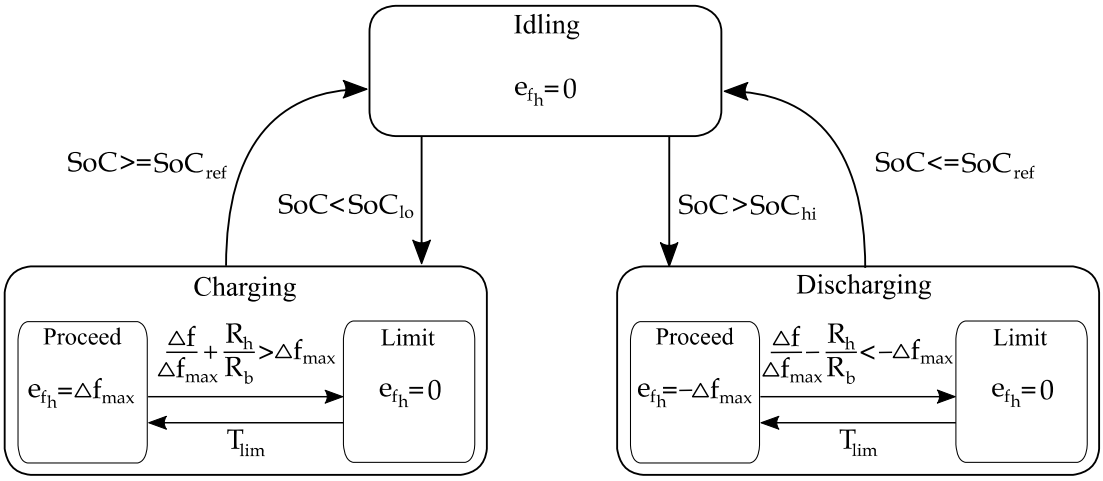

Figure 6.9. Hydro Recharge SoC control Stateflow chart

As was noted in (6.6), the transitions between the three main states are defined based on the SoC signal. The internal substates in the Charging and Discharging states are accounting for the power limitation of the BESS. The respective power limits are defined in the transitions to the Limit substate by scaling the total frequency deviation to the BESS regulation gain. If the limit is exceeded, the HPP charging power is set to zero and remains at that value for at least $T_{lim} = 180\ s$. This value is taken as the time the HPP governor needs to reach a steady state and is implemented to eliminate fast HPP reference changes

caused by the grid frequency oscillating around the BESS power limit. After T_{lim}, the Proceed substate is entered again until another limitation interrupts it or the SoC level reaches the reference.

With the Stateflow SoC control algorithm and (6.8) implemented inside the PPC, the Hydro Recharge unit is complete, and the model can be subjected to qualitative testing through the defined study case in (6.10) and (6.11). The Kaplan turbine model is used as these units were identified as better candidates for HBHS installation. However, it should be stressed that the dynamic behaviour of the Hydro recharge HBHS does not depend on the turbine type, since the regulation power is delivered entirely by the BESS. This further means that the only differences which would be seen during testing are the ones identified between the two turbine types in Figure 6.2, occurring during steps of the HPP power reference.

$$R_{unit} = R_b = R_h = 50\frac{MW}{Hz}, \qquad R_{sys} = R_{FCR-N} - R_h = 7480\frac{MW}{Hz} \tag{6.10}$$

$$SoC_{ref} = 50\ \%, \qquad SoC_{lo} = 40\ \%, \qquad SoC_{hi} = 60\ \% \tag{6.11}$$

Similar to the benchmark model, three qualitative tests are conducted. First, a single step deviation of Δf_{max} is introduced to the model, with the aim of confirming the dynamic behaviour of the Hydro Recharge HBHS and validating the PPC operation. The power response is displayed in Figure 6.10.

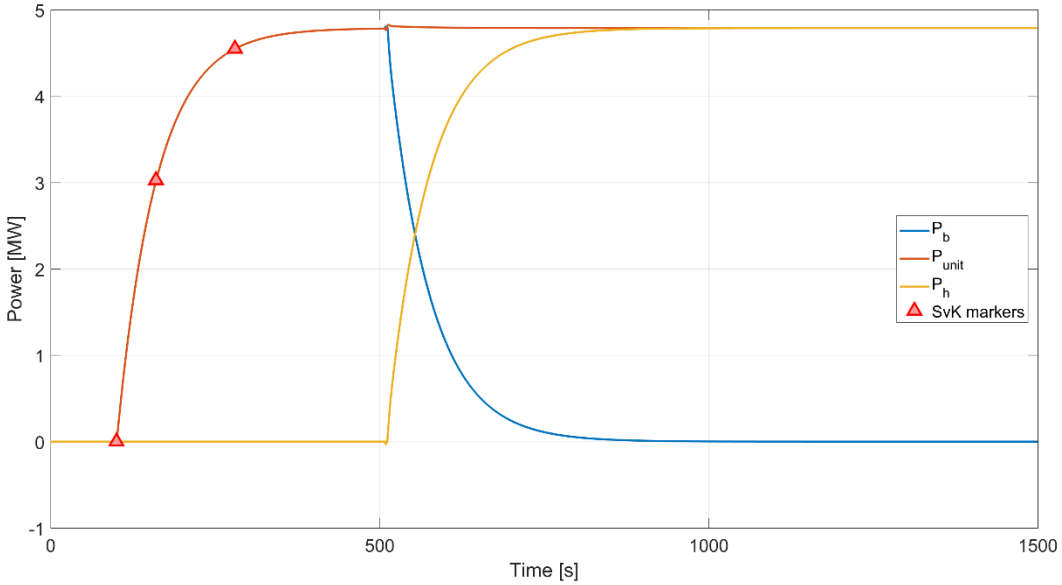

Figure 6.10. Hydro recharge HBHS step response test

From the unit power output, it can be confirmed that the assumption regarding the frequency filter constant was correct. The HBHS is following the SvK markers perfectly, corresponding to a 60-second time constant response. Until a certain point around 500 seconds of

simulation time, the HPP power output is equal to zero. When the SoC falls under the permissible band, the HPP power output increases with regards to R_h and the BESS output decreases respectively. These power changes are defined by the HPP governor speed. The impact of correcting the FCR-N capacity for the backlash can also be seen since, in the charging steady state, the BESS power output is exactly zero. This fact also brings about an important comment. The SoC control algorithm envisions states of charging and discharging the BESS, however, these states do not necessarily correspond to the BESS absorbing or releasing power. Instead, the charging is done indirectly through the regulation power and therefore the actual power exchange between the BESS and grid depends on the grid frequency as well. The HPP is rather substituting the power required by frequency regulation in order to allow for a SoC correction.

Next, the static prequalification test comprising of several frequency steps is performed. The same frequency sequence displayed in Figure 4.3 is introduced to the model, with the endurance requirement of one-hour steps.

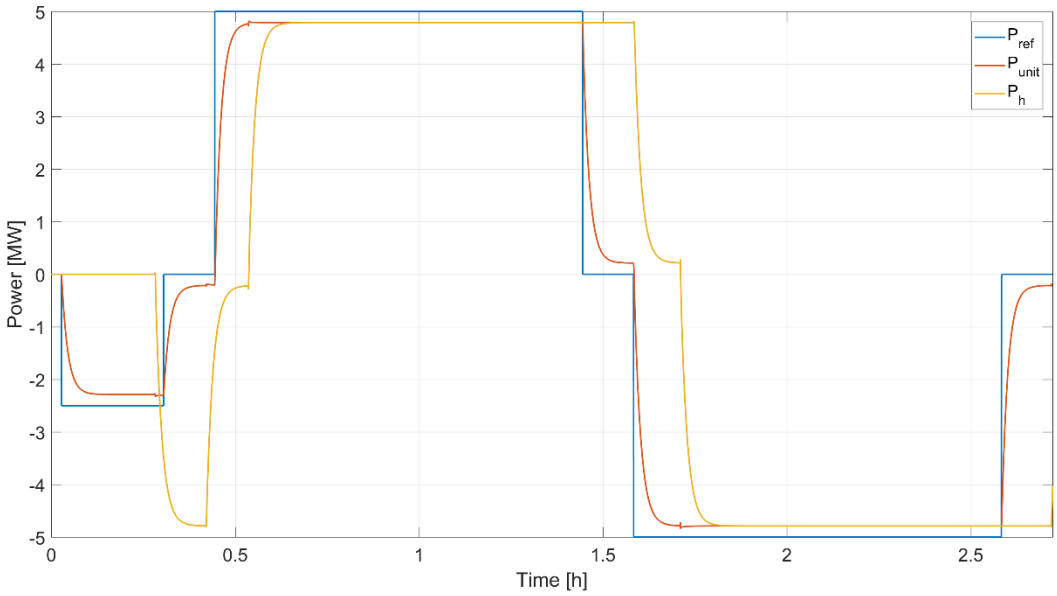

Figure 6.11. Hydro Recharge HBHS static prequalification test power

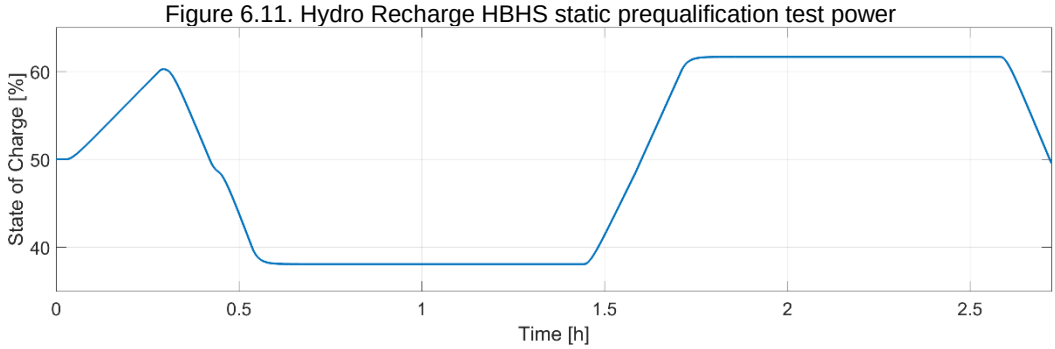

Figure 6.12. Hydro Recharge HBHS static prequalification test SoC

The power responses from the test can be seen in Figure 6.11. Same behaviour is observed with the unit power output following the regulation power reference. This test is a good

opportunity to observe the coordination or lack thereof between the regulation action and SoC control. The BESS state of charge during the test is displayed in Figure 6.12 and gives a clear motivation behind the HPP power steps. The control manages to keep the SoC within the 40 % to 60 % permissible band. Action of the power limitation described in Figure 6.9 is visible at the starts of the two big steps in frequency. At the moment of both steps, the HPP is discharging and charging the BESS respectively via the grid, and during both steps its output is reduced to zero in order not to impose a $2\Delta P_{max}$ power reference on the BESS. Other than this limit, there is no connection between the regulation and recharge algorithms. The test data signifies the same FCR-N capacity and backlash as the benchmark model, which was expected, i.e.

$$2D = 0{,}16\ \%, \qquad C_{FCR-N} = 4{,}79\ MW \tag{6.12}$$

With the static prequalification results displaying the same quality performance of the HBHS unit and the benchmark model, the unit is subjected to the dynamic test next. This test is expected to produce a significant difference to the benchmark tests. The results compared to the benchmark test are displayed in Figure 6.13.

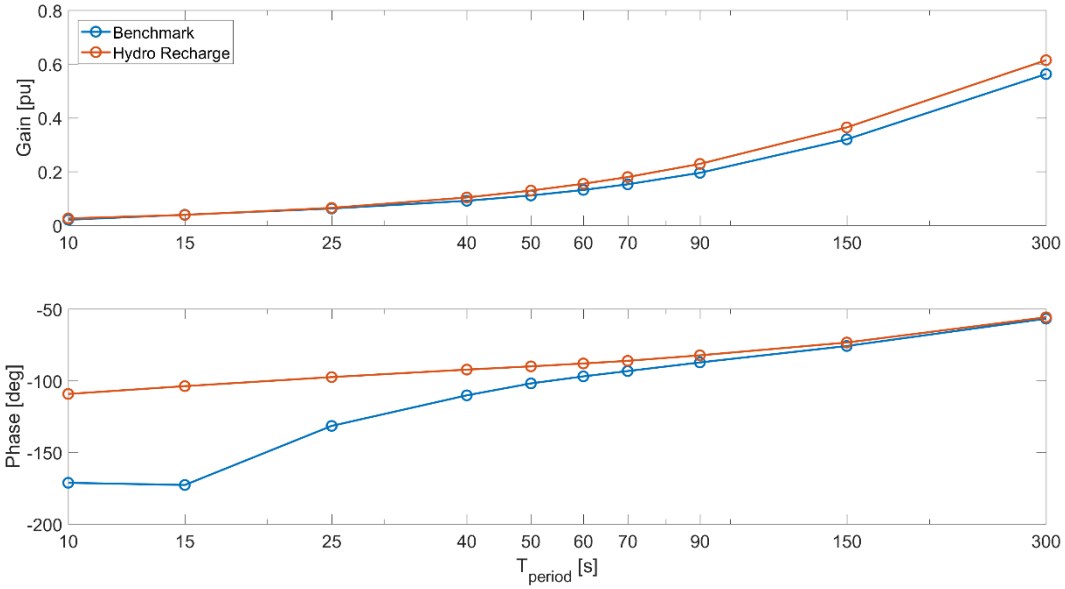

Figure 6.13. Hydro Recharge HBHS dynamic prequalification test

A significant improvement can be seen in both the gain ratio and the phase delay of the HBHS unit compared to the benchmark system. Single HPP units experience a degradation of their FCR-N capabilities with fast frequency oscillations, which is particularly visible in the benchmarked phase delay. The HBHS manages to alleviate this degradation by the BESS action, effectively eliminating the destabilizing behaviour shown in Figure 6.5. Additionally, with slow frequency oscillations, the HBHS manages to deliver more regulation power than the benchmark unit. In general, it can be said that the dynamic performance quality is improved overall, strengthening the previous claims that the HBHS can help qualify certain HPPs during sinusoidal frequency tests. It should be noted that, considering the Hydro

Recharge architecture, further performance improvement is only possible by reducing the unit response time constant and thus going above the response speed required by SvK. This can be concluded from the fact that all the frequency regulation in this unit is provided by the BESS, which reacts almost instantaneously to the filtered frequency measurement.

After the qualitative performance assessment, the quantitative estimation is done by allowing the HBHS to run continuously in the NPS with historical frequency data. The simulation timespan is taken to be the same 30 days of August 2018 as with the benchmark unit. The operation is again exemplified for a five-hour period in Figure 6.14. The obtained 1 168 minutes outside the normal frequency band validate the simulation results. Again, it can be said that the HBHS is providing the provisioned 5 MW of FCR-N in a similar manner to the benchmark. The HPP wear and tear during these 30 days is estimated to be

$$L_{wt} = 8\,153{,}7\ \%, \qquad N_{wt} = 7\,400 \tag{6.13}$$

giving an average movement of 1,10 %, which is an expected value since the full movement corresponding to Δf_{max} amounts to 2 %. The difference compared to the maximum movement is caused by the power limitation in the SoC control algorithm. A significant reduction of HPP wear and tear can be observed compared to the benchmark. The guide vanes and runner blades travel in this case 48,9 % of the distance but, more importantly, they do so in only 6,1 % of the number of movements. This substantial decrease of the number of regulation mechanism movements is considered very beneficial for the service life of Kaplan turbines. Furthermore, the small regulation movements of below 0,5 %, which are considered very inefficient, are practically eliminated.

During the simulated 30 days, the BESS manages to operate continuously, without experiencing SoC issues. The HPP succeeds in containing the SoC close to the permissible band. This is explained by the ability of the HPP to cover the entire regulation power capacity of the HBHS, allowing the HPP to prevent SoC changes in all operating conditions i.e. during all frequency values inside the normal band. This is a necessary condition for guaranteeing truly continuous operation of the HBHS, which will be discussed later. More information about the unit performance can be obtained from the behaviour of the SoC control algorithm. The number of times the Stateflow chart has entered the Charging or Discharging states is obtained to be

$$N_{Char} = 2\,085, \qquad N_{Disc} = 1\,610 \tag{6.14}$$

which allows for the influence of the Limit states to be estimated. Namely, these numbers represent the number of movement commands given to the HPP governor, as can be seen from Figure 6.9. Since they amount to 50 % of N_{wt}, the other 50 % is attributed to the power

limitation. These values also signify the number of times the SoC permissible band limit was reached, giving more insight into the BESS behaviour.

The resulting BESS degradation is evaluated by estimating the lifetime of the batteries in the unit, assuming they are continuously subjected to the operating conditions present during the simulation. These calculations give

$$L_b = 21{,}81\ yrs, \qquad C_{used} = 37{,}24\ \% = 1{,}86\ MWh \tag{6.15}$$

where L_b stands for the lifetime estimation and C_{used} for the BESS capacity that was used during operation. The reason behind the considerably long lifetime estimate can be uncovered from the fact that a just over one third of the 5 MWh capacity is used. This further means that the BESS is substantially oversized for these unit specifications. The possibility of optimizing the unit size and gains, to make the system more cost-efficient, is thus presented.

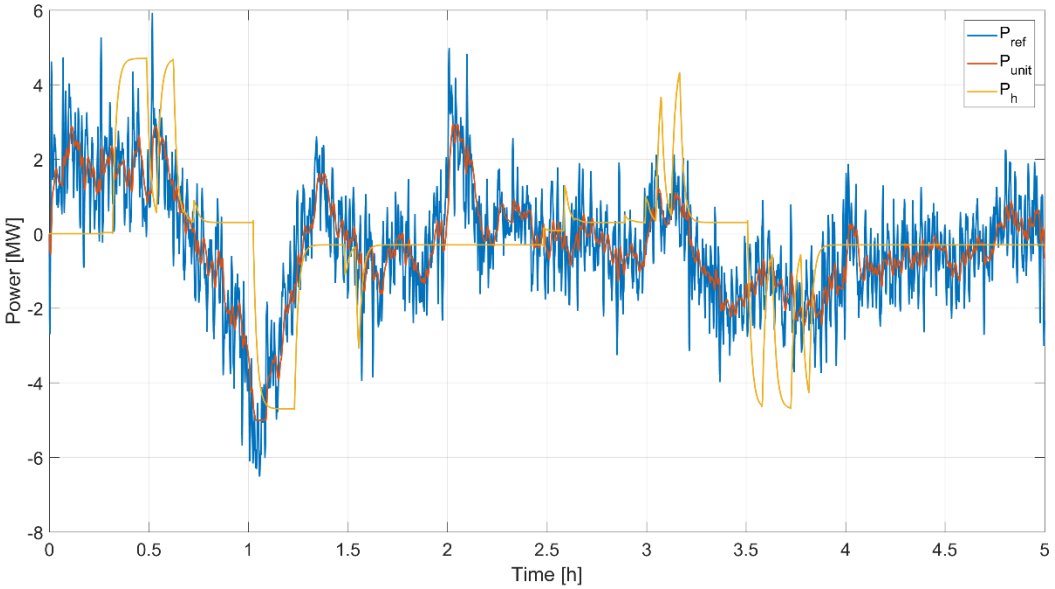

Figure 6.14. Hydro recharge HBHS operation in the NPS

6.3 Frequency Split HBHS

The second HBHS architecture represents a combination of the Hydro Recharge and the benchmark unit. As these arrangements included one of the two elements delivering regulation capacity, the Frequency Split includes both the HPP and BESS delivering FCR-N to the grid, with the measured grid frequency being, as the name suggests, split between them. In addition to providing FCR-N, the HPP is also tasked with compensating the BESS output power based on the SoC measurement. Therefore, both the HPP and BESS model are included and the need for a PPC is also evident, resulting in the model in Figure 6.15, with the same structure as the Hydro Recharge model.

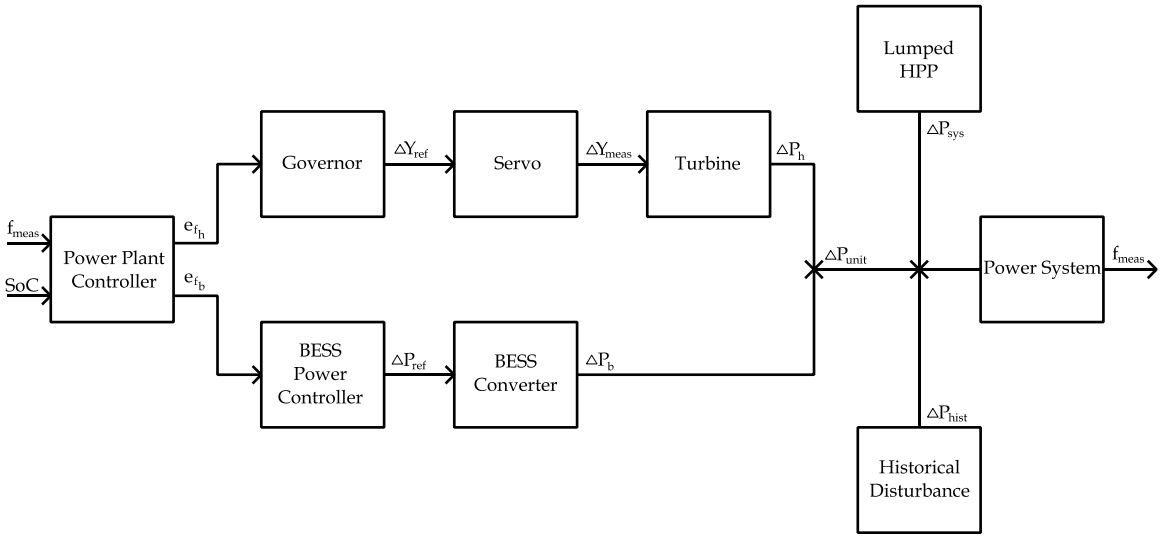

Figure 6.15 Frequency Split HBHS model

Similar to the Hydro recharge, the PPC of the unit is tasked with measuring the grid frequency and generating the frequency error signals for the single HPP and BESS, e_{f_h} and e_{f_b} respectively. The motivation behind having both elements performing frequency regulation together is an attempt to create more flexible FCR-N operation which would play to the individual strengths of both elements. This translates into splitting the frequency in a way that would allow the BESS to react fast and efficiently whilst transferring most of the requested endurance to the HPP. This is performed in a simple manner where the BESS is tasked with following the TSO requirements for FCR-N provision, with regards to the frequency deviation and the HPP power output. This gives the same expression for its frequency error as the Hydro Recharge i.e.

$$e_{f_b}(s) = \frac{1}{T_{unit}s + 1}\left[f_{ref} - f_{meas}(s)\right] - \frac{\Delta P_h(s)}{R_b} = \frac{1}{T_{unit}s + 1}\Delta f(s) - \Delta f_h(s) \qquad (6.16)$$

with the response time constant set to the same 60 seconds and the backlash compensation from (6.9) implemented. As a result of this error signal creation, the BESS, thanks to its superior dynamics, will fulfil the performance requirements for the HBHS independently of the HPP output power. This means that the HPP operation is given more flexibility and can be focused on HBHS endurance and SoC compensation.

The focus on endurance of the HPP is accomplished by splitting the frequency signal in a way that more long-standing references are forwarded to the HPP. In other words, the frequency deviation is heavily filtered in order to create the error signal for the HPP. This can be done in the PPC using a filter with T_{hf}, that, when combined with the governor time constant T_{gov}, will provide the desired slower response characterized with T_{hydro} i.e.

$$T_{hf} = T_{hydro} - T_{gov} \tag{6.17}$$

keeping in mind that this creates a second-order response that can only be approximated with the time constant T_{hydro}. Another option is to change the HPP governor parameters in order to directly implement this increased time constant. Looking at the governor PI controller with droop, this is easily done by recalibrating the integral gain of the controller to

$$K_i = K_i \frac{T_{gov}}{T_{hydro}} \tag{6.18}$$

which will give a pure first-order response with the governor time constant T_{hydro}. Remaining true to the working assumption that the HBHS is supposed to the installed on top of an existing HPP and as such, the HPP should not be altered, the first approach with a PPC filter is implemented setting $T_{hydro} = 300\ s$. This gives the expression

$$e_{f_h}(s) = \frac{1}{T_{hf}s + 1}\left[f_{ref} - f_{meas}(s)\right] = \frac{1}{T_{hf}s + 1}\Delta f(s) \tag{6.19}$$

However, the error signal for the HPP is not complete, as the SoC compensation must be implemented as well. The idea behind the compensation is similar to the one behind the SoC control in the Hydro Recharge HBHS. Namely, when the SoC has gone out of the permissible value band, the HPP adjusts its output power with the aim of charging or discharging the BESS. The power output is adjusted by creating an artificial frequency deviation which is added to the measured one with a sign corresponding to the desired HPP action i.e.

$$\Delta f_{SoC}(s) = \begin{cases} \Delta f_{char}, & SoC < SoC_{lo} \\ 0, & SoC_{hi} \geq SoC \geq SoC_{lo} \\ -\Delta f_{char}, & SoC > SoC_{hi} \end{cases} \tag{6.20}$$

where Δf_{char} is defined freely, in this case as

$$\Delta f_{char} = \frac{\Delta f_{max}}{2} \tag{6.21}$$

The same conditions for state transitions are used as for the Hydro Recharge HBHS, meaning that the compensation is initiated when the SoC is out of the permissible band and stopped when SoC_{ref} is reached, as displayed in the Stateflow chart in Figure 6.16.

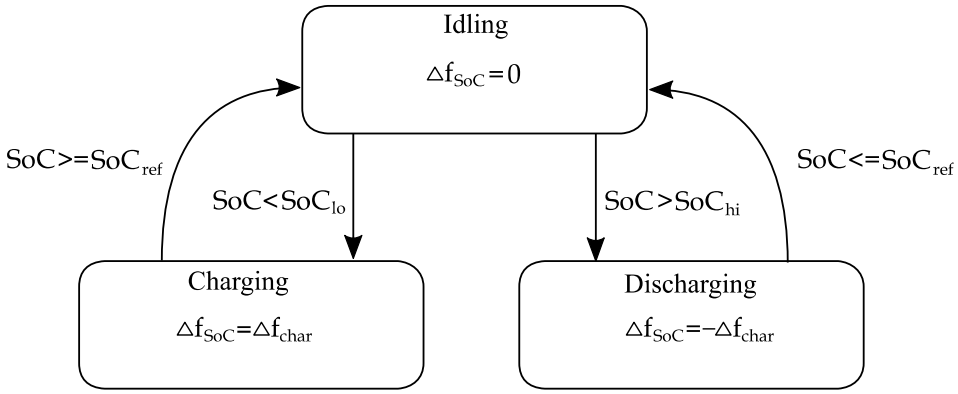

Figure 6.16. Frequency Split SoC compensation Stateflow chart

As can be seen from the Stateflow chart, the BESS power limitation issues encountered with the Hydro Recharge HBHS are not present here, since the individual power limits ΔY_{max} and ΔP_{max} and their combination will limit the HPP output accordingly. With the SoC compensation implemented, the final error signal for the HPP is created as stated below.

$$e_{f_h}(s) = \frac{1}{T_{hf}s + 1}\Delta f(s) + \Delta f_{SoC}(s) \tag{6.22}$$

The implementation of (6.16), (6.22) and the Stateflow SoC compensation algorithm in the PPC completes the Frequency Split HBHS unit.

The three FCR-N qualitative tests are performed with the same study case, repeated in (6.23) and (6.24), but now with the Frequency Split architecture implemented. Again, a Kaplan turbine model is used, as these HPPs are identified as better candidates for the HBHS installation.

$$R_{unit} = R_b = R_h = 50\frac{MW}{Hz}, \qquad R_{sys} = R_{FCR-N} - R_h = 7480\frac{MW}{Hz} \tag{6.23}$$

$$SoC_{ref} = 50\ \%, \qquad SoC_{lo} = 40\ \%, \qquad SoC_{hi} = 60\ \% \tag{6.24}$$

First, a single step deviation of Δf_{max} is introduced to the model, with the aim of confirming the dynamic behaviour of the Frequency Split HBHS and validating the PPC regulation operation. The power response is displayed in Figure 6.17. It is easily visible that both the HPP and BESS react to the frequency change, the BESS doing so instantly and following the SvK speed requirements. After some delay, the HPP power output starts ramping up with a time constant close to the defined $T_{hydro} = 300\,s$. The reaction of the BESS is maintaining the smooth response of the HBHS with the required steady-state FCR-N capacity, which results in a zero steady-state BESS power output. The SoC compensation cannot be seen in this graph since the SoC level does not fall below SoC_{lo} and even if it did, the HPP power limit would limit the recharge power, since $\Delta f = \Delta f_{max}$ during the test. A

control parameter worth mentioning for its use in industry for these systems, is the so-called crossover time, or the time at which the HPP power output surpasses the BESS power output, measured from the frequency step. The name is given since this point is the crossover between the two power signals and is read to be $T_{cross} = 242\ s$ from Figure 6.17.

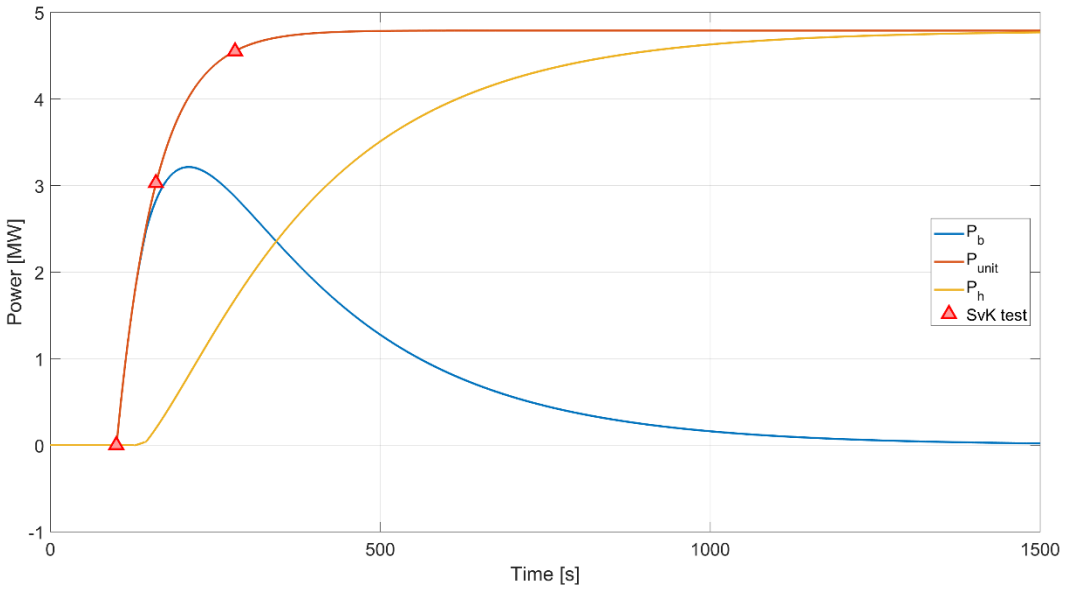

Figure 6.17. Frequency Split HBHS step response test

Next, the static prequalification test for SvK is performed. The frequency sequence displayed in Figure 4.3 is introduced to the model, with the endurance requirement of one-hour steps. The power response of the Frequency Split HBHS can be seen in Figure 6.18, with the SoC during the test given in Figure 6.19.

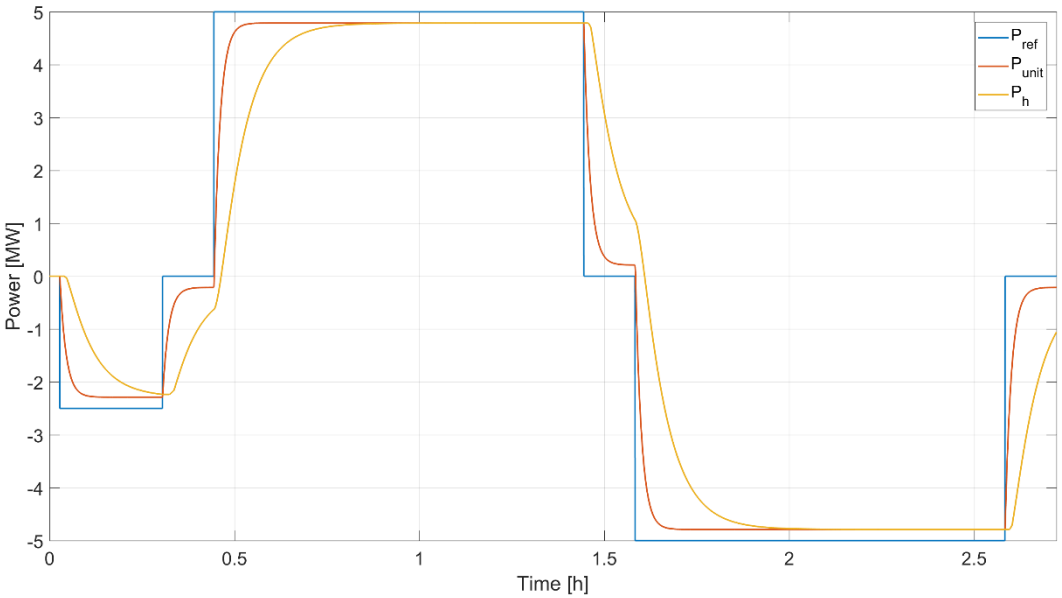

Figure 6.18. Frequency Split HBHS static prequalification test power

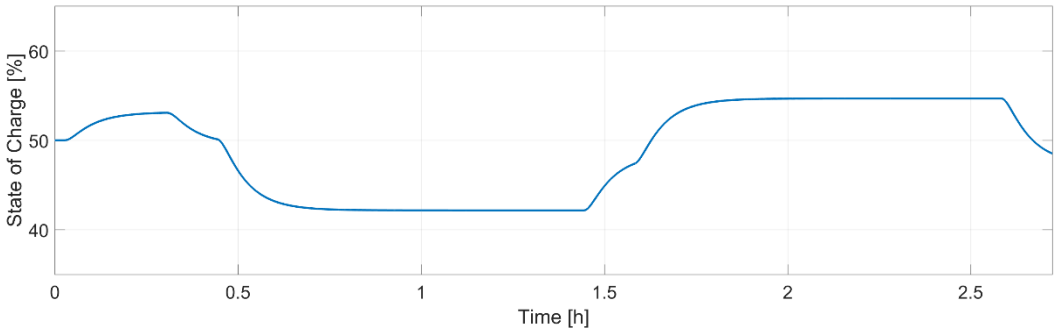

Figure 6.19. Frequency Split HBHS static prequalification test SoC

The power response again demonstrates that the reference is followed by the HBHS as required and in the same manner but more slowly by the HPP. The BESS power output covers the difference between these two signals and is active only until a steady state is reached, which is an explanation as to why the SoC is not exiting the permissible band during this test, as seen in Figure 6.19. This fact already suggests that the approach for the frequency split was correct. The BESS is taking over the faster frequency dynamics but is not experiencing significant stress since the HPP is taking over slower, more energy-demanding dynamics. The test data once again signifies the same FCR-N capacity and backlash as the benchmark model, which was expected, i.e.

$$2D = 0{,}17\%, \qquad C_{FCR-N} = 4{,}79\ MW \tag{6.25}$$

As the same static performance is established for this HBHS architecture as for the benchmark and the Hydro Recharge HBHS, the dynamic prequalification test is conducted next. The 10 different sinusoidal frequency deviations are introduced into the system and the Bode plot in Figure 6.20 is obtained as a result of the testing. Similar performance improvements are seen as with the Hydro Recharge unit test, given in Figure 6.13. This HBHS also manages to alleviate the performance degradation by the BESS action during fast frequency oscillations and deliver more regulation power during slower oscillations. The possibility of the HBHS qualifying certain HPPs for FCR-N deliver is again noted. A comparison between the Hydro Recharge and Frequency Split architectures can also be made. As was mentioned, the BESS is delivering the entirety of the regulation power in the Hydro Recharge architecture, making the frequency dynamics equal to the BESS dynamics. The HPP is delivering regulation power in the Frequency Split unit, however, the HPP response is so slow that it cannot capture most of the oscillations in Figure 6.20. Therefore, differences between the two HBHS architectures are minimal and can only be seen during the tests with the longest time period such as the 150-second and 300-second tests.

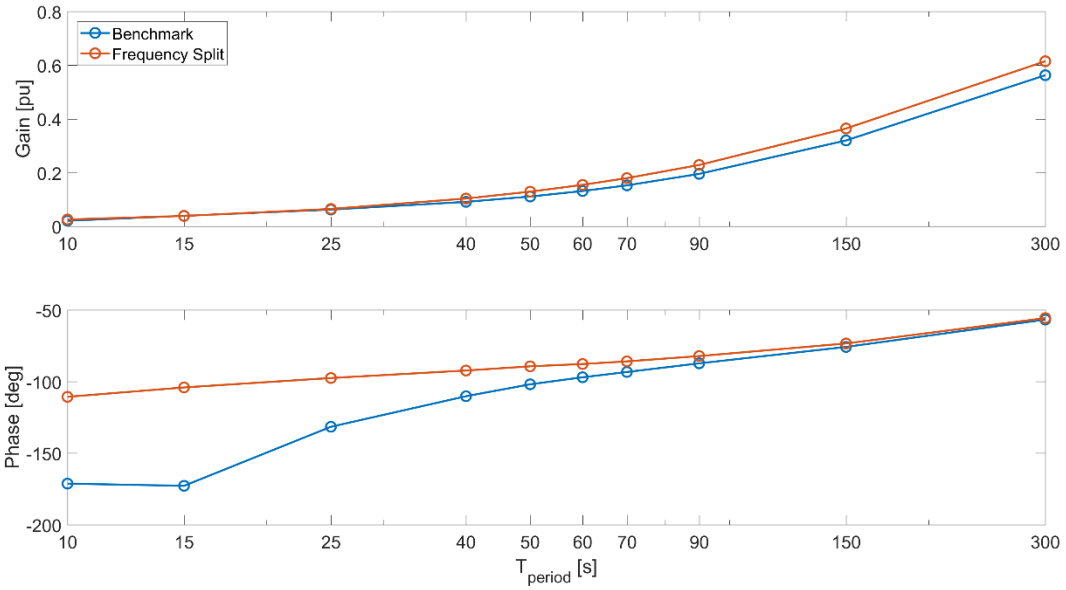

Figure 6.20. Frequency Split HBHS dynamic prequalification test

Finally, the quantitative performance estimation is done by running the HBHS in the NPS during 30 days of August 2018. The operation during five hours of the month is displayed in Figure 6.21 and is validated by the resulting 1 169 minutes outside the normal frequency band. Again, it can be said that the HBHS is providing the provisioned 5 MW of FCR-N in a similar manner to the benchmark. The HPP wear and tear during these 30 days is estimated to be

$$L_{wt} = 2\,333{,}2\ \%, \qquad N_{wt} = 6\,182 \tag{6.26}$$

giving an average movement of 0,38 %. This value is between the benchmark and Hydro Recharge value, which is expected since the Frequency Split is filtering the small movements but is still providing FCR-N from the HPP, which increases the total number of movements. These results again show a drastic reduction of the HPP wear and tear compared to the benchmark, with the HPP regulation mechanism travelling only 14,0 % of the benchmarked distance and doing so in 5,1 % of the movements. This massive decrease in both parameters is very beneficial for the service life of Kaplan turbines. Compared to the Hydro Recharge, the Frequency Split results in the guide vanes travelling just over a quarter of the distance in 16,5 % less movements. Although this comparison is very interesting, it is hard to draw conclusions on behaviour since the approach to frequency regulations differs greatly.

What can be more easily compared is the operation of the BESS. Again, the BESS manages to operate continuously, without experiencing SoC issues. This together with the BESS degradation, evaluated by estimating the lifetime of the batteries in the unit, gives

$$L_b = 47{,}07\ yrs, \qquad C_{used} = 23{,}00\ \% = 1{,}15\ MWh \tag{6.27}$$

What can be seen is that the BESS lifetime more than doubled compared to the Hydro Recharge HBHS, which is well above any battery life expectancy. A similar reason can be given as to why the lifetime estimate is so high from the fact that under 25 % of the storage capacity is utilized. This is a decrease compared to the Hydro Recharge utilizing 37 %. Another reason behind this can be found in the significant decrease of the number of times the SoC compensation algorithm enters Charging and Discharging states compared to the Hydro Recharge, i.e.

$$N_{Char} = 128, \qquad N_{Disc} = 20 \tag{6.28}$$

These facts support the idea behind the Frequency Split architecture, in which both the BESS and HPP are performing frequency regulation. It is concluded that the stress on the BESS is significantly reduced by the HPP participation, additionally reinforcing the assumption that the coordination of both elements is beneficial for both of them individually.

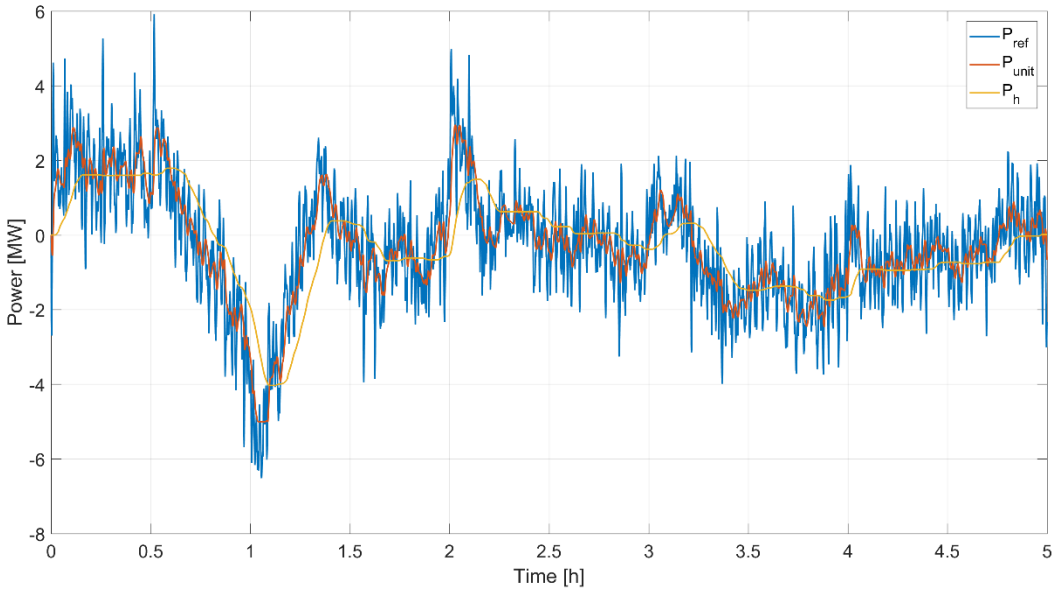

Figure 6.21. Frequency Split HBHS operation in the NPS

Finally, it can be concluded that the Frequency Split architecture gives even more opportunities for performance optimization, considering the oversized BESS and the fact that many parameters in the PPC were set freely. The motivation behind these examples was to explain their operation and present possible performance improvements compared to the benchmark. A true quantitative comparison and the resulting cost-efficiency require the definition of system sensitivity and parameter dependency, which will be done next.

7 HBHS Optimization

During the introduction of the two HBHS architectures, qualitative and quantitative comparisons with the benchmark single HPP were performed. Significant improvements in the dynamic response of the HBHS units were observed. In addition, when running the hybrid units in the NPS with historical frequency data, substantial decreases of the estimated HPP wear and tear were observed. However, for both systems, the same amount of FCR-N was qualified as for the benchmark, following the SvK prequalification test from Figure 4.3, and amount of gain R_h that was used from the HPP was equal to the HBHS gain R_{unit} that is provided to the grid. Furthermore, it was concluded that the BESS was oversized for the defined HBHS specifications.

A very important conclusion can be drawn from these facts. Assuming that the single HPP can qualify for FCR-N provision without the addition of a BESS, this HPP would have the same financial income from FCR-N provision as a potential HBHS in its place with these specifications. Therefore, the capital investment for the BESS installation would have to be justified from the decrease in operational expenses i.e. the reduction of HPP wear and tear. This proves to be very difficult, even with a smaller BESS, considering the lack of experience in the industry with such hybrid systems and the difficulties estimating the financial costs of HPP wear and tear [42]. This further means that the financial viability of the defined HBHS is present only at HPPs which would not be able to pass the future dynamic prequalification tests from Figure 4.4.

The straightforward way of improving the financial viability of the HBHS project is to increase the financial income from the FCR-N. Simply put, this entails qualifying and selling more FCR-N capacity from the HBHS than the HPP regulation capacity. This would set the difference in the gains R_h and R_{unit} as the income difference before and after the BESS installation and could thus make the investment financially viable. In addition to this, other parameters, such as the permissible SoC band, SoC control parameters and HPP regulation response filters can be altered in order to decrease the operational expenses of the HBHS to a possible minimum. These are the considerations motivating the optimization of the two introduced HBHS architectures. First, the following assumptions about the optimization process are adopted:

- The HBHS unit regulation gain is kept constant while the HPP regulation gain is varied.
- The BESS energy capacity is kept constant.

- The HBHS is designed for continuous operation i.e. FCR-N capacity is sold for every hour of simulation time, in order to limit the influence of market dynamics and trends on the optimization.

- The stochastic nature of the grid frequency and its influence on required BESS energy capacity are recognized in the fact that continuous operation cannot be guaranteed for systems with $R_h < R_{unit}$.

- If the HBHS achieves continuous operation for a 30-day simulation with historical data, it is assumed capable of continuous operation with an acceptable statistical margin.

According to the previous assumption of installing the HBHS in existing HPPs, a more natural optimization course could be varying the BESS capacity and regulation gain. However, considering that the HBHS regulation gain is inherited from the BESS and that the BESS degradation estimation is highly dependent on its storage capacity, this approach may prove more difficult for comparing the performance of different architectures. Either way, the obtained ratios between Rb and Rh and the corresponding BESS capacity are independent of their individual size, giving the same result from the chosen optimization approach.

The dynamic behaviour of the HBHS with regards to FCR-N provision is entirely dependent on the BESS and its dynamic characteristics, with no HPP dependency in the Hydro Recharge and very little dependency in the Frequency Split architecture. This further means that, with the aforementioned assumptions, the quantitative performance is evaluated during optimization i.e. the HBHS operation is simulated in the NPS with historical data, for a shorter time period of three days.

7.1 Hydro Recharge Optimization

Applying these assumptions to the Hydro Recharge HBHS architecture and observing possible parameter variations, the following description of the unit is obtained.

$$R_{unit} = R_b = 50\frac{MW}{Hz}, \qquad R_h = var, \qquad R_{sys} = R_{FCR-N} - R_h \tag{7.1}$$

$$C_{rate} = 1 \tag{7.2}$$

$$T_{lim} = var, \qquad SoC_{ref} = 50\ \%, \qquad SoC_{lo} = var, \qquad SoC_{hi} = var \tag{7.3}$$

The HBHS gain is kept constant and invites the same value for the BESS gain, as this element is providing the entire FCR-N capacity in this architecture. The regulation power of

the HPP is variable and defines what are the SoC control power capabilities. It should be noted that the same effect can be achieved with keeping $R_h = R_{unit}$ and varying the error signal e_{f_h} strength to less than Δf_{max}. However, the approach of varying the R_h is used since it is believed to better depict the participation of the HPP in FCR-N and would prove simpler to integrate into other HPP functionalities. In addition to this, the SoC control parameters in (7.3) are set as variables, apart from the reference SoC value, which is defined by the symmetrical requirement of the FCR-N service. This also further dictates that the permissible SoC value band should be symmetrical around 50 %. In general, it can be said that optimization possibilities revolve around the HPP operation, which is understandable since the BESS is bound in inflexible operation delivering FCR-N.

First, the impact of varying the HPP regulation gain R_h and thus the BESS recharge power is examined. In cross-reference with the recharge power strength, a variation of the recharge command timing is implemented. This translates into a range of values set for both R_h and SoC_{lo} and SoC_{hi}. The HPP gain's upper limit is set as the HBHS gain, which was used in the previous examples. The lower limit for the HPP gain is theoretically zero, which would result in a BESS stand-alone operation, thus abandoning the HBHS architecture. Because of this, a lower limit above zero is set. The lower limit for the width of the SoC band is theoretically also zero, which is implemented, while the upper limit is defined by the capacity at 50 %. As waiting until the BESS is empty to recharge it does not correlate with continuous operation, the width of the band is selected to be smaller, finally giving

$$R_h \in [10 \;\; 50] \; \frac{MW}{Hz}, \qquad SoC_{band} \in [0 \;\; 20] \; \% \tag{7.4}$$

which translates into

$$\begin{aligned} SoC_{lo} &= SoC_{ref} - SoC_{band} \in [30 \;\; 50] \; \% \\ SoC_{hi} &= SoC_{ref} + SoC_{band} \in [50 \;\; 70] \; \% \end{aligned} \tag{7.5}$$

The results of running the Hydro Recharge HBHS in the NPS for 3 days, with parameters taking the range of values in (7.4), can be seen in Figure 7.1. The vertical axis displays the HPP gain in per-unit of HBHS gain, while the horizontal axis denotes the width of the SoC band.

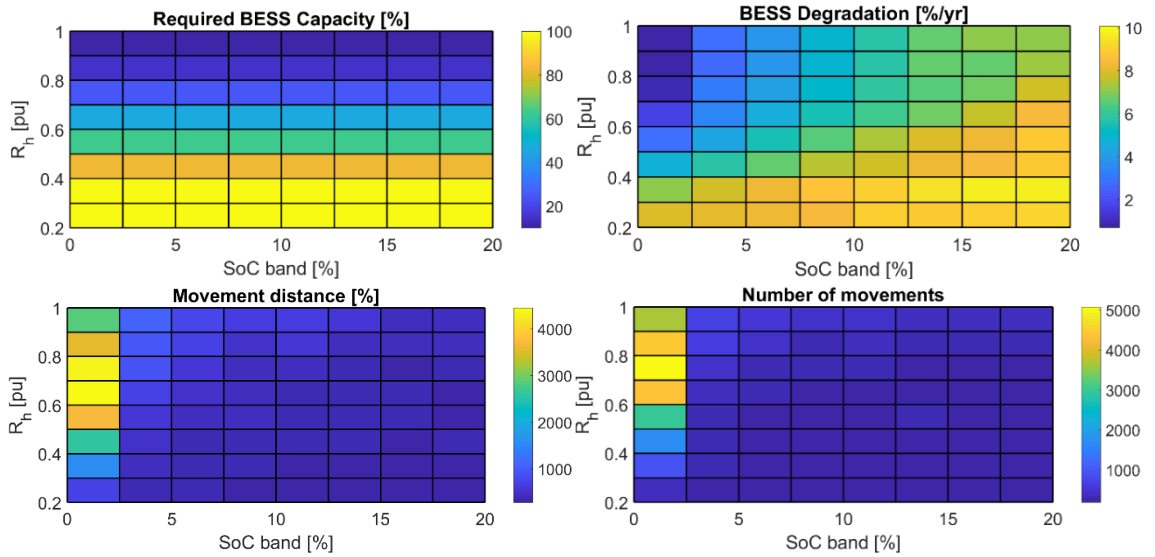

Figure 7.1. Impact of varying the HPP gain and SoC permissible band

The results give several important conclusions, first of which is the fact that the utilized or required BESS storage capacity is strongly dependent on the HPP gain. Values in the vicinity of the 30 %, obtained from the previous test in (6.15) can be seen for HPP gains close to 1 pu. The full capacity of the $C_{rate} = 1$ battery is used when the HPP is providing less than 0,4 pu of FCR-N regulation power, meaning that continuous operation is not possible with these gains. The explanation behind this high dependency is easily given by observing Figure 6.10. When the HPP gain is lower than the HBHS gain, the HPP can only compensate the BESS power output until the frequency deviation reaches the same ratio to 0,1 Hz as the R_h value in per-unit. Therefore, for larger deviations, the HPP cannot compensate the power output and the BESS continues to charge or discharge. As the gain ratio decreases, the amount of frequency deviations which cannot be compensated increases. This is exactly why continuous operation cannot be guaranteed with certainty if $R_h < R_{unit}$. Because of the stochastic nature of the frequency, it is possible that the deviations stay larger than the compensation capability for long enough to deplete or saturate the BESS. Therefore, the issue of continuous operation of the HBHS crosses into the realm of frequency statistics.

A large variance of the BESS degradation, depending on both parameters, is also seen. The lifetime estimation of around 10 years, for low HPP gains and a wide SoC band, increases to over 20 years for high gains and a narrow SoC band. The dependency on the HPP gain is clearly motivated by the required BESS capacity, with deeper BESS cycles occurring with lower gains. The dependency on the SoC band is similarly explained with deeper cycles having to occur for the SoC to be compensated.

A massive spike in the HPP wear and tear is seen for a zero SoC band, which is easily explained by the fact that this setting eliminates the Idling state in the SoC control

from Figure 6.9. This results in the HPP jumping from Charging to Discharging states, all the while operating with the possibility of entering the Limit substate. The wear and tear this setting causes, during three days, is close to the wear and tear after a full month of operation of the example Hydro Recharge unit. After the width of the SoC band surpasses 5 %, the wear and tear estimation holds relatively constant.

With an assumed continuous operation area for a $C_{rate} = 1$ battery obtained as a result of these variations, the influence of another SoC control parameter is examined. The HPP gain is set to 25 MW/Hz to provide continuous operation, and the SoC permissible band is varied again, together with the time limitation for the Limit substate T_{lim}. The theoretical lower limit for T_{lim} is zero while the upper limit can be freely chosen. The SoC band range is further reduced since it has shown that a value larger than zero is needed and that there is no benefit in reaching values of 20 % i.e.

$$T_{lim} \in [0 \;\; 300]\, s, \qquad SoC_{band} \in [2{,}5 \;\; 15]\,\% \tag{7.6}$$

This variance of the SoC control algorithm parameters produces the graphs is displayed in Figure 7.2, where now the time limitation is put on the vertical axis.

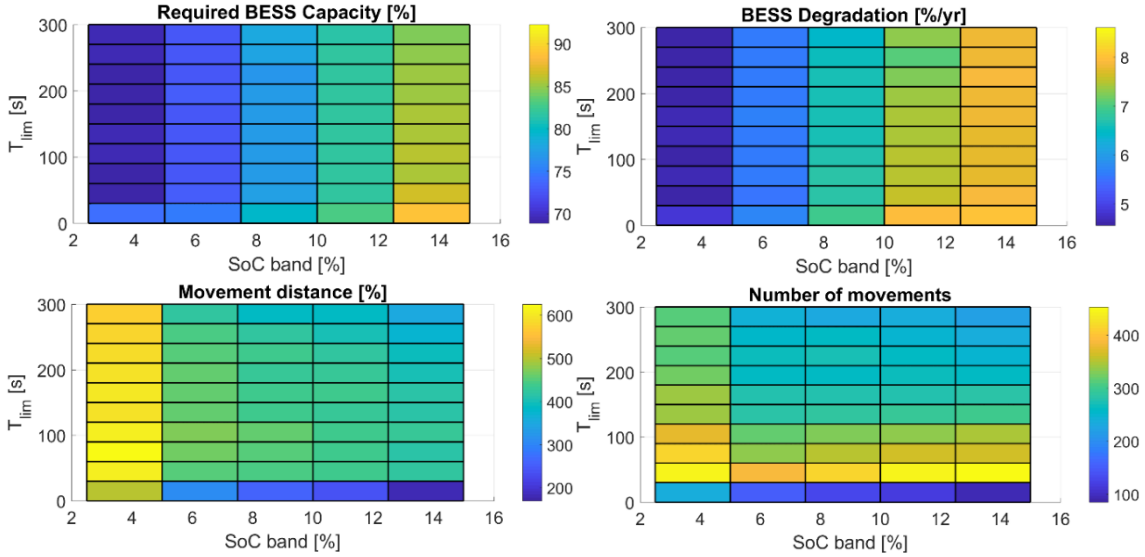

Figure 7.2. Impact of varying the time limitation and SoC permissible band

The variations of required BESS storage capacity and its lifetime are significantly smaller with these parameters than with the HPP gain. The dependency on T_{lim} is only present for values close to zero where they both increase slightly. The obtained dependency of the HPP wear and tear is more complex. The distance travelled by the guide vanes decreases with a longer limitation time, except for $T_{lim} = 0$, for which it drops significantly. This is explained by looking into the Stateflow chart during the simulation and realizing that, for this value, the SoC control algorithm starts to oscillate between the Limit and Proceed substates when the power limitation is reached. This prevents the algorithm from performing correctly

since no constant reference is given to the HPP. This zero setting is thus disqualified. Finally, a more significant decrease in the number of movements is seen with the increase of the time limitation.

From these variances, a possible optimal HBHS specification can be established. As was already mentioned, the desired HPP gain would be one that can deliver continuous operation while utilizing as much of the BESS storage capacity as possible. As a compromise between the BESS degradation and HPP wear and tear, a narrow SoC band, larger than zero, is selected. Lastly, the time limitation is recognized as the least influential parameter and should be set to a relatively large value, like the one used in the example. These optimal specifications are given below.

$$R_h = 25\ \frac{MW}{Hz}, \qquad SoC_{band} = 5\ \%, \qquad T_{lim} = 180\ s \tag{7.7}$$

The operation of such a system can be demonstrated by running the static prequalification test with the 25 MW/Hz gain. The test result is displayed in Figure 7.3.

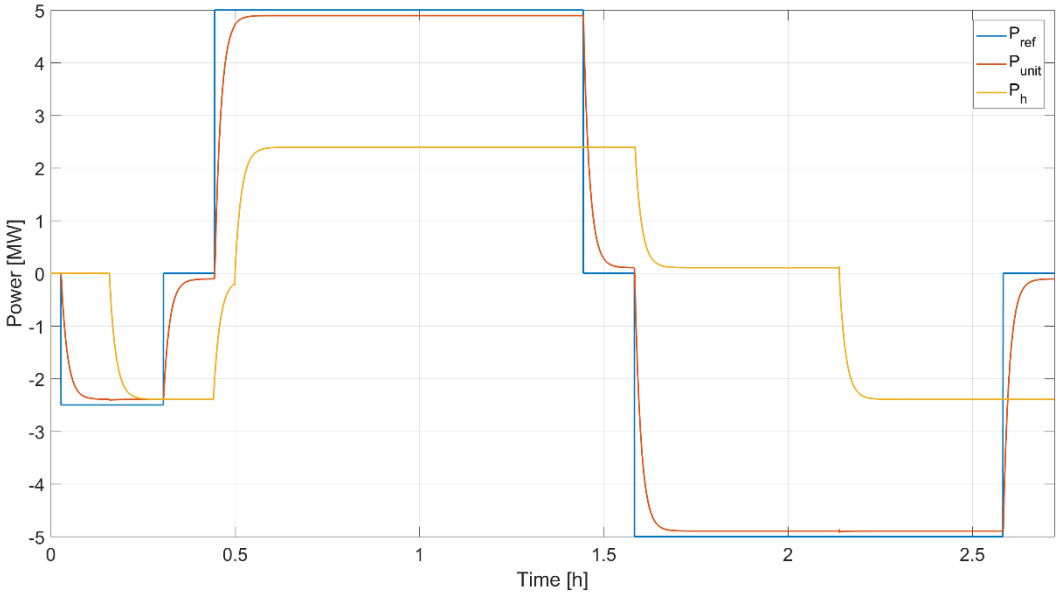

Figure 7.3. Optimal Hydro Recharge HBHS static prequalification test

Independent of the frequency deviation, the maximum power output of the HPP holds at 2,5 MW which corresponds to the set gain. The first step represents a deviation that can be compensated whereas the HPP cannot compensate for the following maximum frequency deviations.

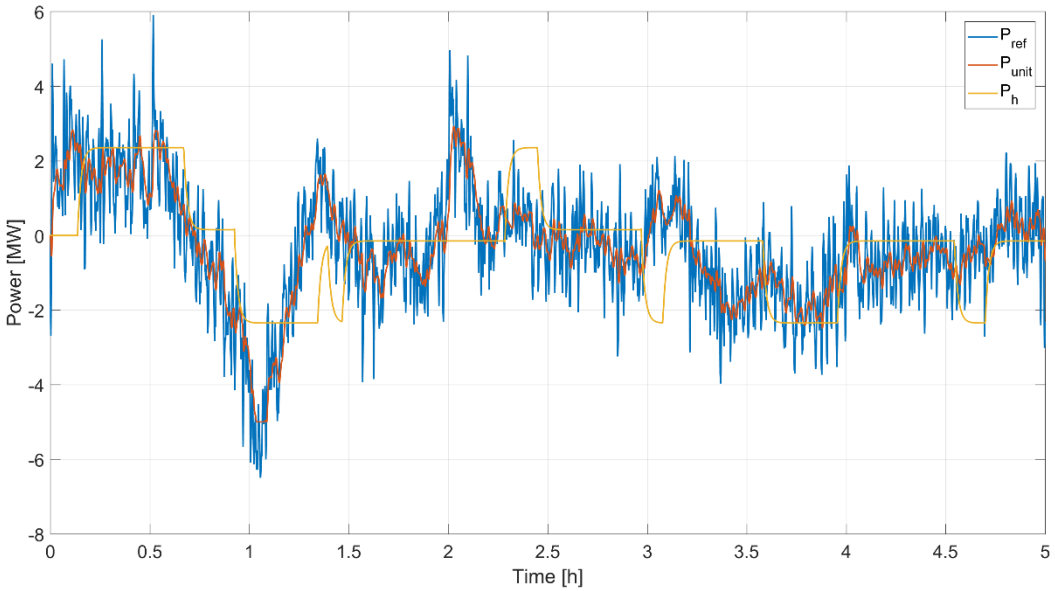

Figure 7.4. Optimal Hydro Recharge HBHS operation in the NPS

Finally, the operation of the proposed optimal HBHS is compared to the benchmark unit quantitatively using the HPP and BESS fatigue parameters. The simulation is again performed for the 30 days in August 2018, with an example displayed in Figure 7.4. The resulting 1 149 minutes spent outside the normal frequency band validate the power system operation. The time is lower since this HBHS effectively added $R_{unit} - R_h$ of FCR-N capacity to the system, according to (7.1). These effects on the power system will be further investigated later. The HPP wear and tear is estimated at

$$L_{wt} = 4\,406{,}4\ \%, \qquad N_{wt} = 2\,644 \tag{7.8}$$

giving an average movement of 1,67 %, which is close to the regulation mechanism maximum of 2 %. The even further reduction of wear and tear compared to that of the example Hydro Recharge HBHS in (6.13) can be attributed to gain ratio and frequency dynamics. Namely, with this gain, the HPP can compensate up to half of Δf_{max}, above which the SoC continues to deviate from the reference, leaving the HPP in the Charging or Discharging state for longer. This is confirmed by the reduced number of entries into these two active states which amount to

$$N_{Char} = 679, \qquad N_{Disc} = 638 \tag{7.9}$$

Additionally, the power limitation is now activated at a larger frequency deviation which occurs less frequently, thus reducing the number of movements. Compared to the benchmark unit, the guide vanes travel 26,4 % of the distance in only 2,2 % of the number of movements. The HPP wear and tear can be compared directly with the benchmark results even when the HPP is delivering less power since the values are normalized with regards to the unit gains and thus the guide vane opening.

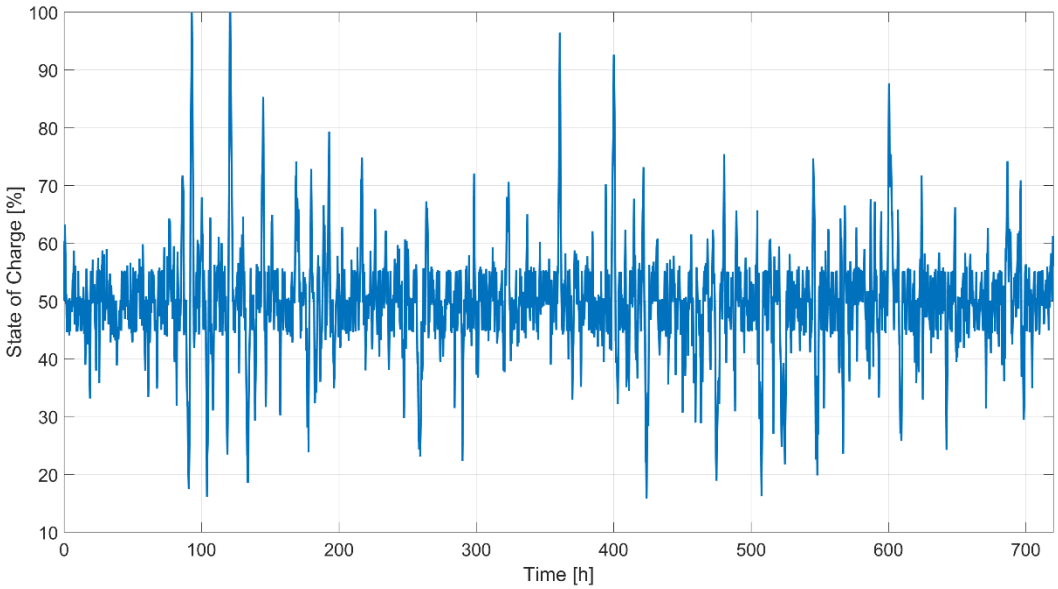

Figure 7.5. Optimal Hydro Recharge HBHS SoC during operation in the NPS

During the simulated 30 days, the BESS manages to operate continuously, with short interruptions, as displayed in Figure 7.5. The SoC does reach 100 % for a total of 20 minutes but it does not reach zero, meaning that it is unable to provide FCR-N for 0,04 % of the operation time. This is deemed low enough to constitute continuous operation, since it is within unit availability and reliability margins. The estimated lifetime of the BESS unit is obtained at

$$L_b = 22{,}29\ yrs, \qquad C_{used} = 84{,}2\ \% = 4{,}21\ MWh \tag{7.10}$$

This result completes the comparison of the optimal Hydro Recharge unit with the benchmark. To conclude, the installation of the Hydro Recharge HBHS unit results in a substantial decrease of the HPP regulation wear and tear and is capable of continuously providing double the FCR-N capacity than the regulation power of HPP. All of this is done using a BESS which is experiencing roughly the same degradation as when the HPP and FCR-N gains are equal.

7.2 Frequency Split Optimization

The same optimization procedure is now followed for the Frequency Split HBHS architecture. Applying the optimization assumptions and identifying possible parameter variations, the following description of the unit is obtained.

$$R_{unit} = R_b = 50\frac{MW}{Hz}, \qquad R_h = var, \qquad R_{sys} = R_{FCR-N} - R_h \tag{7.11}$$

$$T_{hydro} = var, \qquad C_{rate} = 1 \tag{7.12}$$

$$\Delta f_{char} = var, \qquad SoC_{ref} = 50\ \%, \qquad SoC_{lo} = var, \qquad SoC_{hi} = var \tag{7.13}$$

The flexible operation possibilities for the HPP in this architecture dictate that the BESS is designed to satisfy the FCR-N performance requirements, giving limited optimization possibilities for the BESS parameters. Therefore, the performance optimization is again focused on the HPP response and SoC compensation algorithm. For the HPP, its gain and time constant of its regulation response T_{hydro} are set as variables. For the SoC algorithm, the strength of the compensation power defined as Δf_{char} and the SoC permissible band are set as variables. In general, more optimization possibilities are present than for the Hydro Recharge architecture, which is expected considering the combined participation of both HBHS elements in frequency regulation.

Firstly, the HPP gain R_h is varied together with the recharge error signal given to the HPP Δf_{char}. These two parameters represent the total power output capacity and the capacity dedicated to the SoC compensation respectively, which gives a clear need for their cross-referencing during optimization due to their possible impact on one another. The limits for the variance of the HPP total gain are set in the same way as for the Hydro Recharge: from a small participation in order to constitute a hybrid system, up to the HBHS unit gain. The limits of the SoC compensation error signal are set in per-unit of the maximum frequency deviation, following the nature of the signal. As such, the theoretical maximum is Δf_{max}, while the theoretical minimum is zero, which would result in a stand-alone BESS delivering $R_{unit} - R_h$ of FCR-N capacity. Therefore, a value above zero is taken for the same reasons as for the HPP gain, giving

$$R_h \in [10\ \ 50]\ \frac{MW}{Hz}, \qquad \Delta f_{char} \in [0{,}2\Delta f_{max}\ \ \Delta f_{max}] \tag{7.14}$$

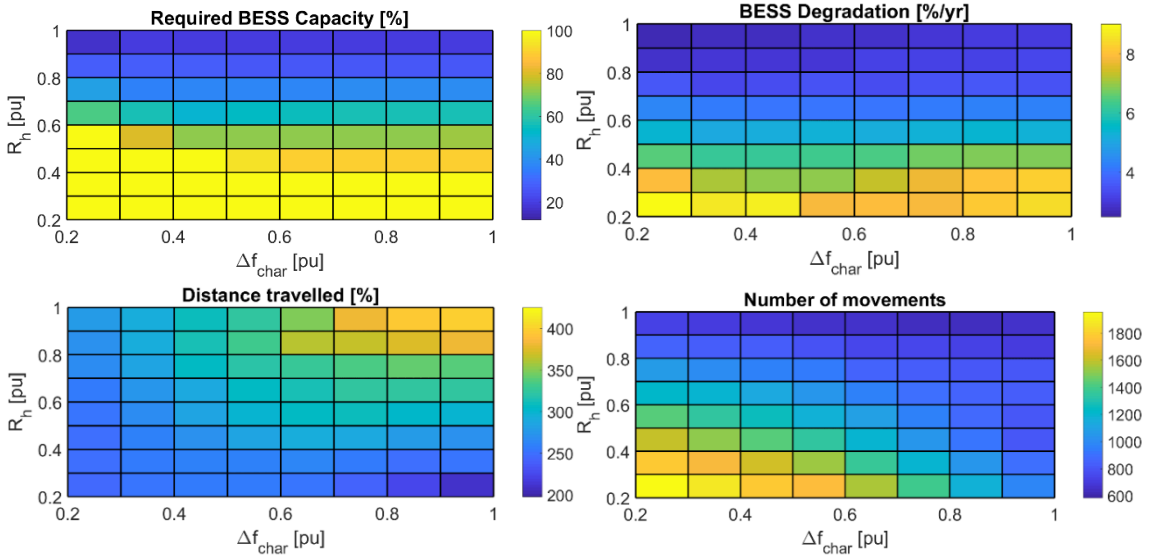

Figure 7.6. Impact of varying the HPP gain and SoC compensation power

Similar results to the Hydro Recharge HBHS can be observed in Figure 7.6. The required BESS storage capacity is again highly dependent on the HPP total gain with a dependency on the SoC compensation signal as well. The system is predicted to be able to function continuously with the HPP providing around half of the regulation power with a compensation signal of at least 0,5 pu of the maximum deviation. This dependency on the SoC signal is expected since a higher error value results in a higher charging or discharging power reference for the HPP. On the other hand, the BESS degradation does not show a strong dependency on the SoC compensation since the power reference does not influence the cycle depth or number. If a higher power reference is present, it only means that SoC_{ref} will be reached faster, while the frequency deviation continues to dictate the depth and number of cycles. A more complex dependency of the HPP wear and tear is obtained. Two characteristics govern this result, first of which is the fact that, the higher the HPP gain, the more regulation action it is providing, resulting in less stress on the BESS and less SoC variation. The second is that, a higher SoC signal will result in a more frequent maximum power reference for the HPP, according to (6.22), which then lasts for longer. Assuming a medium HPP gain, the results suggest a higher SoC signal value should be used, since the number of movements will be significantly decreased while the distance will increase slightly. A true inter-dependency of these two parameters is seen in this example.

Next, the total HPP gain is set to 25 MW/Hz, as the value that indicated continuous operation with the most BESS capacity utilized, and the SoC compensation parameters are varied together to observe their inter-dependency. In addition to the introduced SoC compensation signal, the width of the SoC permissible band is varied in the range introduced for the Hydro Recharge i.e.

$$SoC_{band} \in [2{,}5 \;\; 15]\%, \qquad \Delta f_{char} \in [0{,}2\,\Delta f_{max} \;\; \Delta f_{max}] \tag{7.15}$$

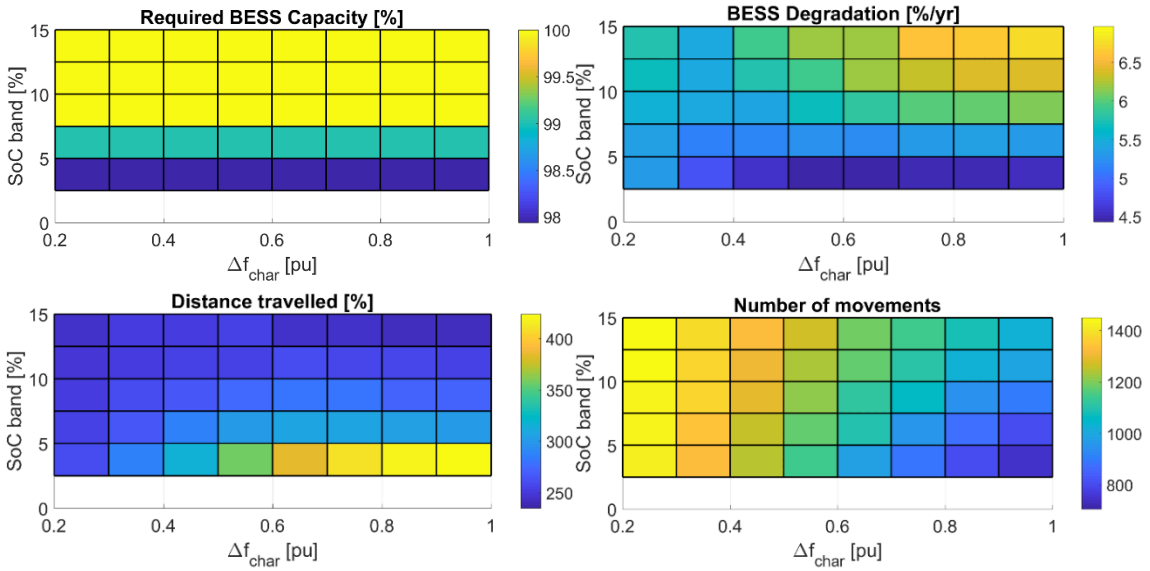

Figure 7.7. Impact of varying the SoC compensation signal and permissible band

The results of these variations can be seen in Figure 7.7. An expected increase of the required storage capacity and BESS degradation is seen for a wider SoC permissible band. However, the significant increase of the distance travelled by guide vanes disqualifies the 2,5 % SoC band value. In addition, the positive effects of a higher SoC compensation value on the HPP wear and tear are confirmed. Based on these results, a narrow SoC band larger than 2,5 % can be suggested, together with a high SoC error signal.

Finally, the impact of varying the HPP regulation response speed in the form of the approximated time constant T_{hydro} is examined. The test is performed with a SoC permissible band of 5 % and a SoC compensation power of 0,8 pu. The limits for the time constant variation are set freely since it is an entirely internal parameter for the HBHS. The theoretical lower limit is the 60-second response of the HPP governor, giving

$$T_{hydro} \in [60 \;\; 600]\; s \tag{7.16}$$

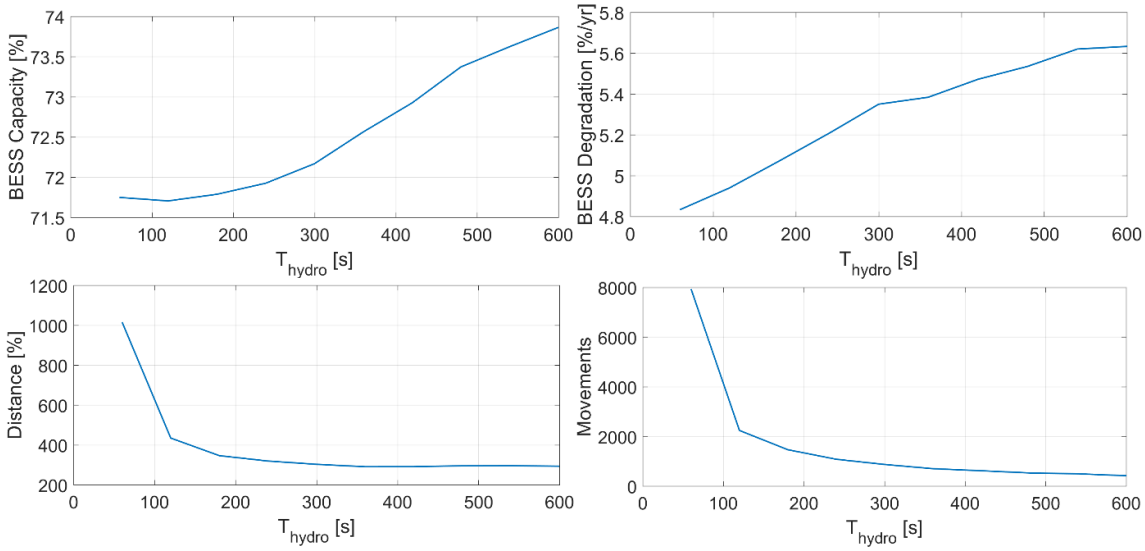

Figure 7.8. Impact of varying the HPP regulation response time constant

The impact of increasing this time constant to more than the standard governor value can be seen in Figure 7.8. From the BESS operation aspect, a slower HPP regulation response results in a higher power difference for the BESS to provide, as exemplified in Figure 6.17. This in turn results in the linear increase of the capacity requirements and, more importantly, in the degradation of the BESS. The more interesting phenomenon can be seen in the behaviour of the HPP wear and tear with the time constant increase. Namely, both the distance and the number of movements decrease drastically for the initial values of the time constant, whereas the wear and tear hold steady after the time constant reaches 200 to 300 seconds. This exponential behaviour can be interpreted from the aspect of NPS frequency dynamics. An exponential decrease indicates a presence of frequency oscillations with the corresponding time constants from 60 to 200 seconds, which coincides with previous research on frequency dynamics [15]. Oscillations with a longer time period are not present

and thus the movement of the HPP corresponds to the slower frequency trends. These considerations are very valuable for the Frequency Split architecture, as the idea behind the unit was for the HPP to handle exactly these, more durable, frequency trends.

After varying all the parameters, a possible optimal Frequency Split HBHS specification can be established. As was already mentioned, the desired HPP gain would be one that can deliver continuous operation while utilizing as much of the BESS storage capacity as possible. In order to limit the fatigue of both elements, a narrow SoC band and a high SoC compensation signal are used. Lastly, the HPP response time constant is set to filter most of the faster frequency oscillations.

$$R_h = 25\ \frac{MW}{Hz}, \qquad \Delta f_{char} = 0{,}8\ \Delta f_{max}, \qquad SoC_{band} = 5\ \%, \qquad T_{hydro} = 240\ s \tag{7.17}$$

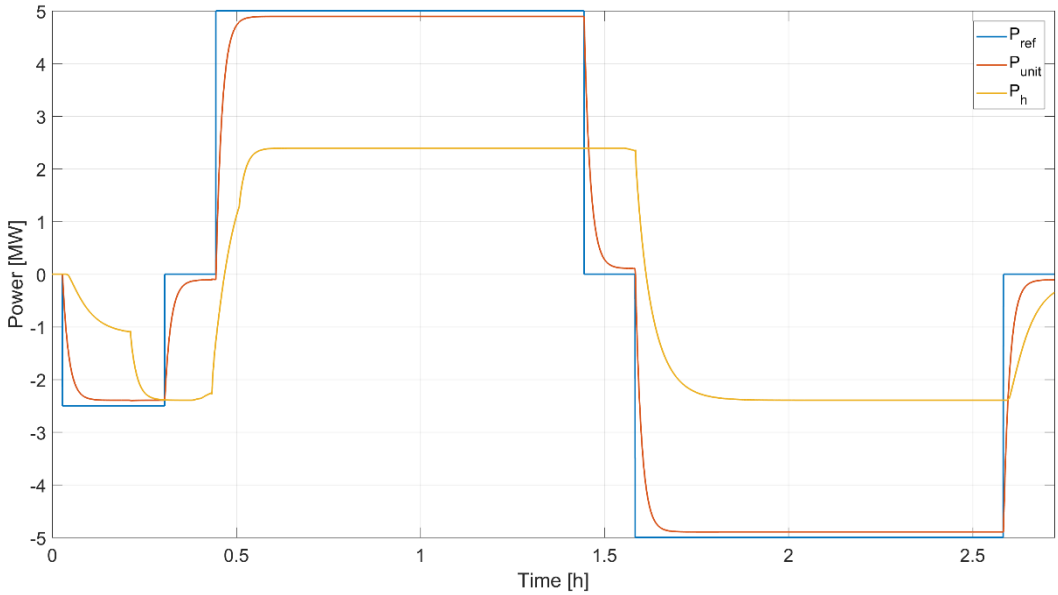

Figure 7.9. Optimal Frequency Split HBHS static prequalification test

The operation of the proposed optimum Frequency Split HBHS is exemplified in Figure 7.9, where the result of running the static prequalification test is displayed. Now, the action of the SoC compensation algorithm is visible during the first frequency step. At the point when the SoC drops below 45 %, the HPP power output increases to maximum, where half is the result of the regulation action and half of the SoC compensation.

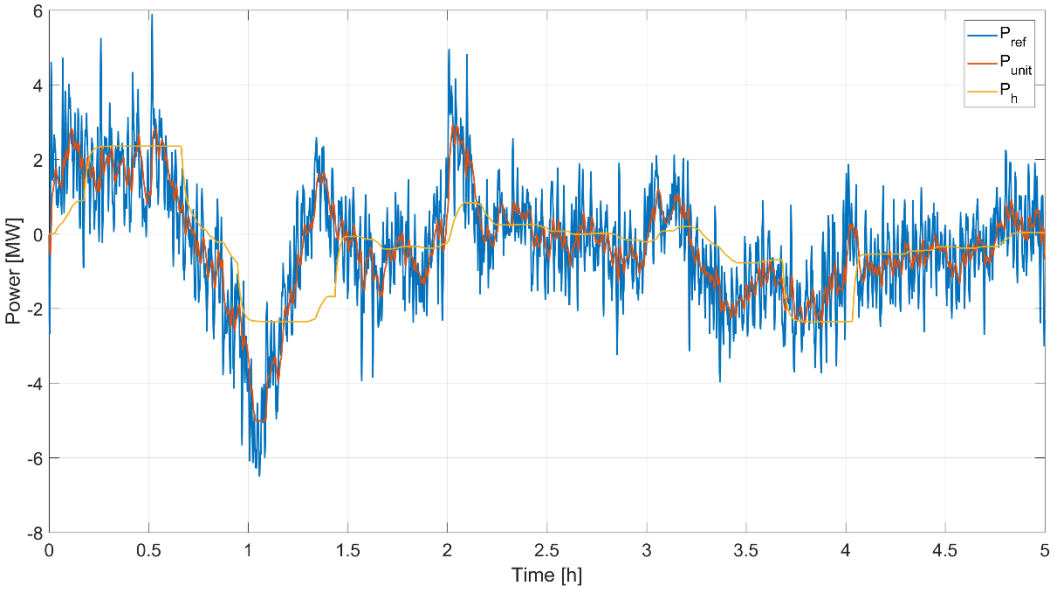

Figure 7.10. Optimal Frequency Split HBHS operation in the NPS

Finally, the operation of the proposed optimal HBHS is compared to the benchmark unit. The simulation is performed again for the 30 days in August 2018, with an example displayed in Figure 7.10. The resulting 1 153 minutes spent outside the normal frequency band validate the power system operation. The HPP wear and tear is estimated at

$$L_{wt} = 3\,602{,}5\ \%, \qquad N_{wt} = 14\,553 \tag{7.18}$$

giving an average movement of 0,25 %. The higher number of movements compared to the optimized Hydro Recharge HBHS is attributed to the fact that the HPP is now participating in frequency regulation. This is confirmed by the lower number of entries into the SoC compensation active states, which amount to

$$N_{Char} = 461, \qquad N_{Disc} = 423 \tag{7.19}$$

signifying that most of the wear and tear on the HPP is caused by the regulation action. Compared to the benchmark unit, the guide vanes travel 21,6 % of the distance in 11,9 % of the number of movements. Compared to the optimized Hydro Recharge HBHS, the guide vanes travel an 18 % shorter distance but perform five and a half times more movements.

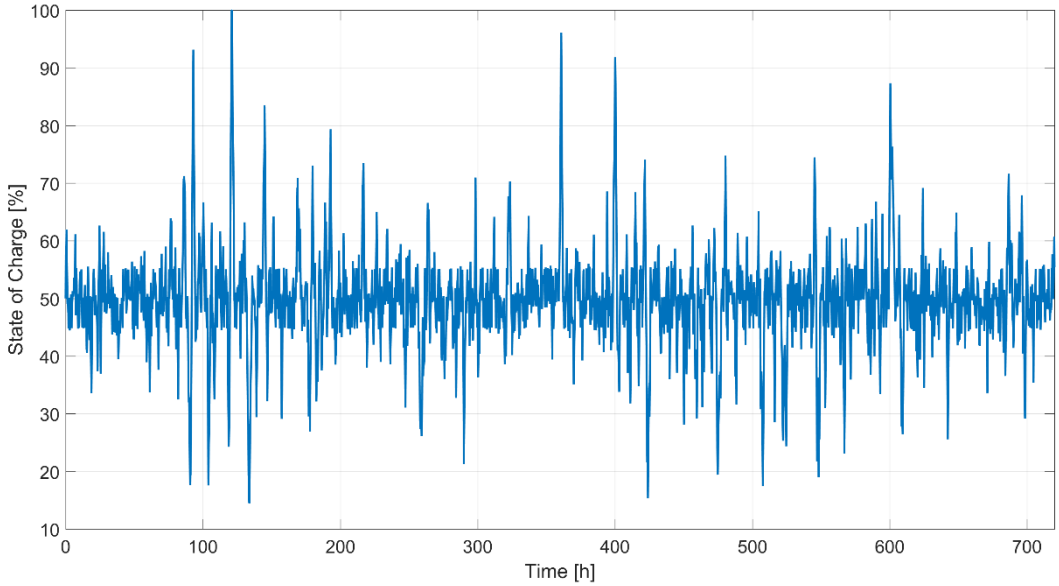

Figure 7.11. Optimal Frequency Split HBHS SoC during operation in the NPS

During the simulated 30 days, the BESS manages to operate continuously, with short interruptions, as displayed in Figure 7.11. The SoC again reaches 100 % for a total of 9 minutes, while it does not empty entirely, which means that it is unable to provide FCR-N for 0,02 % of the operation time. This is again deemed low enough to constitute continuous operation, since it is within unit availability and reliability margins. The estimated lifetime of the BESS unit is obtained at

$$L_b = 25{,}82\ yrs, \qquad C_{used} = 85{,}57\ \% = 4{,}28\ MWh \tag{7.20}$$

which demonstrates that the BESS is experiencing less stress during operation than in the Hydro Recharge HBHS, as was expected due to the participation of the HPP in frequency regulation.

To conclude, the installation of the Frequency Split HBHS unit results in a substantial decrease of the regulation wear and tear that a single HPP experiences and provides double the FCR-N capacity than the HPP regulation. All of this is done with the BESS experiencing less stress than in the Hydro Recharge HBHS, on the account of more movements performed by the HPP regulation mechanism.

Interesting conclusions can be drawn by comparing the proposed optimal Hydro Recharge and the Frequency Split HBHS, as well as their operation with the HPP gain of 50 MW/Hz. Looking at the optimized proposals, it is easily seen that, although both architectures result in massive reductions of fatigue compared to the benchmark, the Hydro Recharge imposes less stress on the HPP during operation, particularly in the number of movements of the regulation mechanism. On the other hand, the Frequency Split imposes less stress on the BESS during operation and is more capable of controlling the SoC. This

indicates that, in order to choose between the two HBHS architectures for a specific application, one would have to quantify the value of both BESS degradation and HPP wear and tear for that specific application. Another observation is the similar performance of the two HBHS units as compared to the benchmark, in spite of the fact that the unit architectures are entirely different. The explanation behind this can be derived if it is imagined that Δf_{char} is equal to Δf_{max}. Then, the HPP response as a result of the SoC compensation algorithm becomes the same as the Hydro Recharge unit's response to the SoC control algorithm, in the Charge and Discharge states. The difference between the two then only exists in the Idling state, where the Frequency Split HPP participates in regulation whereas the Hydro Recharge HPP remains dormant. Taking into account that the BESS response is governed by the HPP reaction, this gives practically identical behaviour of the two HBHSs when the SoC is outside the permissible band.

Comparing the optimal HBHS architectures to their counterparts with an HPP gain of 50 MW/Hz, two different trends are observed. The optimization of the Hydro Recharge HBHS reduced the estimated amount of HPP wear and tear, whereas this estimation has increased for the Frequency Split HBHS. Again, this comparison can be made since the wear and tear is normalized with regards to the HPP gain. The stress the BESS is experiencing is roughly the same for the Hydro Recharge with both gains and the Frequency Split with a 25 MW/Hz HPP gain. The only application that shows significantly less BESS degradation is the Frequency Split HBHS with equal gains. These performance trends suggest that the Frequency Split HBHS is better suited for an application with equal or similar HPP and HBHS gains i.e. $R_h = R_{unit}$.

The optimal settings for this full Frequency Split HBHS can also be taken from the optimization process since these operating points were included. Observing Figures 7.6 to 7.8, the optimal settings are determined to be

$$R_h = 50\ \frac{MW}{Hz}, \qquad \Delta f_{char} = 0{,}3\ \Delta f_{max}, \qquad T_{hydro} = 240\ s \tag{7.21}$$

$$C_{rate} = 4, \qquad SoC_{band} = 20\ \% \tag{7.22}$$

which are very similar to the ones with reduced HPP gain in (7.17). The SoC compensation error was significantly reduced to minimize HPP wear and tear, and the BESS size is only a quarter of the $C_{rate} = 1$ system. The SoC permissible band is also scaled with the BESS capacity to prevent an increase in HPP regulation action. For the same 30-day simulated operation, these settings result in

$$L_{wt} = 2\ 887{,}9\ \%, \qquad N_{wt} = 10\ 500 \tag{7.23}$$

$$L_b = 7{,}86\ yrs, \qquad C_{used} = 56{,}12\ \% = 0{,}70\ MWh \tag{7.24}$$

The HPP increases the distance travelled for 24 % and the number of movements made for 70 %, compared to the previous test on the $C_{rate} = 1$ BESS in (6.26). However, the comparison with the benchmark unit reveals that the distance the guide vanes travel is 17,3 % while the number of movements performed is 8,6 %. Furthermore, the 5 MW and 1,25 MWh BESS is able to operate continuously without any difficulties, but while reporting a significantly shorter lifetime than in (6.27).

The conclusion that a balance between the HPP wear and tear costs and BESS costs needs to be found for the optimal settings is applicable to these results as well. For example, if the costs of the HPP wear and tear are high, changing the battery system every seven years does not pose a financial problem. On the other hand, if the HPP wear and tear costs are relatively low, a bigger BESS, which would have a significantly longer lifetime, would give more time for the HPP wear and tear savings to turn a profit.

7.3 Model Parameter Sensitivity

As with every optimization process, the sensitivity of the obtained results to the variance of model parameters needs to be considered. Therefore, a discussion is given, with the result being the identification of critical model parameters which could significantly influence the outcome of the optimization and should therefore be accurately measured and modelled for a specific application.

The NPS model was built using full-scale measurements of system inertia and damping. The behaviour of the model was tested after its introduction and validated during every optimization simulation. The influence of the power system on the HBHS performance can only be seen through the historical frequency data used, because of the way in which the historical power disturbance is created and matched to the frequency data. Therefore, the optimization is sensitive to the historical frequency data. This was also mentioned during the creation of optimization assumptions, where a 30-day period was taken as an acceptable sample. Now, this sensitivity to frequency data is further explored in order to improve the robustness of the optimization results and to gather insight into the dependency of the HBHS operation on the frequency quality. This is considered valuable as the grid frequency behaviour is constantly evolving.

The benchmark HPP and two architectures, the example Frequency Split with full HPP gain, defined in (6.23) and (6.24), and the optimal Hydro Recharge HBHS with half the HPP gain, defined in (7.7), are simulated to run 30 days in the NPS during three different months. One month with worse and one with better frequency quality than August 2018 are selected, and the same performance and fatigue indicators are evaluated for all three frequency samples, as can be seen in Table 7.1. The HPP wear and tear estimations increase with the deterioration of frequency quality for all three models. On the other hand,

the trends of BESS degradation do not follow the frequency quality. For example, the month of August demonstrates the best operating conditions for the optimal Hydro Recharge BESS, while December the worst. This indicates that the time outside the normal frequency band does not fully represent the frequency quality and is therefore not the only relevant parameter for HBHS operation. Nevertheless, the sensitivity of the model to this frequency quality parameter is determined with these results. It is concluded that the estimations of fatigue for both the HPP and BESS are sensitive to the frequency data with an average variance of around 12 %, while the comparison of benchmark and HBHS operation reduces that sensitivity. Therefore, the conclusions drawn in the previous work are deemed valid. This sensitivity further stresses the importance of the statistical approach to frequency data and simulating model operation for a longer frequency sample.

Table 7.1 Model sensitivity to historical frequency data

Model	**Frequency sample**	**Frequency outside** $[min]$	**HPP distance** L_{wt} [%]	**HPP movements** N_{wt}	**BESS lifetime** L_b $[yrs]$	**BESS capacity** C_{used} [%]	**HBHS out of service** $[min]$
Benchmark HPP	May 2018	1 270	17 131	123 992	/	/	0
	Aug 2018	1 170	16 670	122 011	/	/	0
	Dec 2018	1 028	12 844	109 037	/	/	0
Frequency Split HBHS	May 2018	1 267	2 516	7 653	43,60	22,2	0
	Aug 2018	1 169	2 333	6 182	47,07	23,0	0
	Dec 2018	1 027	2 337	4 804	44,26	23,5	0
Optimal Hydro Recharge HBHS	May 2018	1 247	4 928	3 000	21,45	93,1	116
	Aug 2018	1 149	4 406	2 644	22,29	84,2	20
	Dec 2018	1 004	3 802	2 115	19,92	99,8	33

The lumped and single HPP models were built using theoretical parameter ranges and empirical test data. The sensitivity of the model to different HPP parameters should be estimated by analysing the timescale of different component dynamics. Following this, the governor parameters are the most influential on the HPP response and, as such, can influence HBHS operation. In order to minimize this sensitivity, the performance was compared to SvK markers during testing and well-known standard governor values were used. Because of much faster dynamics, the sensitivity to servo and turbine parameters is disregarded, except for the backlash effect. As was seen in Figures 6.2 to 6.4, the backlash effect has a significant influence on the dynamic and steady-state response of the HPP unit. The changes in steady-state power output as a result of backlash could influence the optimization procedure, which is why it is classified as a critical parameter. In general, the dynamics of the HBHS mostly depend on the BESS response, as pointed out during the HBHS introduction, reducing its sensitivity to HPP parameters. In addition, the presented optimization results were obtained for a Kaplan turbine, which means they are valid for a Francis turbine as well since, due to its superior dynamics.

The model sensitivity to different BESS parameters should also be estimated by analysing the timescale of BESS transients. From this, it is immediately concluded that the model is not sensitive to BESS dynamic performance, as all transients can be considered practically instantaneous with regards to frequency regulation.

The model sensitivity to the fatigue estimations for both the HPP and BESS is evident from the presented work. The HPP wear and tear estimation has already been modified during the modelling to reduce its sensitivity on the sampling time. However, the movement counter remains very sensitive to the changes in its settings, which is why it was tuned to produce results similar to existing literature models. This identifies the wear and tear counter settings as critical model parameters and brings into question the absolute counter value. Nevertheless, the comparisons of counter values between different HBHS units still hold. The BESS degradation estimation is entirely dependent on the SoC value and the empirical expression in (5.44). Therefore, the round-trip efficiency of the BESS can immediately be identified as a critical parameter for the required storage capacity and degradation estimation, and thus for the optimization. In addition, the capacity fade expression is also classified as a critical parameter, however, the same considerations are true as for the movement counter. While the absolute values of BESS lifetime can be questioned, its comparison between different HBHS units still hold.

8 Impact on the Nordic Power System

Up to this point, the HBHS was developed and optimized from the perspective of a single unit i.e. the perspective of its owner or operator. With the architectures and corresponding settings for the HBHS defined, it is now prudent to explore the impact installing a larger number of HBHS units would have on the NPS and its frequency quality.

The total FCR-N gain present in the system and used in the project is 7530 MW/Hz. As was said before, this is almost exclusively provided from HPPs and was represented by the lumped HPP model. It was also said that the motivation behind the development of the HBHS is improving the frequency conditions in the NPS. Assuming the load disturbance remains the same, the frequency quality can be improved either by modifying the existing FCR-N resources or by activating additional FCR-N resources. Therefore, two possible scenarios can be seen for improving the frequency quality using HBHS units:

- the replacement of activated FCR-N capacity, provided by HPPs, with the capacity provided by HBHSs and
- the activation of additional FCR-N capacity generated by the HBHS, alongside the existing activated HPP capacity.

Using the conclusions reached in previous work, the former scenario would practically entail installing the Frequency Split HBHS with full HPP gain or the Hydro Recharge HBHS while reducing the HPP gain by half. Both solutions would result in the same FCR-N capacity delivered to the grid. The latter scenario, on the other hand, would practically entail the installation of the Hydro Recharge HBHS with double the power rating of the HPP. This would result in the double the FCR-N capacity delivered to the grid, increasing the total by the HPP gain i.e. half the HBHS gain.

The latter scenario is expected to have a more significant impact on the frequency quality, since it constitutes adding new FCR-N assets, as opposed to speeding up the response of existing assets. Since the frequency quality in the system is considered as issue, it is assumed that the scenario of activating additional FCR-N capacity is more likely and it thus explored. By varying R_{unit}, an increasing amount of Hydro Recharge HBHS units is introduced into the power system model and the simulation is ran for the three different months of 2018, to take into account the sensitivity to frequency data. This is necessary since the frequency sample used represents the initial condition of the power system and the result is thus highly dependent on it. This is confirmed when the results are displayed in Figure 8.1.

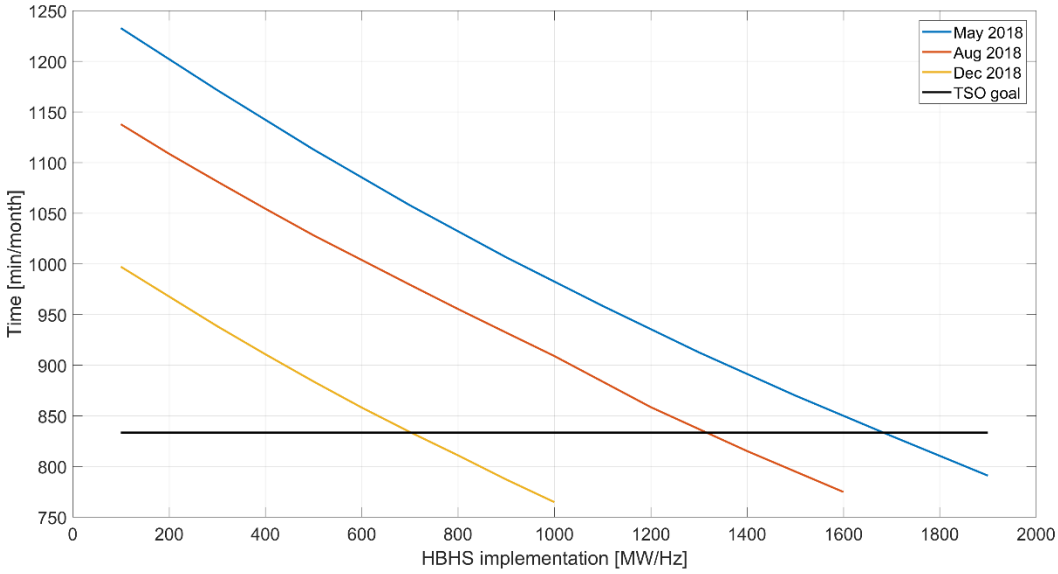

Figure 8.1. Estimate of minutes outside the normal frequency band

The number of minutes spent outside the normal frequency band decreases almost linearly with the activation of additional FCR-N capacity from the HBHSs, for all three frequency samples. Furthermore, this linear decrease seems to have the same slope for different frequency samples. This is confirmed when a polynomial fit is done for the trends in Figure 8.1.

$$T_{May} = -0{,}244\, R_{unit} + 1\,239\, min$$

$$T_{Aug} = -0{,}242\, R_{unit} + 1\,153\, min \quad (8.1)$$

$$T_{Dec} = -0{,}257\, R_{unit} + 1\,017\, min$$

It is easily seen from (8.1) that the reduction of time outside is constant with regards to the HBHS gain, while its absolute value is dependent on the time outside the normal frequency band without any HBHS installed for that month. This allows for the creation of a formula that produces the HBHS gain necessary to reach the TSO goal of 10 000 minutes per year from the time spent outside the normal frequency band T_{out} i.e.

$$R_{unit} = \frac{T_{out} - 833\, min}{0{,}248} \quad (8.2)$$

Using the Fingrid measurements of 1 097 minutes outside per month, this formula gives an HBHS capacity of 106 MW and 106 MWh and thus the same amount of BESS needed to be installed in the NPS to reach the TSO goal of 833 minutes. It should be stressed that these calculations are given assuming the HBHS frequency regulation bids would be continuously activated. This assumption further means that the TSOs are purchasing 806 MW of FCR-N instead of the used capacity of 753 MW, amounting to a 7

% increase. However, it is noted that the sensitivity of this result to the change of system inertia and damping should be explored as well.

Another interesting observation is made when examining the impact this large-scale implementation would have on the individual HBHS units themselves. Namely, for the same 30-day period, the HPP wear and tear is slightly reduced with the increase of the HBHS implementation gain, compared to the single unit analysed in Section 7.1. A more significant increase of the BESS lifetime is also observed, with the best effect visible on the amount of time the BESS is out of service. This signifies an improvement of the operating conditions for the individual units with the large-scale implementation, especially for the BESS.

9 Conclusions

Due to the differences that exist in frequency product markets and prequalification testing in different Nordic countries, Sweden was selected as the study-case location for this project. Following this, the FCR-N product was selected as the service the HBHS is to provide to the power system, since the market analysis and price identified it as the one with highest profitability potential. After an analysis of existing HPPs providing frequency support, units which house Kaplan turbines and have higher running hours, were identified as good candidates for the HBHS installation. It was established that Kaplan turbines can experience more difficulties to satisfy proposed FCR-N provision requirements, due to their two-tier regulation system. It was concluded that units with higher running hours are favourable because of their lower cost and higher availability of running the HPP in the HBHS. With these system specifications, the study-case was fully determined.

A model of the HBHS performing frequency regulation in the NPS was built as a platform for evaluating unit performance. The model creation was governed by the relatively long timescale of frequency regulation dynamics, while the parameters were taken from industry standards and full-scale test data. The model performance was compared to full-scale tests on existing HPPs. The HBHS performance was evaluated in a qualitative and quantitative manner. The performance quality was evaluated by running the HBHS model through current and proposed FCR-N provision tests, as defined by SvK and ENTSO-E respectively. The ability of the HBHS unit to satisfy FCR-N performance requirements was checked and the qualified power capacity was obtained. The quantitative assessment was based on the fatigue that both the HPP and the BESS experience during operation. For the HPP, the fatigue was quantified in the distance the regulation mechanism i.e. guide vanes and runner blades travel whilst regulating the power output and the number of movements they make. The BESS fatigue was quantified in the resulting energy capacity fade of the Li-ion batteries which was used to project a lifetime estimate for the BESS. The capacity fade used depended on the number and depth of the cycles the BESS performed, as well as the average state of charge (SoC).

Two different HBHS architectures were introduced: the Hydro Recharge and the Frequency Split. Their operation principles were defined and the Power Plant Controller (PPC) housing the required functions and control laws was developed. The qualitative comparison showed a significant improvement of HBHS dynamics during the sinusoidal dynamic provision test, compared to the single HPP benchmark. Both architectures exhibited similar improvements in dynamic performance while qualifying the same capacity of FCR-N through the existing step sequence provision test. The quantitative comparison with the benchmark HPP showed that the Hydro Recharge HPP regulation mechanism travelled 48,9 % of the distance in 6,1 % of the number of movements, delivering the same

regulation power in the same time period as the benchmark unit. For the Frequency Split HBHS, the HPP regulation mechanism travelled 14,0 % of the distance 5,1 % of the number of movements, delivering the same service. From this and the estimated BESS lifetime, it was concluded that the Frequency Split is the architecture with superior performance when the HBHS and HPP have equal regulation gains.

The BESS was significantly oversized for the studied HBHS units, motivating the exploration of an optimal ratio between the HPP and BESS regulation gains and the BESS storage capacity. Additionally, unconstrained parameters of the HBHS were varied in an attempt to obtain additional reductions in fatigue for both HBHS elements. A ratio of half the HBHS unit gain was found as necessary to be provided by the HPP, for a BESS with a $C_{rate} = 1$ implemented in both architectures, in order to enable continuous operation of the HBHS. Optimal settings of the SoC control and compensation algorithms, as well as frequency measurement filters, were obtained for a minimum combined fatigue of the HPP and BESS. These optimal settings resulted in further reductions of the HPP wear and tear when applied in the Hydro Recharge architecture, with the HPP delivering half the power compared to the benchmark unit. For the Frequency Split HBHS, the HPP wear and tear increased compared to the full gain application. It was, therefore, concluded that the Hydro Recharge architecture is better suited for applications with reduced HPP gain than with full gain. The comparison between the two architectures for applications with reduced HPP gain was not given because of its dependency on the HPP wear and tear cost estimation, which needs to be done on a case-by-case basis. Using the optimization results, the full gain Frequency Split HBHS operation was simulated again with corrected parameters and a $C_{rate} = 4$, which resulted in similar wear and tear and continuous operation. All of these results are summarized in Table 9.1 for a better overview and understanding.

Table 9.1 Overview of HBHS architectures' performance compared to benchmark

Model	R_{unit} $\left[\frac{MW}{Hz}\right]$	R_h $\left[\frac{MW}{Hz}\right]$	**BESS capacity** $[MWh]$	L_{wt} [%]	N_{wt} [%]	**BESS lifetime** L_b $[yrs]$	**HBHS availability** [%]
Benchmark HPP	50	50	/	100	100	/	100
Hydro Recharge HBHS	50	50	5	48,9	6,1	21,8	100
Frequency Split HBHS	50	50	5	14,0	5,1	47,1	100
Optimal Hydro Recharge HBHS	50	25	5	26,4	2,2	22,3	99,96
Optimal Frequency Split HBHS	50	25	5	21,6	11,9	25,8	99,98
Full Frequency Split HBHS	50	50	1,25	17,3	8,6	7,9	100

In general, considerable reductions in HPP wear and tear were obtained for both HBHS architectures and both HPP gains, while imposing an acceptable level of stress on the BESS. If the HBHS is installed in order to enable the HPP to pass the FCR-N provision tests whilst qualifying the same regulation power, the Frequency Split architecture is recommended, with a BESS sized for $C_{rate} = 4$. Secondly, if the HBHS is installed with the aim of providing a higher FCR-N capacity to the power system, the proposed gain ratio of 50 % is given for a BESS sized for $C_{rate} = 1$, with the preference between the two architectures depending on the actual implementation case. In the end, the result's sensitivity to different model parameters is discussed and a large-scale implementation of proposed HBHS units is explored. It is concluded that, with current frequency conditions, a cumulative capacity of some 106 MW and 106 MWh of installed HBHSs would reduce the number of minutes outside the normal frequency band under the 10 000-minute goal set by Nordic TSOs, with the TSOs required to increase the purchased capacity by 53 MW.

The work conducted in this project opens several interesting directions for its future continuation and development. The most direct continuation would be an economic analysis and financial viability study of the proposed HBHS units, which would consider current market trends and help further limit the optimization parameters, according to their cost-efficiency, and thus improve the results. Another point of interest would be to examine the influence of the static HPP operation on the HBHS regulation performance. This would entail more precise modelling of different HPP operating points along the efficiency curve and taking into account water constraints and production planning. In other words, these continuations entail the expansion of the model to include static operation points and market dynamics, which were disregarded in this project. Another direction involves a more holistic approach to the HBHS concept and that is increasing the service portfolio of the HBHS, first by examining different frequency regulation products, and then by examining entirely different services such as synthetic inertia, peak shaving and voltage support.

10 Acknowledgements

I would like to take the opportunity to thank everybody involved in the truly unique experience that was this Master Thesis project. First and foremost, I would like to express my gratitude to Oriol Gomis Bellmunt, my Thesis supervisor at UPC for all that he has done during the past six months. Even though I had been performing my project several thousand kilometers away, I have always felt I had the support I needed to follow through. Thank you for your understanding and encouragement, which allowed me to pursue this project with my own plan and goals. Thank you for your constant counseling and advice, which was never limited to this project. I plan to take apply what I have learned from you in my future career and all aspects of life. It was an honour having you as my supervisor.

Secondly, I would like to thank Fortum for the opportunity to carry out my work as their Master Thesis student and providing me with everything I needed during the entire project. I would like to say thank you to my Fortum supervisor Alessandro Ferraris for introducing me to the project, company and industry. It was a pleasure discussing my work with you and hearing your valuable ideas for the future. Thank you very much for taking the time to go on several site visits with me as well. Next, I wish I could express my gratitude to my Fortum manager Hans Bjerhag, but it will hardly come across as enough. Thank you for the wonderful introduction to Fortum, thank you for giving us students your undivided attention when we needed it, and for making us feel always welcome at the company. I have always felt like I had you to turn to for professional advice and guidance, as well as an insight into Swedish culture and customs. Finally, I wish to thank all the Fortum employees I have had the privilege to meet. Thank you for the opportunity to learn more about your fields of expertise and to share my project and ideas.

11 Bibliography

[1] ENTSO-E, “Nordic Balancing Philosophy,” 2016.

[2] Fingrid, “Frequency quality analysis for 2016,” 2017. [Online]. Available: https://www.fingrid.fi/globalassets/dokumentit/fi/kantaverkko/suomen-sahkojarjestelma/frequency_quality_analysis_2016_public.pdf.

[3] Fingrid, “Frequency quality analysis for 2017,” 2018. [Online]. Available: https://www.fingrid.fi/globalassets/dokumentit/fi/kantaverkko/suomen-sahkojarjestelma/frequency_quality_analysis_2017.pdf.

[4] R. Eriksson, N. Modig, and A. Westberg, “FCR-N Design of Requirements (Draft),” *ENTSO-E Rep.*, 2017.

[5] Nord Pool, “The power market,” 2017. [Online]. Available: https://www.nordpoolgroup.com/the-power-market/. [Accessed: 06-May-2019].

[6] E. Byström, “Senior Advisor at Fortum, interview held on 2019-02-20,” Stockholm, 2019.

[7] A. Oudalov, D. Chartouni, C. Ohler, and G. Linhofer, “Value Analysis of Battery Energy Storage Applications in Power Systems,” in *IEEE PES Power Systems Conference and Exposition*, 2006.

[8] B. Xu, A. Oudalov, J. Poland, A. Ulbig, and G. Andersson, “BESS Control Strategies for Participating in Grid Frequency Regulation,” in *IFAC Proceedings Volumes*, 2014, vol. 19.

[9] W. Yang, P. Norrlund, C. Y. Chung, J. Yang, and U. Lundin, “Eigen-analysis of hydraulic-mechanical-electrical coupling mechanism for small signal stability of hydropower plant,” *Renew. Energy*, vol. 115, 2018.

[10] W. Yang, J. Yang, W. Guo, and P. Norrlund, “Response time for primary frequency control of hydroelectric generating unit,” *Electr. Power Energy Syst.*, vol. 74, 2016.

[11] L. Saarinen, “The Frequency of the Frequency - On Hydropower and Grid Frequency Control,” Uppsala University, 2014.

[12] J. Muikku, “Hydro Turbines in Power System Balancing,” Lappeenranta University of Technology, 2018.

[13] E. Dahlborg, “Frequency control - Pay for performance,” Uppsala University, 2015.

[14] H. Chavez, R. Baldick, and S. Sharma, “Governor Rate-Constrained OPF for Primary Frequency Control Adequacy,” *IEEE Trans. Power Syst.*, vol. 29, no. 3, 2014.

[15] C. Odelbrink, “Design of an Alternative Frequency Controller for Hydropower Stations,” Uppsala University, 2014.

[16] H. Olsson, “Future frequency control services in the Nordic power system,” Uppsala University, 2017.

[17] A. Oudalov, D. Chartouni, and C. Ohler, “Optimizing a Battery Energy Storage System for Frequency Control,” *IEEE Trans. Power Syst.*, vol. 22, no. 3, 2007.

[18] N. Andrenacci, E. Chiodo, D. Lauria, and F. Mottola, “Life Cycle Estimation of Battery Energy Storage Systems for Primary Frequency Regulation,” *Energies*, vol. 11, no. 12, 2018.

[19] R. Bucher and A. Schreider, “Live test results of the joint operation of a 12.5 MW battery and a pumped-hydro plant,” in *HYDRO 2018*, 2017.

[20] C. Jin, N. Lu, S. Lu, Y. V. Makarov, and R. A. Dougal, “A Coordinating Algorithm for Dispatching Regulation Services Between Slow and Fast Power Regulating Resources,” *IEEE Trans. Smart Grid*, vol. 5, no. 2, 2013.

[21] D. Risberg, “Intraday Trader at Fortum, interview held on 2019-03-08,” Stockholm, 2019.

[22] M. Amelin and L. Söder, *Efficient Operation and Planning of Power Systems*, 11th ed. Stockholm: KTH Royal Institute of Technnology, 2011.

[23] Svenska kraftnät, “Overview of the Requirements on Reserves.” [Online]. Available: https://www.svk.se/en/stakeholder-portal/Electricity-market/information-about-reserves/.

[24] Prequalification Working Group - FCP project, “Technical Requirements for Frequency Containment Reserve Provision in the Nordic Synchronous Area (Draft),” 2017.

[25] V. Granberg, “Power Portfolio Manager at Fortum, interview held on 2019-02-06,” Stockholm, 2019.

[26] Svenska kraftnät, “Trade and Pricing.” [Online]. Available: https://www.svk.se/en/stakeholder-portal/Electricity-market/information-about-reserves/.

[27] Svenska kraftnät, “Mimer - Primärreglering,” 2019. [Online]. Available: https://mimer.svk.se/PrimaryRegulation/PrimaryRegulationIndex. [Accessed: 05-Mar-2019].

[28] J.-O. Silver, “Senior Power Portfolio Manager at Fortum, interview held on 2019-02-28,” Stockholm, 2019.

[29] Svenska kraftnät, “Application for Frequency Containment Reserve Provision,” 2018. [Online]. Available: https://www.svk.se/en/stakeholder-portal/Electricity-market/information-about-reserves/prequalification/.

[30] Svenska kraftnät, “FCR-N Test Program Template,” 2018. [Online]. Available: https://www.svk.se/en/stakeholder-portal/Electricity-market/information-about-reserves/prequalification/.

[31] International Energy Agency, “Hydropower.” [Online]. Available: https://www.iea.org/topics/renewables/hydropower/. [Accessed: 05-Mar-2019].

[32] P. Breeze, *Hydropower*. Academic Press - Elsevier, 2018.

[33] F. Diaz-Gonzalez, A. Sumper, and O. Gomis-Bellmunt, *Energy Storage in Power Systems*. John Wiley & Sons, Ltd, 2016.

[34] C. K. Tan, M. M. Aman, N. A. Rahim, S. R. S. Raihan, and M. Sufyan, “Sizing and

applications of battery energy storage technologies in smart grid system: A review," *J. Renew. Sustain. Energy*, vol. 11, no. 1, 2019.

[35] L. Saarinen, P. Norrlund, U. Lundin, E. Agneholm, and A. Westberg, "Full-scale test and modelling of the frequency control dynamics of the Nordic power system," *IEEE Power Energy Soc. Gen. Meet.*, 2016.

[36] L. Saarinen, P. Norrlund, and U. Lundin, "Field Measurements and System Identification of Three Frequency Controlling Hydropower Plants," *IEEE Trans. Energy Convers.*, vol. 30, no. 3, 2015.

[37] T. Olenius, "Project Manager at Fortum, interview held on 2019-03-12," Stockholm, 2019.

[38] P. Kundur, *Power System Stability And Control*. McGraw-Hill Inc., 1993.

[39] Fingrid, "Frequency - historical data," 2019. [Online]. Available: https://data.fingrid.fi/en/dataset/frequency-historical-data. [Accessed: 07-May-2019].

[40] H. Bjerhag, "Senior Expert Hydropower at Fortum, interview held on 2019-05-09," Stockholm, 2019.

[41] W. Yang, P. Norrlund, L. Saarinen, J. Yang, W. Zeng, and U. Lundin, "Wear Reduction for Hydropower Turbines Considering Frequency Quality of Power Systems: A Study on Controller Filters," *IEEE Trans. Power Syst.*, vol. 32, no. 2, 2017.

[42] W. Yang, P. Norrlund, L. Saarinen, J. Yang, W. Guo, and W. Zeng, "Wear and tear on hydro power turbines - Influence from primary frequency control," *Renew. Energy*, vol. 87, 2016.

[43] D. I. Stroe, M. Swierczynski, A. I. Stroe, R. Teodorescu, R. Laerke, and P. C. Kjaer, "Degradation Behaviour of Lithium-Ion Batteries based on Field Measured Frequency Regulation Mission Profile," *2015 IEEE Energy Convers. Congr. Expo. ECCE 2015*, 2015.

[44] D. I. Stroe, V. Knap, M. Swierczynski, A. I. Stroe, and R. Teodorescu, "Operation of a Grid-Connected Lithium-Ion Battery Energy Storage System for Primary Frequency Regulation: A Lifetime Perspective," *IEEE Trans. Ind. Appl.*, vol. 53, no. 1, 2017.

[45] Adam Nieslony, "Rainflow Counting Algorithm - MATLAB Central," *2014*. [Online]. Available: https://se.mathworks.com/matlabcentral/fileexchange/3026-rainflow-counting-algorithm. [Accessed: 16-Apr-2019].